The Effect of Humidity and Moisture Content on the Tone of Musical Instruments

by

Matthew James Borland

A thesis
presented to the University of Waterloo
in fulfillment of the
thesis requirement for the degree of
Doctor of Philosophy
in
Systems Design Engineering

Waterloo, Ontario, Canada, 2014

I hereby declare that I am the sole author of this thesis. This is a true copy of the thesis, including any required final revisions, as accepted by my examiners.

I understand that my thesis may be made electronically available to the public.

Abstract

The purpose of this research work is to investigate the relationship between humidity and tone in musical instruments. A basic hypothesis that motivates this work is that normal seasonal variations in relative humidity are thought to alter the tone of instruments constructed from wood. These changes in tone are believed to be due to changes in the dimensions and material properties of an instrument that are a result of wooden components absorbing and adsorbing water in equilibrium with their ambient environmental conditions.

To investigate this hypothesis an experiment was conducted with a guitar acclimatized at different relative humidity levels. Sample sounds recorded at each humidity level were then evaluated by the test subjects using a three alternative forced choice listening test paradigm. Subjects were readily able to distinguish sounds recorded at different humidity levels, supporting the claim that changes in ambient humidity can create perceptible differences in instrument tone.

A finite difference model was then developed to produce simulated sounds as a function of moisture content (MC being the weight percentage of a piece of wood that is water). The model was validated and further listening tests were conducted to determine the perceptual limit of MC differences. The just-noticeable difference value for MC change was established to be 0.7% MC difference. To be considered imperceptibly stable with respect to tone, materials used to replace traditional soundboard woods would need to have less variability than the equivalent material property changes due to this 0.7% MC difference.

Testing of an acetylated plate in terms of its vibration and material properties followed. An increase in both stiffness and density was noted, yet even after modification the vibration properties of the plate were observed to remain within an acceptable range of material properties typical of soundboard grade woods [1]. Instrument builders would likely welcome this new material, as long as its properties can be shown to not vary significantly from traditional choices.

A second component of this thesis concerns the application of wavelets in musical analysis. Psychoacoustical signal parameters (PSPs) are a tool used to quantify aspects of sounds, such as brightness or percussiveness. These PSPs are often calculated using the Fast Fourier Transform (FFT), an algorithm that has certain limitations. To address the deficiencies of the FFT a wavelet transform was employed and conventional PSPs were reformulated in the wavelet domain to improve their accuracy. Tonal differences due to changes in MC were shown to be well suited to analysis by wavelet PSPs where improved sensitivity was observed in comparison to the conventional methods.

Finally, an acoustical study of the development of the piano from the clavichord to the modern grand piano was conducted. An improved bass response and the presence of more energy in the upper partials, particularly in these bass notes, were concluded to be due to an increase in soundboard area, the introduction of longer string scale lengths, and the use of wound strings for bass notes.

Acknowledgements

I would like to thank my supervisor, Dr. Stephen Birkett, for his support and assistance in the undertaking of my PhD. Stephen has always given me the freedom to investigate topics and problems that I'm passionate about, something a researcher like me truly appreciates. Thanks also go to Dr. Jeffery Jones from Wilfrid Laurier University for access to his facilities and his undergrad psych students who acted as my test subjects. David Breitman from Oberlin College also provided access to a wonderful set of historic pianos and great hospitality, which was much appreciated. Support from Accsys Technologies plc. in preparing acetylated wood samples used as part of this thesis was also greatly appreciated. Vicky Lawrence, Kristen Deckert, Colleen Richardson, and the other SYDE staff are also owed a thank you for all the support and answers to my many questions, and for providing help when I've needed it. I would also like to thank Dr. Paul Calamai and Dr. Carolyn MacGregor for their support of my teaching pursuits and the opportunities they've given me during my PhD to develop those skills. Finally, thanks to Kate for her love and support.

Contents

List of Tables

List of Figures

Chapter 1

Introduction and Literature Review

1.1 Introduction

The study of musical instruments in an engineering context is a rapidly developing field. As complex vibratory systems made of organic materials, they present a significant challenge, but when the results of an engineering analysis are interpreted in the context of a psychological or emotional response by a listener the problem becomes much more complex. This thesis aims to explore the role of material properties, particularly the moisture content of wood, and their effect on the tone of an instrument. Novel wavelet domain analysis methods will be developed to do this, finite-difference modelling will be employed, and psychoacoustic listening tests will be conducted to validate the results of experimentation; all within the context of perception.

1.1.1 Musical Instrument Design

The design of musical instruments has evolved over hundreds, if not thousands, of years in a largely empirical manner as small changes in design are tested and implemented through a trial and error process to suit the prevailing or desired musical sound of the time period. The research work in this thesis focuses on two instruments, the guitar and the piano, which share several commonalities in design and construction. Guitars and pianos are both built with a thin wooden soundboard that is attached through a bridge, to a string which is free to vibrate. Sound is produced in these instruments by exciting the string, which then transfers vibrational energy to the soundboard, which in turn acts as a transducer that produces pressure waves in the air which a listener then perceives as sound.

The guitar is the simpler of the two instruments and consists of a soundboard, resonating box, neck, bridge and strings. The string has terminations at the bridge

and the nut (or where a player presses a string against a fret with their finger) and is generally excited by a plectrum or the finger of the player (with or without fingernail). The parts of the guitar are seen in figure 1.1. The guitar's design varies most significantly from the piano with the presence of an air cavity that contributes 'air modes' to the modal space of the instrument in addition to soundboard and back vibration modes. The soundboard of a guitar is typically 2-3 mm thick and in the most highly regarded instruments is constructed from old growth softwoods such as sitka spruce or Norway spruce which are preferred for their vibrational properties [1, 5]. Backs and sides are generally made from hardwoods that are often chosen as much for their aesthetic appeal as their vibrational properties.

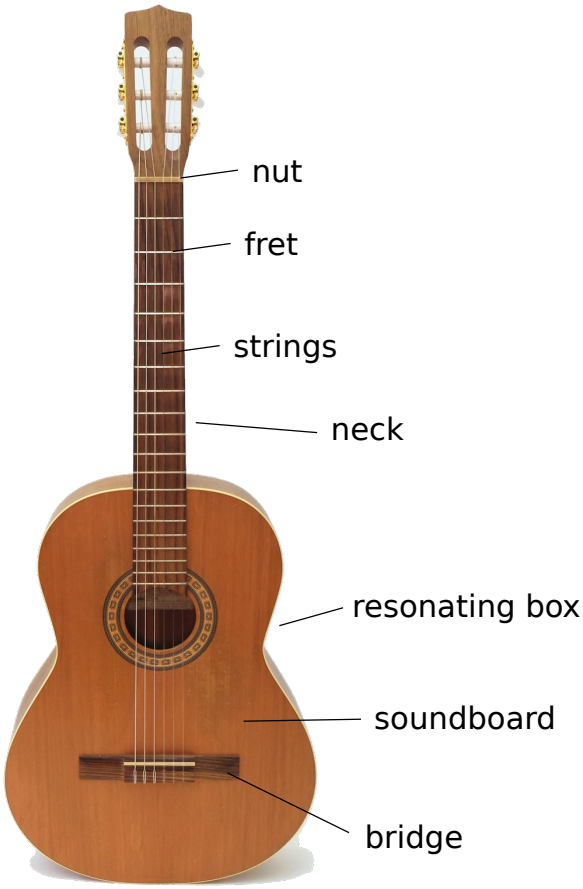

Figure 1.1: Typical components of a guitar.

The piano, on the other hand, is an exceptionally complex system of mechanical parts. A player applies force to a key, which, through a mechanical action, launches a hammer at a string (or group of strings). The hammer velocity and hardness determine the energy transfer to the string which is set into motion, where both transverse and longitudinal string vibrations are transduced via the bridge and the

soundboard panel into pressure waves a listener perceives as sound. The components of a typical modern grand piano are illustrated in figure 1.2

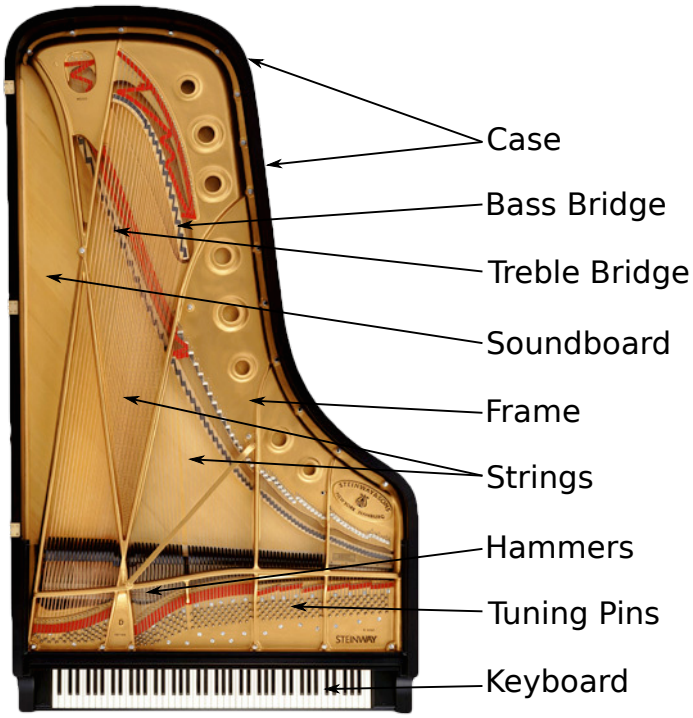

Figure 1.2: Typical components of a grand piano[2].

One important point to emphasize is the importance of perception in the analysis of a musical instrument. The ultimate purpose of an instrument is to allow an artist to create an emotional response to their performance, a purpose which can sometimes be lost in the midst of modal analysis or vibration measurements. A listener's perception of the sound of an instrument will be the final judge of its quality for any practical purpose, and it is with this in mind that this research work aims to provide instrument designers and builders with a better understanding of the role humidity plays in musical instrument tone.

1.1.2 Ambient Humidity and Wood

Wood is a hygroscopic material, that is, a material that can readily absorb and adsorb moisture from its environment [3]. Typically this means that wood moves towards an equilibrium moisture content (EMC) in balance with the current humidity level. The amount of moisture contained within a piece of wood has a significant effect on its dimensions and material properties [3, 4] and it is this property that requires careful consideration from musical instrument designers and builders. The

current moisture content (MC) of a piece of wood is not always equal to its EMC, as a certain amount of time (several hours to days) is required for that piece to come into equilibrium. One of the challenges when working with wood as an engineering material is to understand its behaviour under different moisture conditions and to design appropriately to allow for this natural variation to occur.

To understand MC you must first be able to measure it and there are three main ways to do this: resistance methods, capacitance methods, and oven drying [3]. In the resistance method two metal spikes are inserted into the wood sample and a resistance value is measured using a specialized ohmmeter. This resistance value, combined with the distance between the spikes and the wood density, is then attributed to a MC level. The capacitive method is similar, but without the destructive nature of the resistance method. In the capacitive method a thin charged plate is placed on the wood sample and for a given density and thickness a capacitance is measured and equated with a MC level. This method once again relies on the knowledge of the density of a wood sample, which is often not measured directly, but is looked up from reference tables of typical density values for a particular species. The final method, oven drying, is the most accurate, but can also be the most damaging. In this method the mass of a wood sample is measured at a desired MC, then the sample is oven dried until it contains no moisture and the mass is measured again. This approach provides the basic definition for MC where the formula is:

$$\mathrm{MC} = \frac{M - M_0}{M} \tag{1.1}$$

where M is the current mass of the sample and M_0 is the oven dried mass of the same sample. Drying wood samples to 0% MC can cause serious warping and cupping and is not suitable when a non-destructive measurement is necessary.

With the ability to measure MC we can now consider the different effects this moisture has on the wood's structural components. There are three primary grain directions found in all wood samples which are each affected differently by changes in MC: longitudinal (along the length of the tree), radial (from the centre of the tree outwards), and tangential (tangential to the radial direction). An illustration of these primary grain directions is shown in figure 1.3.

In terms of dimensional change the radial and tangential directions undergo significant amounts of shrinkage and swelling, while in the longitudinal direction shrinkage is typically considered to be negligible [3]. From a maximum moisture condition (green wood with approximately 25-30% MC) to an oven dry state (0% MC) the shrinkage percentage for sitka spruce in the tangential direction is 7.5% and in the radial direction is 4.3% [3] (i.e. a 10 cm wide board could shrink by 0.43 cm in the radial direction from green to oven dry state). These shrinkage percentages are typical of most wood species, with the tangential direction experiencing more shrinkage than the radial direction, however, each species has its own unique

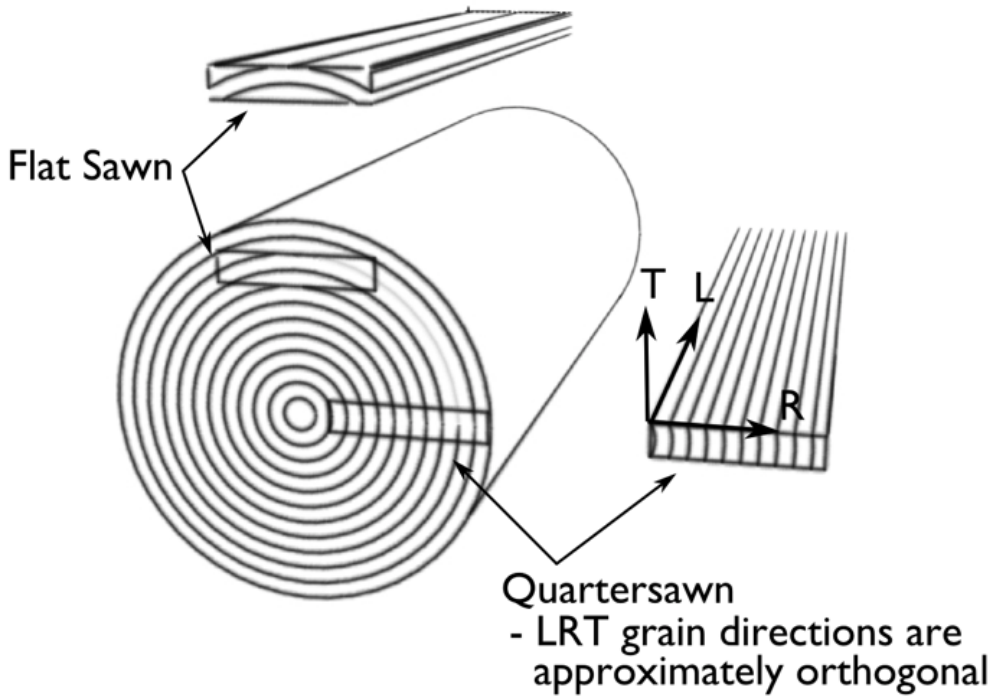

Figure 1.3: Primary grain directions: longitudinal (L), radial (R), and tangential (T). Flatsawn and quartersawn pieces of lumber are also indicated, with flatsawn lumber being more prone to warping and cupping and quartersawn lumber behaving more like a rectangular orthotropic material (which is less susceptible to warping and cupping, but still subject to expansion and contraction) [3].

shrinkage properties that need to be considered when using wood as an engineering material.

Choosing certain cuts of wood, particularly quartersawn wood, decreases a piece of lumber's propensity to warp or cup, but does nothing in terms of the overall dimensional and material property changes that occur as wood absorbs and adsorbs water. A quartersawn piece of wood which has properties that are approximately orthotropic is a dramatic improvement over flat sawn lumber in terms of warping, but even perfectly quartered lumber still requires careful consideration in the design process as all untreated woods will expand and contract through the seasonal humidity variations found in most climates. In the case of the piano this is most significantly seen in the soundboard which is made of quartersawn strips edge glued together to produce a large continuous panel. In the radial direction of a grand piano soundboard (approximately perpendicular to the bridge) this can mean expansion across a span of 1.2 m or more in the radial direction. Using standard formulae [3] for wood expansion an unrestricted soundboard made of sitka spruce would then vary in this radial span dimension by as much as 1.65 cm from the dry winter months (5% MC) to the moist summer months (14% MC). In a piano, however, the soundboard is not unrestricted, but is rigidly constrained within a frame referred to as the case. This physical constraint leads to issues of cracking and geometric instability, exactly the kinds of problems that provide the basic motivation of this thesis.

1.1.3 Musical Instrument Tone

The tone of a musical instrument has three main descriptive perceptual components: pitch, loudness, and timbre [6]. The pitch of a note is closely associated with the fundamental frequency of a harmonic or inharmonic sound and its relation to defined scales like the equal temperament scale common in western music. A piano emitting a sound with a fundamental frequency of 440 Hz has a pitch of A4, or A above middle C (see appendix for note names and fundamental frequency values). Loudness refers to the perception of a sound property that is roughly related to the amplitude of its vibration. The human hearing response is not equal across all frequencies so corrections are applied to determine loudness depending on the frequency content of a sound. Loudness is also measured on a logarithmic scale (dB) because of the logarithmic quality of human hearing. Finally, timbre is defined as the sound 'quality', a property that differentiates musical sounds of equal loudness and pitch by the complex harmonic structure inherent to different types of instruments. Psychoacoustical signal parameters are commonly used to quantify these timbral differences by analyzing the temporal and frequency domain properties of a sound [7].

Ultimately the perception of musical instrument sounds must be understood in the context of human perception and with this in mind researchers depend on listening tests to draw conclusions about tone. Listening tests usually consist of

playing a series of recorded sound samples in a controlled condition and having the subject respond to various questions about the sound samples. The primary method that will be used in this thesis is the three alternative forced choice (3AFC) procedure. In this technique subjects are presented with three sound samples, two of which are identical (the 'a' sample), and are asked to identify the sample that is unique (the 'b' sample). The presentation order of the sound samples is randomized (i.e. one of aba, aab, or baa) and subjects are considered to be able to perceive a difference between the 'a' and 'b' samples if their correct identification rate is higher than the 33.3% average they would get if they were just randomly guessing [8]. In this way the degree to which two similar sounds are different can be established with higher correct identification rates corresponding to more highly perceptible differences.

The 3AFC method can also be extended to be used in establishing a just-noticeable difference (JND) level[9]. The JND level represents the smallest difference in a stimuli that is perceptible by a subject and occurs when their average correct identification rate approaches the 33.3% response that occurs for random guessing. To employ this technique the 3AFC test is adaptive, starting out with large, highly perceptible differences between the 'a' and 'b' samples that are gradually reduced until the subject is unable to consistently perceive a difference and begins to randomly guess. This JND represents the degree of dissimilarity that a subject is able to perceive and, accordingly, is useful as a design criteria in establishing acceptable performance limits.

In the case of a musical instrument these performance limits could relate to the tonal properties that correspond to several design aspects. If the goal of musical instrument design is to create a stable tone then the structural geometry and material properties could be designed to vary within the JND limits without having to achieve the somewhat unrealistic goal of being perfectly stable. The primary reason for tonal instability, as mentioned above, is the variation in material properties and swelling/shrinkage due to MC changes experienced by wood. An example of this is the downbearing angle of the strings at the bridge that is established by the amount of crown, or arching, present in a piano soundboard. This arch is built into piano soundboards to increase the effective stiffness and define the angle at which the piano strings attach to the bridge. Both the string angle and amount of downbearing are known to affect tone [10] and as the soundboard absorbs water and expands, the curvature or crowning will increase and create variations in these properties. This downbearing concept is illustrated in figure 1.4.

Guitars can also feature a similar arching of the soundboard in their design and any other changes in instrument geometry due to swelling and shrinking will have similar effects on the vibrational and tonal properties of all musical instruments made of hygroscopic materials like wood.

This natural variation makes the job of a musical instrument builder very difficult, as ideally they would spend a great deal of time fine tuning their instrument under one set of moisture conditions. Unfortunately their instruments are expected

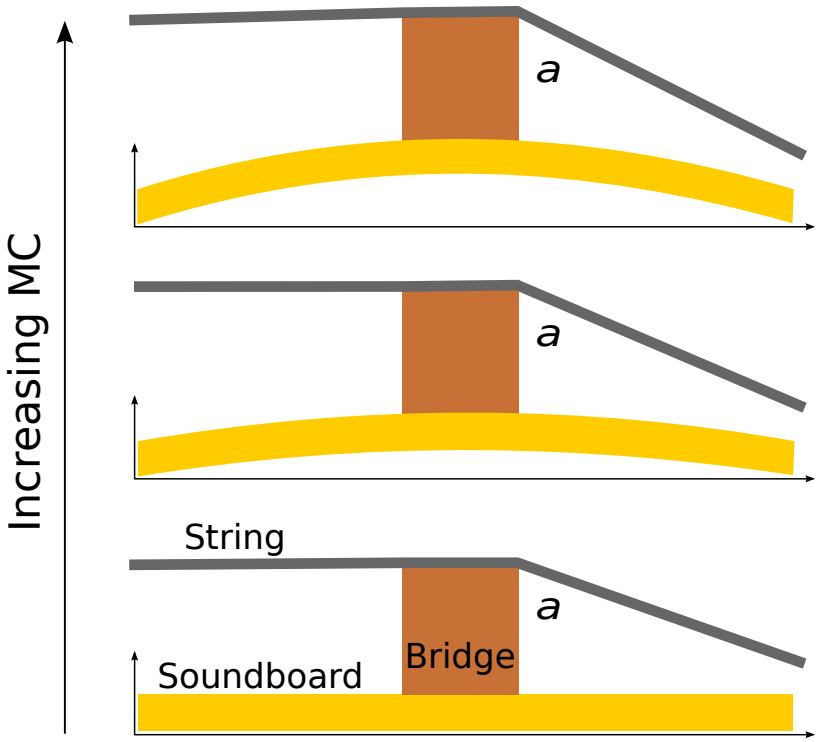

Figure 1.4: Downbearing at the bridge of a piano due to string angle (a) and soundboard curvature. Increased MC creates increased curvature and downbearing angle at the strings which increases the downward force component due to string tension at the bridge. The amount of curvature is greatly exaggerated in this figure for illustrative purposes.

to perform in a wide array of moisture conditions that are completely out of their control. If stable alternatives to replace wood are available that can accurately reproduce its complex tonal qualities a builder would be able to fine tune the sound of their instruments with confidence. Exploring the idea of tonal stability will be a focus of this thesis.

1.2 Literature Review

A review of relevant literature is provided next to establish the background research applicable to the problem areas described in the introduction. The five main areas of study are presented in sections below: Wood as an Engineering Material, Numerical Modelling for Sound Synthesis, Psychoacoustical Evaluation, Wavelets and Signal Parameters, and Wood Properties and Stabilization.

1.2.1 Wood as an Engineering Material

The Wood Handbook [11] published by the U.S. Department of Agriculture's Forest Product Laboratory provides an excellent basis for understanding the mechanical and engineering properties of wood. Chapter 4 of the cited document is devoted to the mechanical properties of wood and is an important source of material property data. Many different wood species are sampled for material properties such as modulus of elasticity, specific gravity, and hardness, among others, and the basic relationship between the primary grain directions is discussed. The effect of other factors on mechanical properties such as varying grain angle, the inclusion of knots, and, most relevantly to this thesis, moisture content are introduced. The overall conclusion from this work is that wood's natural variation requires careful consideration when used as an engineering material as there are many factors that affect its behaviour. That said, a scientific approach is possible if attention is paid to wood's natural variability.

A second text of great importance in the wood research field is Hoadley's *Understanding Wood* [3], a book that represents a summation of many years of research in the field of wood technology. It provides chapters on wood as an engineering material, material properties, and the relationship between wood properties and moisture content. The discussion in this last chapter introduces the concepts of bound and free water and the basics of determining equilibrium moisture content of a wood sample. A direct relationship is drawn between increasing relative humidity and MC and the expansion and contraction of wood is predicted using basic equations and knowledge of the fiber saturation point. Methods for coping with dimensional change in wood due to natural variations in relative humidity are also discussed including both design methods that pay careful attention to grain direction and chemical stabilization methods that aim to reduce the hygroscopicity of the material. It might be argues that one simple solution to reduce moisture exchange might be to simply coat the wood with a surface finish like varnish. Hoadley

points out that, although surface finishes may slow moisture exchange, none are able to completely stop it. Hoadley's work provides the fundamentals needed for any discussion of wood as an engineering material, particularly in the context of moisture exchange due to seasonal variations in relative humidity. Musical instrument builders such as luthier Antonio de Torres (1817-1892) have applied these concepts throughout the centuries in an informal manner [12] to cope with dimensional change and the challenges of working with a material like wood, but Hoadley expresses them more formally and provides a basic understanding of the use of wood in an engineering context.

Taking the scientific understanding of MC and wood further, Pérez, et. al. [4] investigate the modal response of a thin plate of musical instrument soundboard wood for its modal properties under varying humidity conditions. Using modal analysis they calculate the dynamic moduli of a quartersawn sample of Norway Spruce in the longitudinal and radial directions. Shear modulus is also calculated from the data and the measurements are repeated from 0%MC to 25%MC to provide a curve fit of these parameters as a function of moisture content. In general it is shown that these moduli tend to increase in value with decreasing MC (i.e the drier the material is, the stiffer it is), but below 5%MC the increase in stiffness either reaches a maximum or slightly decreases. This work provides an excellent overview of the effect of moisture on the mechanical properties of a musical instrument soundboard and will be used as the basis for parameterizing the thin plate model developed in chapter 3.

When discussing wood as a material for use in musical instruments it should be clear by this point that there is not a 'one-size fits all' solution. The mechanical properties required for frame components vary greatly from those of soundboard components and also among different types of instruments. Wegst [1] and Yoshikawa [5] present two different classification schemes that attempt to identify ranges of material property values that would satisfy the different structural and vibrational roles found in the different parts of musical instruments.

Wegst's [1] study measures a large variety of musical instrument woods for speed of sound, density, loss coefficient, and Young's modulus. The materials are then classified by instrument type or sound production role (i.e. is it a frame component or is it a soundboard) and are presented on plots comparing speed of sound to density or Young's modulus to loss coefficient. Clear patterns emerge in these plots that show distinct regions of material properties that are associated with different types of instrument parts. Soundboard woods, for example, have low density and high speed of sound, whereas woods used for woodwind instruments have higher density and lower speed of sound values. Wegst's classification plots provide excellent target values when searching for stable alternatives to replace wood in the construction of musical instruments, as any new materials used to replace wood (while still retaining a traditional 'wood' sound) should be chosen to have properties that fall within these typical property value ranges.

Similarly Yoshikawa [5] investigates the material property differences between

woods used in soundboards and frame boards, but uses an alternative formulation for derived material properties believed to be relevant to these two categories of wood. A variety of traditional woods used for both purposes are tested for their vibration properties which are then plotted to observe if any distinction exists between the two applications of the different woods. Several different combinations of parameters are derived, with the transmission parameter, cQ (where c is speed of sound and Q is related to the inverse of attenuation), and the anti-vibration parameter, ρ/c (where ρ is density and c is speed of sound), are observed to have almost orthogonal behaviour for the two types of wood used in musical instruments. Soundboard woods generally have low values of anti-vibration parameter and high values of transmission parameter that fall near one regression line, while frame components have high values for both anti-vibration and transmission that fall along a regression line orthogonal to the soundboard line. These regression lines provide clear targets for the material properties of any material that would be used to replace wood in the soundboard or frame of a musical instrument.

Both of these classification studies present interesting results, but unfortunately do not present any information regarding the MC of the wood samples they used to determine the material properties that define their classification schemes. With an understanding of the role of MC in wood properties [3] this is an important omission that will warrant further investigation later in this thesis.

1.2.2 Numerical Modelling for Sound Synthesis

The evolution of sound synthesis is well documented in Bilbao's *Numerical Sound Synthesis* [13] where he ultimately employs the computationally expensive finite difference method for simulation, but in earlier work Bilbao [14] introduces the digital waveguide network (DWN) method and its application in musical sound synthesis. The DWN approach relies on a series of interconnected passive delay lines that are used to approximate the behaviour of a partial differential equation (PDE) in a discrete manner. Passivity, or the property of elements to neither create or destroy energy is the key aspect of DWNs, and it is this property that ensures the stability of the system. Energy is shunted around the waveguide network and the next state of any node in the system is simply calculated as a sum of adjacent nodes at previous time steps, with the possibility of including lossy behaviour through special nodes. As its name suggests this method is well suited to solving the wave equation and for sound synthesis, as it is computationally efficient. DWNs are expanded upon throughout the text into 2D and 3D versions incorporating ever more complex modifications to attempt to model losses and complex physical interactions more accurately. When applied to musical instruments a 1D delay line can be used to model the behaviour of strings and tubes, with frequency dependant losses applied as a lumped filter combining the losses of all the nodes together at the end of the network. This approach retains the computational efficiency of the method, but highlights the main difference between DWNs and other methods like the finite difference approach. To run efficiently DWNs create ideal lossless energy networks

that are then filtered to achieve a desired output, whereas other computationally more expensive methods incorporate more complex loss schemes directly into the problem formulation for each discrete component of the model [13, 15, 16].

Fontana and Serafin [17] extend the DWN method pioneered by the Center for Computer Research in Music and Acoustics (CCRMA) [18] to model a simplified trapezoidal shaped violin. To do this a 3D trapezoidal waveguide mesh is used to model the air resonances of the body and to determine the impulse response of the air cavity. A DWN model of the bowed violin string is then filtered using the air resonance impulse response to create the final output sound; in this manner retaining the computational efficiency of the DWN method. This approach of applying filters to represent the more complex components or behaviours of an instrument is typical of the approach used by the DWN method as the main goal of this approach is to create real-time synthesis, not explicitly replicate the complete dynamic behaviour of the system being modelled. The goal of simulating a simplified violin in real time is achieved in this case, but there is no comment as to how well the simulation actually compares to a real violin's tone or physical behaviour.

Moving beyond the DWN approach Chaigne and Lambourg [15] present a time-domain formulation of both isotropic and orthotropic plates including damping. An experimental approach is used to examine the frequency dependent nature of damping in different types of material and to compare the results with a finite difference model of damping. The time domain formulation is considered to accurately represent the observed behaviour of aluminum, glass, carbon fibre, and wooden plates and is employed in a subsequent paper [19] as part of an impacted plate model used for sound synthesis. By increasing the complexity of the governing equations they increase computational costs, but also allow for the physics of the system to be more directly simulated.

Continuing on from earlier work, Chaigne et. al [19] then developed a finite difference model of a damped thin plate for both orthotropic and isotropic cases in conjunction with an impact model that is used to excite the plates. The Kirchoff-Love thin plate assumption provides the basis for the model which is extended with the damping model from their previous work [15]. The Rayleigh integral is used for simplicity to determine the sound pressure at an observation point away from the plate and the synthesized sounds are compared to measured sounds for validation purposes. The frequency values of the harmonic peaks of the FFT of the measured and simulated sounds are found to compare excellently, but the magnitudes of each peak are observed to vary significantly. The overall impression of the simulated sounds is considered to be good, but a more complicated radiation model is considered to be necessary to improve the accuracy of the results, particularly for large dimension wood plates.

With the fidelity of musical instrument simulations observed to be increasing, it is at this point that Derveaux et. al [16] extend the work of Chaigne with a complete guitar model including string excitation, soundboard plate vibration, air resonances, and radiation. A 1D damped string model is attached at the bridge to a

Kirchoff-Love plate representing the soundboard. The guitar back and sides are not considered to vibrate, but do define the boundaries of the air cavity inside the guitar. To simplify the model only the transverse vibration of the soundboard is considered and an acoustic field which connects the air cavity via the soundhole to the rest of the acoustic field is used. Even with the number of simplifications employed the full 3D model is quite complex. Using a fictitious domain method introduced by Glowinsky [20], Derveaux et al. present a complete formulation of the model and create simulated guitar sounds. When compared to sound pressure, admittance, and modal results of real instruments published in the guitar literature Derveaux's results were considered to be 'compatible'. The primary physical limitation of the model is considered to be the inability to accurately include the geometry of the bracing found on a guitar soundboard. Other improvements suggested by Derveaux are the inclusion of more accurate air-soundboard coupling models, 2D string models that include polarization, as well as the vibration of the neck of the guitar. The inherent complexities of presenting a complete model of a guitar become apparent, and it should be noted that in comparison to the structural complexity and size of a piano the guitar can be considered to be a relatively simple musical instrument.

Bilbao's second text [13] on system modelling for sound synthesis abandons the DWN approach in favour of the finite difference method, despite the added computational costs associated with the technique. The change in modelling paradigm is in response to the ever increasing computing power available and the ability of the finite difference method to directly model the partial differential equations that define the physics of a particular system. In this manner losses can be explicitly defined as part of the PDE's and more realistic dynamic modelling can be realized. The text develops the finite difference method from the simplest 1-dimensional equations to 2-dimensional plate vibration, including both linear and non-linear cases, and, most importantly for this work, a thin plate orthotropic model with losses suitable for modelling the wood soundboards of musical instruments.

Bilbao's text provides a thorough overview of the numerical methods and detailed analysis of the use of finite difference modelling in sound synthesis. His method will be used extensively for the modelling found in this thesis.

1.2.3 Psychoacoustical Evaluation

The field of psychoacoustics is well established and Ing and Ing [9] provide an overview of the just noticeable difference (JND) technique and its application in acoustics. Two classes of JND tests are introduced, those that play both stimuli sounds being compared simultaneously, when for example comparing the loudness of sounds with two different pitches, and JND tests that play two different sounds one after another, used when comparing two similar sounds. When conducting the second kind of test the researcher must be careful to ensure several experimental design parameters do not affect the results. First, the pause between successive

sounds should be more than 0.1 s, but less than 2 s to ensure the results are independent of the pause duration as longer wait times require auditory memory to play a larger role and generally will increase the observed JND level. A second important aspect of JND testing identified is that the loudness that the sample sounds are presented at can have an effect on subject performance. Sound-pressure levels of 40 dB or higher are considered to be adequate to ensure loudness is not affecting the perception of the sound stimuli. General experimental results for frequency, phase, loudness, and masked JND tests are also presented as experimental guidelines for researchers. The importance of experimental design and ensuring that any variation in stimulus is only with respect to the desired sound property is emphasized.

As an example application of this technique Henrich et. al [21] examine the perceptual relevance of several glottal flow parameters used in a speech synthesis model to determine JND levels. Test signals are simulated in a synthesis program and an adaptive 3AFC approach is used to determine if listeners can hear a difference between sample sounds. The subjects ranged in age from 23 to 58 years of age and no gender differences were observed in terms of the overall results. For any particular sound parameter being examined the subject starts out comparing two sounds with a large difference in the parameter and are presented with three sound samples in random order, two of sound 'A' and one of sound 'B'. They are then asked to identify which sound was unique (i.e. not repeated) with correct responses seeing the difference between the two stimuli reduced, while incorrect responses would result in an increase in the difference in the parameter being examined. JND levels for the glottal parameters are then established using this method, with the final JND level being calculated from the average of the last few tests.

Another discussion of the JND technique in terms of timbre perception is presented by Rahne et. al. [8]. Timbre is a fundamental aspect of musical perception and in this paper the researchers develop a psychoacoustical test to determine timbre differences which vary only in spectral shape for the purpose of improving musical perception in people with cochlear implants. The authors note that several JND tests have been conducted previously using real instrument sounds, but since these sounds vary in more than one timbre dimension the results are hard to discuss. To alleviate this problem a synthesis algorithm is used to vary sound parameters only in terms of the amplitudes of ten harmonic components present in the sounds used in the experiments. In this way the harmonic shape is easily controlled, while other tonal parameters like pitch and loudness remain constant. Test subjects are then presented with a 3AFC test and instructed to identify which sample sound is unique. The spectral difference between the sound stimuli is then adjusted according to their response for the next test. After two correct responses the step size is halved, while after one incorrect response the step size is doubled. After a number of tests the subject should approach their perceptual limit and will begin to randomly guess, at which point the JND step size will remain constant and the JND level is established. Rahne et. al conclude that their test methodology is capable of accurately identifying JND levels in terms of timbre parameters and

is applicable in the testing of other relevant timbre properties other than spectral shape.

Following a solid, well-defined experimental protocol is a key aspect of all three of the discussed works and a similar 3AFC method will be used later in this thesis to determine a JND level for MC difference. The importance of isolating the desired attribute in the testing procedure is an important aspect of the experiments discussed by Rahne et. al. [8], and will require special attention in chapter 3.

1.2.4 Wavelets and Signal Parameters

One of the challenges of psychoacoustics is to find quantitative descriptors of sounds that can then be linked to the perception of those sounds. Peeters [7] provides an overview of a number of signal analysis parameters that can be used to quantify the properties of sounds for exactly this purpose. The parameters are divided into several categories dependent on their method of classification and include temporal, spectral, energy, harmonic, and perceptual features. All of the psychoacoustical signal parameters (PSPs) defined in this paper are calculated in either the time domain, frequency domain, or a combination of both, and thus rely heavily on the discrete Fourier transform. Peeter's set of PSPs will be extended to the wavelet domain later in this thesis to provide an alternative analysis approach that does not suffer from the limitations of the Fourier transform in terms of representing aperiodic signal components.

The wavelet transform is an analytical technique that is somewhat difficult to understand. Instead of breaking down a signal into pure frequency components, as in the Fourier transform, the wavelet transform instead uses short, finite length wavelets that do not immediately lend themselves to direct interpretation. Torrence and Compo [22] present an excellent introduction to the wavelet transform and its application to analyzing time domain data that can help a reader understand the basics of this exciting method of signal decomposition. Many different approaches can be used to calculate the wavelet transform of a signal and the differences between the discrete wavelet transform (DWT) and continuous wavelet transforms (CWT) are explained, with a complete description of the application of the continuous transform provided by Torrence and Compo. The basic concept of the wavelet transform is to decompose a time domain signal into a time and wavelet domain using 'wavelets' instead of pure sinusoids. In comparison to the traditional Fourier transform the wavelet transform has several advantages: the ability to choose from several different decomposing waveforms, the ability to increase both time and frequency resolution at the same time, and the ability to more accurately represent aperiodic signals. The disadvantages of the CWT are that it is computationally more expensive and that it requires a shift in mindset when interpreting results. The decomposing wavelet used in the CWT is not a pure periodic sinusoid, as in the Fourier transform, but is instead a finite length wavelet composed of several different frequency components. When interpreting the results an equivalent

Fourier frequency can be calculated at a particular wavelet scale, but the CWT is often reported with a scale axis that refers to the period of the wavelet used in the transform. The advantage of the CWT over the DWT is that it does not require an orthogonal wavelet basis for decomposition, but it does produce a transform with redundant data. The DWT provides the most compact representation of the time domain data in the wavelet domain, and is thus well suited to data compression tasks, but the 'redundant' information provided by the CWT is actually useful in signal analysis tasks as it takes the form of increased time resolution.

To demonstrate the technique Torrence and Compo analyze weather data using the CWT and clearly illustrate the beneficial aspects of wavelets in examining signals with both periodic and aperiodic components. They also present statistical methods for comparing two different time series data sets using wavelets. It can be concluded that the wavelet transform provides a complementary analysis method to the traditional Fourier transform that is useful for certain types of time series. Musical sounds often consist of both a short aperiodic component associated with the instrument's excitation and a periodic component that is related to the steady vibration of a moving body such as a string [23] and are well suited to analysis by the wavelet transform.

An example of this application in musical sound analysis is presented by He and Scordilis [24] who attempt to determine the amount of compression that is acceptable without a perceived loss of quality using a wavelet transform approach to compression. The discrete packet wavelet transform (DPWT) is employed in a multi-step process with progressively more compression and masking of portions of the signal that are considered to be inaudible. This DPWT method is compared to a discrete Fourier transform (DFT) version of the same algorithm and shows that the the wavelet method is superior to the Fourier technique both in terms of computational costs and temporal resolution. Informal listening tests are reported, but only a simple observation that the compressed sounds are indistinguishable from the original sounds for both the DFT and DPWT methods is reported. The strengths of the wavelet approach are confirmed by this study as a more accurate representation of the original time series data is achieved versus the Fourier transform, even at a lower bit-rate.

This ability to more accurately represent signals with both periodic and aperiodic components, like sound recordings of music, will be employed later in this thesis to reformulate PSPs in the wavelet domain and analyze historic pianos and variations in MC.

1.2.5 Wood Properties and Stabilization

The chemical modification of wood to improve stability is not a new topic, even to musical instrument design. The Yamaha corporation has a patent [25] for an acetylated soundboard for use in pianos, with another example provided by Yano and Minato [26]. These researchers explored the role of chemical modification

in the control of the vibrational properties of wood in an attempt to show that timbral differences in the sound of a musical instrument are not determined only by the geometry and structural design, but can also be controlled by the use of chemical treatments of the wood used in an instrument's soundboard. Sample strips of sitka spruce are treated with an aqueous solution of saligenin of varying concentration then air and vacuum dried. Samples are then allowed to acclimatize for a week at normal indoor humidity conditions and then are finally subjected to a formaldehyde treatment. Decreases in hygroscopicity are expected, but Yano's purpose is actually to create a frequency dependent change in damping as a result of the treatment. The results of vibration testing indicate that 5% saligenin solutions are the most effective in terms of the added mass from the treatment and the overall effect on damping values. The general behaviour is to increase damping more at lower frequencies than at higher frequencies, which Yano argues will effectively make the wood 'resound uniformly' in the audible frequency range. A decrease in hygroscopicity and a corresponding improvement in dimensional stability are also noted. It is important to note that achieving a uniform frequency response is not the point of these experiments, but instead the point is to demonstrate that chemical modifications can be used to create frequency dependent changes in the vibrational properties of soundboard woods used in musical instruments.

The acetylation technique employed by Yamaha for piano soudboards [25] had previously been developed extensively by Rowell who gives an excellent general overview in his article *Acetylation* [27] in the Forest Products Journal. This article aims to provide an introduction to the science behind this wood stabilization method and outline its strengths and weaknesses. Acetylated wood falls into the class of chemical stabilization, as it uses an esterification process that reacts acetic anhydride with the hydroxyl groups present in wood's microstructure to produce acetylated wood and acetic acid as a by-product. Normally it is at these hydroxyl groups where water bonds to the chemical structure of wood, but because the hydroxyl groups in the cell wall are already occupied water molecules are effectively blocked, in a macroscopic sense, from being absorbed. Several different chemical processes have been developed to catalyze the reaction or generally increase the reaction rate of acetylation, which is limited by the diffusion properties of the wood species being acetylated. Rowell suggests that the best method of acetylation is also the simplest in terms of chemical processes: acetic anhydride and solid wood are reacted under vacuum at 120°C, with higher reaction temperatures increasing the reaction rate.

The degree of acetylation in a sample is referred to by its weight percentage gain (WPG), which is calculated in a similar manner to MC. Through various tests an ideal value of 20% WPG due to the added esters that replaced the hydroxyl groups has been established, as above 20% the wood properties are considered to degrade due to deterioration of the cell walls in the wood fibre. At a WPG of 20% the wood sample will absorb far less moisture from the atmosphere and will correspondingly have a smaller variation in MC than untreated wood. Rowell illustrates how an untreated sample of pine varies from 5.8%-21.7%MC at 30%-90%

relative humidity, whereas the acetylated sample varies from 2.4%-8.4%MC under the same conditions. This reduction in the amount of absorbed water results in increased dimensional stability, the primary goal of the acetylation process. Other properties of wood are also improved, such as resistance to rot, fungus, and marine organisms, as well as the mechanical properties of wet wood. The acetylation process has also been shown to have excellent long term-stability, with little to no loss of WPG of the ester groups after cyclic exposure to low and high humidity over a 20 year period. Rowell concludes that the only limiting factor in the adoption of acetylated wood is the added cost associated with its production, something that is currently being addressed by the development of new processing techniques [28].

The degree of acetylation was assessed by Ramsden et. al. [29] who present a study of Scots pine to determine the effect of WPG on its tensile modulus of elasticity and dimensional stability. A 50/50 mixture of xylene and acetic anhydride was used to treat the samples for a reaction time of 1-4 hours at 145°C. This treatment provides samples ranging from the untreated 0%WPG condition to samples with slightly greater than 30% WPG for testing. Tensile modulus was measured for each of the samples with an Instron material testing machine and was shown to increase in value from the untreated sample to the sample treated for 1 hour (roughly a 15%WPG). For samples treated for longer than 1 hour the tensile modulus tended to decrease compared to the 1 hour treatment, but all acetylated samples had higher tensile moduli than the untreated samples. Dimensional stability was also shown to increase significantly with untreated samples observed to have a 12% volume increase when immersed in water while samples treated for 4 hours increased in volume by less than 5% when immersed. Ramsden concluded that a compromise must be made between gains in dimensional stability and the deterioration of mechanical properties at high WPGs, with his research indicating a WPG of 15-20% being ideal. The tradeoff between increased stiffness and mass is a particularly interesting one for musical instrument builders and will be discussed further in chapter 6.

Acetylation is not the only possible way to chemically occupy the hydroxyl bonds found in wood and Li et. al. [30] have explored the use of other anhydrides for this purpose. In their research acetylated, propionylated, butyrylated, isobutyrylated, and hexanoylated woods were prepared without catalysts at several different reaction temperatures under reduced atmospheric pressure. All the treatments showed increased weight percentage gains (WPG) with increasing reaction temperature and time, and increasing dimensional stability with increased WPG. The anhydrides with lower molar masses were observed to require lower reaction temperatures to achieve desired WPGs and butyrylated, isobutyrylated, and hexanoylated were considered to create an undesirable byproduct odour upon reaction. Li et. al. conclude that acetic or propionic hydrides are best suited for use as wood modifiers due to their less pungent odour and lower reaction temperatures. This research clearly indicates the complex criteria by which materials used to replace traditional wood products will be judged.

Several other chemical treatments have also been examined by Obataya et.

al. [31] with relation to the resulting vibrational properties of wood after treatment. Formaldehyde, acetylation, polyethylene glycol impregnation, and hematoxylin impregnation are applied to sample blocks of sitka spruce which are then left to acclimatize in an indoor environment for more than 1 month. The test samples are then tested at 25°C and 60% RH to determine dynamic Young's modulus, E/γ, and the loss tangent, $\tan\delta$. The effect on E/γ by the acetylation method is to generally reduce E/γ versus the untreated sample at all humidity levels, whereas the hematoxlyin impregnated samples showed little to no change from the untreated sample with regards to this parameter. In terms of $\tan\delta$ the acetylation and formaldehyde treatments both showed a consistent decrease compared to the untreated sample, whereas the hematoxylin impregnation was less consistent, showing variable levels of decrease at low relative humidities, while showing an increase in $\tan\delta$ above 90% relative humidity. The major difference between the treatment techniques should be noted: the impregnation methods effectively fill the wood cells with a plasticizing agent, unlike the formaldehyde and acetylation methods which chemically alter the wood structure by occupying hydroxyl groups. Obataya concludes that all four methods increase dimensional stability, but they are not all consistent in terms of their effect on vibrational properties. From the data presented in the paper the acetylation and formaldehyde methods appear to provide the more consistent modifications in vibrational properties in comparison to the impregnation methods.

Acetylated wood stabilization will be evaluated in chapter 7 of this thesis to test its suitability as a stabilized alternative for use in musical instruments.

1.3 Contributions of This Thesis

The contributions of this thesis fall into three main areas: the exploration of the effect ambient humidity has on wood, and subsequently, the tone of musical instruments; the development of wavelet domain signal parameters for the evaluation of tone in musical instruments; and the evaluation of a stabilized wood product as a replacement for traditional soundboard materials.

Although anecdotally observed, there is little research clearly demonstrating the perceptibility of tonal differences in musical instruments as a function of change in humidity. To explore this concept a guitar is examined at three humidity levels for modal, impedance, and psychoacoustical signal properties, as well as ultimately being compared through a 3AFC listening test to determine if differences in tone are perceptible. The listening tests produce promising results in terms of the perceptibility of the differences and lead directly into the next stage of the project: a finite difference model of an orthotropic thin wooden plate.

This finite difference model provides precise control of the moisture content being simulated in the wood, something that is not possible when using a real wooden plate or instrument and acclimatizing it in a humidity controlled chamber. The sound samples created by the model can then be used in further 3AFC tests

to determine the JND level of tonal differences due to changes in MC with an increased degree of resolution and consistency in terms of initial conditions. Before establishing a JND for these kinds of differences a psychoacoustical verification is performed to ensure the model is accurately simulating the real behaviour of a guitar soundboard, and more importantly, the perception of the sound output of an orthotropic wooden plate with varying humidity. Listening tests similar to those mentioned above are repeated using the orthotropic model to create the sound samples and results of both studies are then compared for validation purposes. The model's performance is found to closely replicate the results of the earlier guitar study and the model is considered to be satisfactory enough to proceed to a more detailed study to determine the just-noticeable difference (JND) level for moisture content change. An adaptive 3AFC approach is used with further listening tests to establish this JND level (i.e. the smallest amount of change in moisture content in the soundboard that is perceptible by a listener), the purpose of which is to determine a reasonable design criteria for material stability in terms of acoustical properties in musical instrument construction. The overarching goal of this research work is to design musical instruments that have stable properties under typical humidity conditions found in winter (low humidity) and summer (high humidity) months. By establishing the lower perceptible limit in terms of MC change the material used as a replacement for wood would not have to be perfectly stable under all conditions, just stable enough to only vary within the range established by the JND test.

The second component of this thesis is an exploration of the application of wavelet methods in psychoacoustics. This topic is introduced first by applying the wavelet transform in place of the Fourier transform to produce a 'time-frequency', or wavelet domain, representation of a signal. The wavelet domain is useful because it provides a researcher with a more accurate representation of the signal compared to a standard Fourier domain representation of the time domain signal when that time domain signal contains finite length, aperiodic components. Musical instrument sounds contain both periodic and aperiodic components associated with the free vibration and excitation of the system respectively [23], and as such are well suited to examination using wavelet techniques. To provide a quantitative psychoacoustical wavelet analysis a number of psychoacoustical signal parameters (PSPs) currently formulated in the Fourier and time domains are reformulated to be calculated in the wavelet domain. An exploration of idealized impactive components and their effect of Fourier and wavelet versions of these signal parameters is then provided to illustrate the increased accuracy of the wavelet domain representation of the signal. To further illustrate the application of wavelet domain PSPs a comparison of the tonal development from early fortepianos to modern grand pianos is also provided.

Finally, the evaluation of a stabilized wood product as a replacement for traditional soundboard wood is explored. Stabilized wood products are known to have greatly improved dimensional properties, but their applicability as tone wood in musical instruments has not been tested in terms of relevant vibratory, acoustical,

and psychoacoustical properties. These types of properties are examined to provide an assessment of an acetylated wooden soundboard for use in musical instruments.

Chapter 2

Preliminary Evaluation of Guitar Tone and Moisture Content

2.1 Introduction

Musical instruments are complex systems that depend on many parameters to control their output sound quality. In this chapter the effect of relative humidity level on the tone of a guitar is investigated to determine if changes in relative humidity create perceptible changes in tone. The hygroscopic nature of wood means that as relative humidity varies the equilibrium moisture content of the wood will also change accordingly; in turn affecting the material properties of the wood [3] and the tone of the instrument.

Changes in humidity are anecdotally thought to affect an instrument's tone with instrument builders typically attempting to precisely control humidity conditions during the construction process [12], but there is little objective research available to quantitatively show that these changes are perceptible. Research, however, indicating the type of mechanical changes to expect in terms of wood's material properties as its moisture content (MC) changes is extensive [3, 11, 32, 33, 34]. Generally speaking, increased moisture content will increase the density of a wood sample, while decreasing most other properties such as Young's modulus or shear modulus [11].

The purpose of this study is to investigate the hypothesis that changes in moisture content are perceptible as a change in the tone of a musical instrument. Psychoacoustical listening tests were employed to determine if this hypothesis is true for a set of guitar sounds recorded under a range of indoor relative humidity levels typical of seasonal variations in North America [3].

2.2 Background

Moisture content is a term derived to relate the total amount of water present in a wood sample to its oven dried state (i.e. having no moisture content or 0% MC). The MC value is expressed as a percentage and represents the portion of the sample's mass that is absorbed water, see equation 1.1. For wood in an environment with a constant relative humidity an equilibrium state will eventually be reached that is referred to as equilibrium moisture content (EMC). If given a long enough time to acclimatize to a certain relative humidity a wood sample will always reach an equivalent EMC, and thus relative humidity is often used interchangeably with the concept of MC in wood. Finishes on wood such as lacquer, oil, or shellac, act to retard moisture transfer and increase the time it takes a sample to reach EMC, but given enough time even samples treated with surface finishes will eventually absorb water and move towards EMC [3]. The general relationship seen in figure 2.1 between RH and EMC is similar for different types of wood.

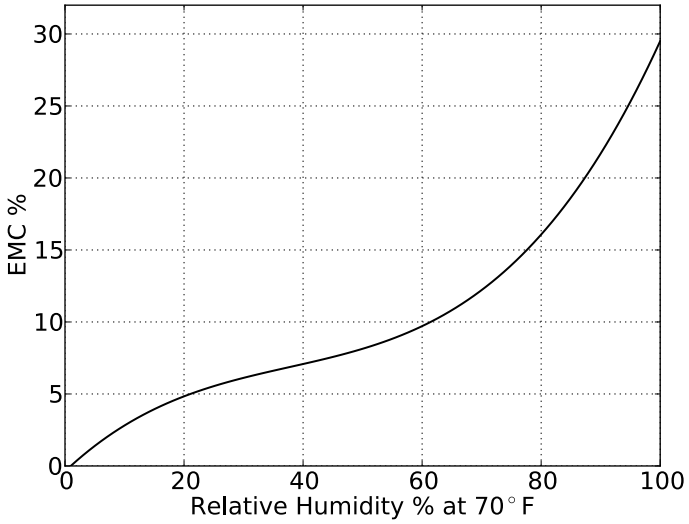

Figure 2.1: Relationship between equilibrium moisture content and relative humidity for white spruce; a fair approximation for most wood species [3].

The absorption of water will have three relevant general effects on wood: increased density, decreased material moduli properties, and dimensional change [3]. Musical instruments that are constructed of wood are resultantly subject to these kinds of changes when MC fluctuates due to relative humidity variations, and it is these effects which are hypothesized to alter the tone of wooden instruments. When building instruments like guitars and pianos (and many others), careful attention is paid to choices in wood, grain direction, and surface finishes, all in an attempt to produce a stable sound under variable humidity conditions. That said, musical instruments are often finely tuned and it is possible that the natural variation of

wood as a function of MC could significantly effect the vibratory and acoustical performance of an instrument. An example of this kind of issue mentioned earlier from piano building would be the curvature, or crown, of the soundboard that acts to add stiffness and establish the down bearing angle (the angle that the strings attach to the bridge) of the instrument. Wood contraction will decrease the curvature of the soundboard with decreasing MC and in turn decrease the down bearing angle between the string back length and speaking length. Structural stiffness due to the arching effect will decrease and the overall mass of the soundboard will be reduced as moisture is lost. All of these changes will have an effect on tone, but the question remains as to how perceptually relevant these changes are and what magnitude of change in these kinds of material and structural properties is perceivable.

A more technical explanation of the effect of MC on wood properties can be found in *Understanding Wood* by Hoadley [3] and the *USDA Wood Handbook* [11], specifically chapter 4. The mechanism for moisture transfer in wood is through the exchange of free water (water that is found within the wood cell cavities) and bound water (water that is held within the cell walls through physical attractive forces at the molecular level). Free water is easily shed by the wood after it is harvested and once all this water has been adsorbed the wood reaches a fiber saturation point where any remaining water is bound within the cell walls. Typically this occurs at 30% EMC, but varies among wood species. Below the fiber saturation point bound water is lost as the material equalizes itself with the relative humidity of its environment. At this point the wood begins to shrink and increase in strength as EMC decreases [3]. Moisture content is used interchangeably with the term EMC, but technically EMC is a moisture level in equilibrium with relative humidity, while MC is simply the current moisture level whether or not the material has reached equilibrium.

To discuss the tonal changes due to MC variations one must first understand timbre, or sound quality. Timbre is what differentiates the tone of one instrument from another and corresponds to parameters of a sound related to its attack, decay, temporal envelope, and frequency content. To quantify timbre we use psychoacoustical signal parameters such as spectral centroid and temporal centroid that have been shown to be connected to perceived brightness [35] and the percussiveness of a sound [7].

In the current research work it is hypothesized that tonal differences will be perceptible when subjects listen to test samples of a guitar recorded after it has been acclimatized at different relative humidity levels (and associated MC levels). To verify this hypothesis a three alternative forced choice (3AFC) test is used to establish if test samples are perceptibly different. The 3AFC test works by asking participants to choose which sample is unique in a set of three samples where two are the same and one is different. If subjects are unable to perceive a difference between the samples and are effectively randomly guessing they would on average achieve a hit rate of 33.3%. The concept behind this method is that performance higher than this 33.3% random guessing effort would indicate a perceptible difference is present in the test samples. This approach has been used to determine the

perceptibility of the tainting of cooked trout by diesel fuel [36], to train subjects who had received cochlear implants to improve speech performance [37], and is quite commonly employed in the field of psychoacoustics to determine the perceptibility of differences in sounds [38, 8, 39].

2.3 Method

Sample sounds for this study were recorded from a steel string guitar that was stabilized at different levels of relative humidity in a small humidity chamber. A guitar was chosen because its small size was convenient, it required little expertise in terms of tuning/preparing the instrument for playing, and because the internal wood surface of the guitar body is not treated with any finish, thus allowing more rapid equalization of the wood's moisture content with the relative humidity level in the chamber. The guitar used in this study is a Seagull steel-string model with laminated sides and back, and a solid cedar top. Ultimately three humidity levels were chosen for testing: 30%, 60%, and 80% at 20°C, corresponding to 7%, 9%, and 11% MC. These relative humidity levels were selected to be typical of the indoor moisture variations found in many parts of North America due to seasonal weather patterns [3].

Measuring MC is not a simple task and is especially difficult when the wood samples are very thin, as is the case for the wood in the soundboard and body of a guitar. The resistance method is not preferred as it is destructive and it only measures one resistance value between two points on a sample. The capacitive method is non-destructive and measures a larger sample area, but does not perform well with very thin samples (less than 1/4 inch in thickness) typical of the sounding boards of musical instrument construction. For the purposes of the experiment the capacitive method was chosen and a thicker wood sample was used as a surrogate for the measurement of moisture content. Ultimately the accuracy of using these methods to determine the actual MC of the wood in the guitar could be called into question (i.e. is it actually at 7% MC), but the relative difference between samples (i.e. the 2% difference between the 7, 9, and 11% cases) can be considered to be reliable. The only more reliable method would be to dry the guitar to 0% MC in an oven and then measure the mass of the guitar as it acquires moisture from the air. This method, however, would be destructive to the guitar and incompatible with testing the same guitar at multiple MC levels.

To create a set of stimuli for listening tests the sounds of a guitar being played were recorded using a Behringer ECM 8000 microphone in a laboratory under identical conditions. A mechanical plucking device was created to ensure consistency in terms of excitation, and the guitar was tuned to standard tuning before each session. The plucking device consisted of a plectrum attached to weight and lever. The weight was dropped from a repeatable position allowing for a silent actuation of the guitar pluck. Each of the six open strings, notes E2, A2, D3, G3, B3, and E4, was recorded at each MC: 7%, 9%, and 11%. Only the open strings of the guitar

were used in this study to avoid the possibility of tonal differences due to fingering technique. Recordings were made outside of the small humidity chamber use to acclimatize the guitar with a RH of approximately 70%. Several sound samples were collected for each note and only samples that were repeatable, determined by examining the cross-correlation of the waveforms, were used in the study. The selected recorded sounds were then corrected for pitch differences using an autocorrelation method to ensure tuning differences between the three MC samples were within 5 cents, a level below an established perceptible limit of 10 cents [40], with 100 cents being equivalent to one semitone. After pitch correction was complete the samples were windowed to ensure each sample had a similar duration and were adjusted using peak amplitude normalization to ensure equal loudness. This loudness normalization method was considered adequate due to the similarity of the sound samples being compared. These samples contain the sound of the pluck and are referred to herein as the 'plucked' samples. A second set of samples was also created with a different windowing technique that selected only the region after the initial excitation peak of each sound, excluding the pluck portion. This sample set was created to compare results with the 'plucked' dataset to establish if the initial pluck is an important characteristic in the discrimination of the sound samples. The second dataset is referred to as the 'windowed' dataset.

A 3AFC task was created to determine if humidity variations are perceptible as changes in tone [41]. In this 3AFC task the subject was presented with three short sound samples in succession where two of the samples (sample 'a') were identical and one was different (sample 'b'). Samples were presented in random order (i.e. one of b-a-a, a-b-a, or a-a-b) and the subject was instructed to indicate which sample they believed to be different. Within subject testing was conducted simultaneously for the six notes described above. This kind of task was repeated 75 times for a number of different combinations of different sounds, but not the full set of possible sounds to avoid any possible fatigue effects. Participants were allowed to replay the sound sample as many times as they liked and were not restricted in terms of response time. All of this was conducted using a Python script and a computer interface. Sennheiser HD 280 Pro headphones [42] were used with an M-Audio soundcard [43] for audio playback and subjects were seated in an Industrial Acoustics Company sound isolation chamber [44]. Subjects were selected from a university student population and ranged in age from 17 to 23 years of age. In total 30 subjects participated in the study, with one subject being excluded because they did not follow the provided instructions while completing the test. The participants answered a short survey assessing their musical experience and were also subjected to a hearing test. Of the 29 subjects 17 were musically experienced and 19 were assessed to have normal hearing (they passed a hearing screening at the threshold of 25 dB HL for pure-tone frequencies of 0.5-8 kHz using a MADSEN Midimate 622 - Diagnostic audiometer). These groups provide a basis for later comparisons in terms of their performance on the 3AFC task. Subjects were remunerated with course credit for their participation and had the right to withdraw without penalty.

2.4 Results

2.4.1 3AFC Testing

On completion of the participant testing an individual's correct identification (hit rate) was calculated for the different test blocks discussed above. A histogram of the overall average for all participants for all test samples is shown in figure 2.2 where a normal distribution is observed. A mean of 0.77 and a standard deviation of 0.09 is shown where a hit rate of 1.0 would represent a perfect score and the null hypothesis that the participants could not distinguish between the sounds and are randomly guessing would yield a hit rate of 0.33.

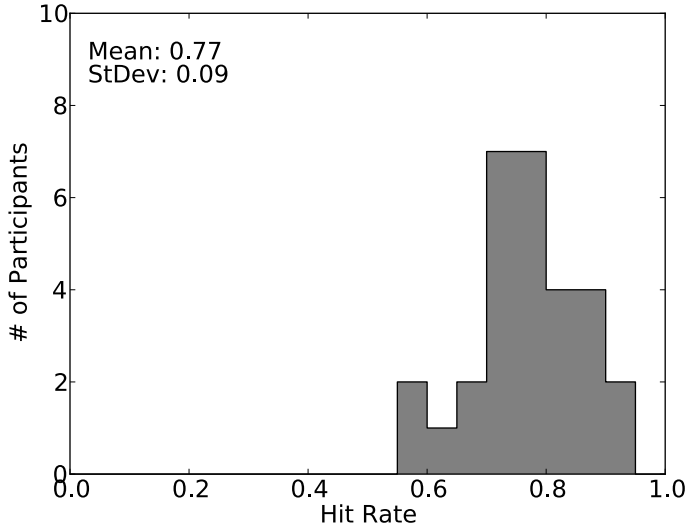

Figure 2.2: Histogram of the average hit rate for all participants for all types of stimuli. A mean hit rate of 0.77 indicates that on average participants correctly responded 77% of the time with a standard deviation of 9%.

Beyond just looking at the subjects' performance on average for all the different types of stimuli there are several sub-groups of data that can be compared. One of these is the comparison between 3AFC tests where a 7% and 9% MC (2% MC change), 9% and 11% MC (2% MC change), and 7% and 11% MC (4% MC change) are used as stimuli. It is anticipated that due to the larger change in MC in the comparison between 7% and 11% MC samples that the participants should have a higher hit rate on this comparison than on the other two types of comparisons which should be similar in performance. A box plot showing whiskers as max and min, a box outlining quartiles, and a mean value for the three types of comparison are shown in figure 2.3.

A oneway ANOVA on the 7-9%, 9-11%, and 7-11% treatments resulted in an F-value of 20.1 and a p-value of 3.7×10^{-5}, indicating that one of the treatments

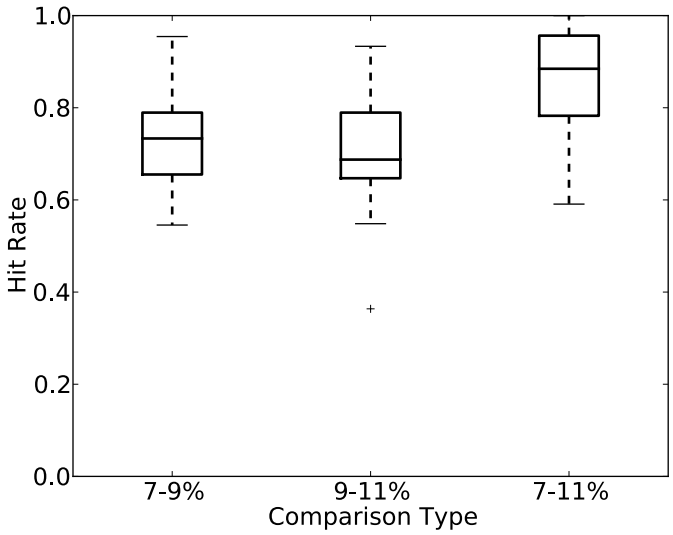

Figure 2.3: Box plot of the three test cases: 7-9%, 9-11%, and 7-11% with whiskers indicating maximum and minimum values, a box outlining quartiles, a line indicating mean value, and a cross indicating any outliers.

has had a significantly different effect than the other treatments. Further t-test comparisons of the treatments showed that as hypothesized the 7-11% comparison had a statistically significant increase in hit rate even when adjusted using the Bonferroni correction where the number of hypotheses is 5: pitch, hearing issues, musical experience, and MC difference. For a critical p-value of 0.05 the adjusted p-value will be 0.01. A similar adjusted p-value criterion is used for the remaining comparisons in this section and chapter 3.

Plotting the hit rate for each note also provides an insight into the effect of pitch on perception of changes in guitar tone due to changes in moisture content. Figure 2.4 provides box plots for each of the six notes tested for all participants. A general trend of increasing mean hit rate can be seen with increasing pitch and ANOVA indicates an F-value of 10.05 and a p-value of 2.0×10^{-8} indicating a significant difference in hit rate for at least one of the notes.

A comparison between 'plucked' and 'windowed' tests is shown in figure 2.5. The 'windowed' tests show a higher average hit rate than the 'plucked' tests and a similar distribution. A t-test on these two groups showed a t-value of -2.82 and a p-value of 0.007, indicating a significant difference between the two groups which could be interpreted as the differences in the 'windowed' tests being more readily perceived than in the 'plucked' tests.

Participants were also classified by musical experience to test the hypothesis that musically experienced people would more readily perceive changes in tone. Musically experienced participants were identified as those who had 2 or more years of training/playing experience. A box plot is shown in figure 2.6 for each

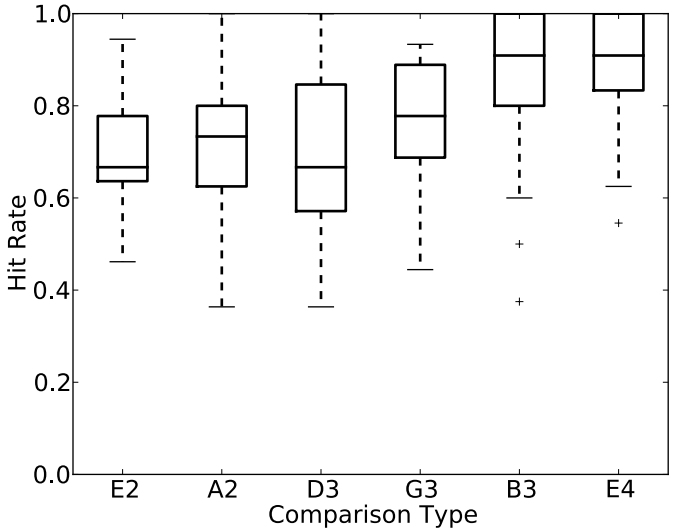

Figure 2.4: Box plot of hit rate for each note of the guitar with whiskers indicating maximum and minimum values, a box outlining quartiles, a line indicating mean value, and a cross indicating any outliers.

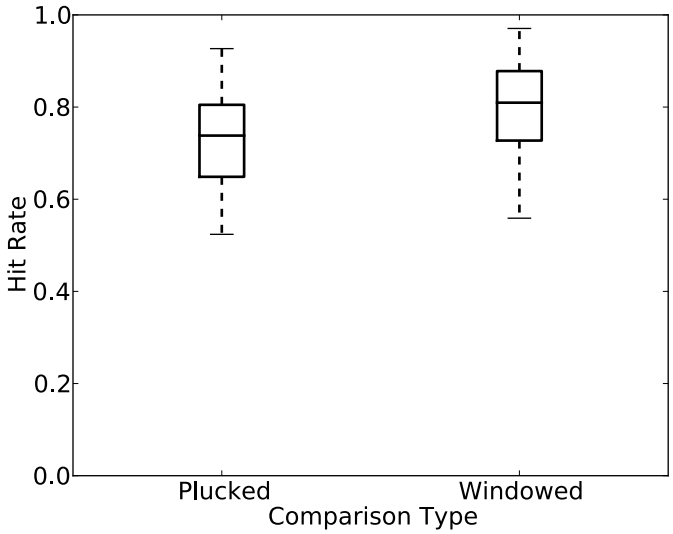

Figure 2.5: Box plot of hit rate for 'plucked' and 'windowed' tests with whiskers indicating maximum and minimum values, a box outlining quartiles, a line indicating mean value, and a cross indicating any outliers.

group for all tests. A t-test on these two groups showed a t-value of -2.59 and a p-value of 0.015, indicating a slightly significant difference between the two groups.

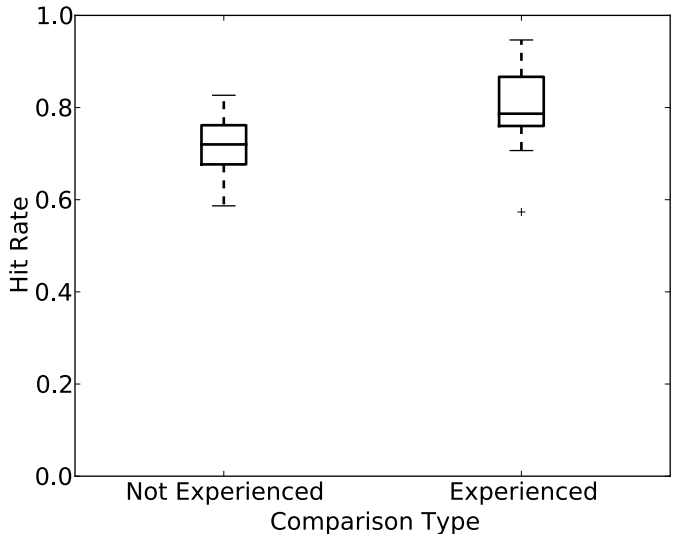

Figure 2.6: Box plot of non musically experienced and musically experienced subjects with whiskers indicating maximum and minimum values, a box outlining quartiles, a line indicating mean value, and a cross indicating any outliers.

Finally, participants were classified by their performance on the hearing test into two groups, as normal hearing or as having a hearing issue. Figure 2.7 shows the box plot for these groups. A Welch's t-test calculated a t-value of 0.80 and a p-value of 0.43, indicating that there is no statistically significant difference between the performance of these groups.

The hit rate and standard deviation for all comparison types is provided in table 2.1.

2.4.2 Psychoacoustical Signal Analysis

Examining the sample sounds in terms of psychoacoustical signal parameters is a good starting point to relate changes in tone perceived by the test subjects to physical properties of the guitar.

Spectral centroid (SC) is defined as the centroid of the frequency spectrum of a sound and has been shown to be an indicator of brightness [35, 7]:

$$\mathrm{SC} = \frac{\sum f(x) \cdot x}{\sum f(x)} \tag{2.1}$$

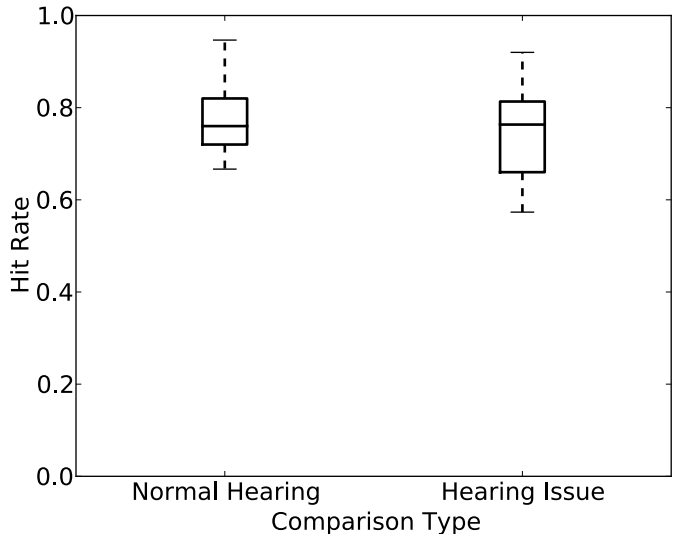

Figure 2.7: Box plot of normal hearing and hearing issue subjects with whiskers indicating maximum and minimum values, a box outlining quartiles, a line indicating mean value, and a cross indicating any outliers.

Table 2.1: Summary of Subject Data by Groups

Group	Mean Hit Rate	Std Dev
All Users All Tests	0.76	0.09
All Users Plucked Tests	0.73	0.10
All Users Windowed Tests	0.8	0.10
7% - 9%	0.72	0.10
9% - 11%	0.72	0.12
7% - 11%	0.85	0.12
Musically Experienced	0.80	0.09
Not Musically Experienced	0.72	0.07
Normal Hearing	0.78	0.08
Hearing Issue	0.74	0.11

where x is the frequency bin of the FFT of the time signal, $f(x)$ is the magnitude of the FFT, and the sum is over all relevant x (i.e. for an appropriate frequency band). The spectral centroid for each note plotted at each of the three MC levels is shown in figure 2.8.

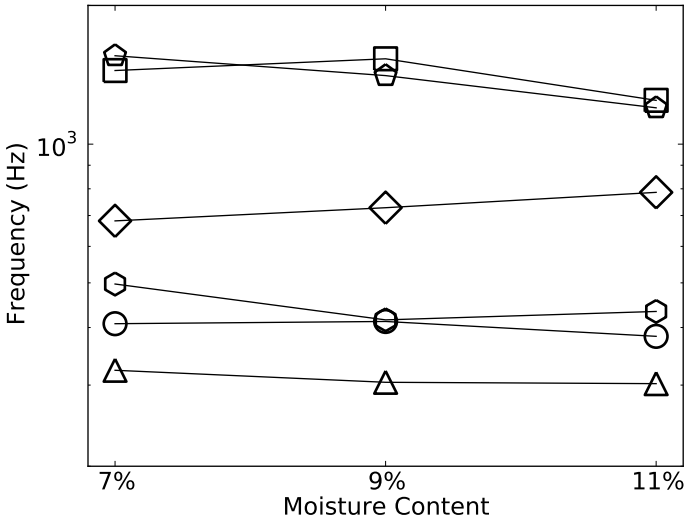

Figure 2.8: Spectral centroid of all notes at different MC levels. Different notes are denoted by markers as follows: E2 (○), A2 (△), D3 (⬡), G3 (◇), B3 (□), and E4(⬠).

Notes can be seen to have increasing or decreasing values of spectral centroid with increasing moisture content. Figure 2.8 illustrates that although trends do seem to exist with changes in moisture content, they are not always directly proportional to these changes. It can be concluded, however, that changes in MC do cause observable differences in SC, regardless of the direction of the trend.

Temporal centroid (TC) is defined as the centroid of the energy envelope of the time signal of the sound [7]:

$$\mathrm{TC} = \frac{\sum_{t=0}^{t_w} e(t) \cdot t}{\sum_{t=0}^{t_w} e(t)} \tag{2.2}$$

where $e(t) = (y(t))^2$ is the energy envelope, y is the signal amplitude, and t is the time. The time window, t_w, used in this calculation may be selected as appropriate and in the calculations in this paper is set to be $t_w = 1\,\mathrm{s}$. Figure 2.9 shows a similar result to that of the spectral centroid, with general trends with increasing moisture content, but with some notes seeing increasing temporal centroid values, while others see decreasing temporal centroid values.

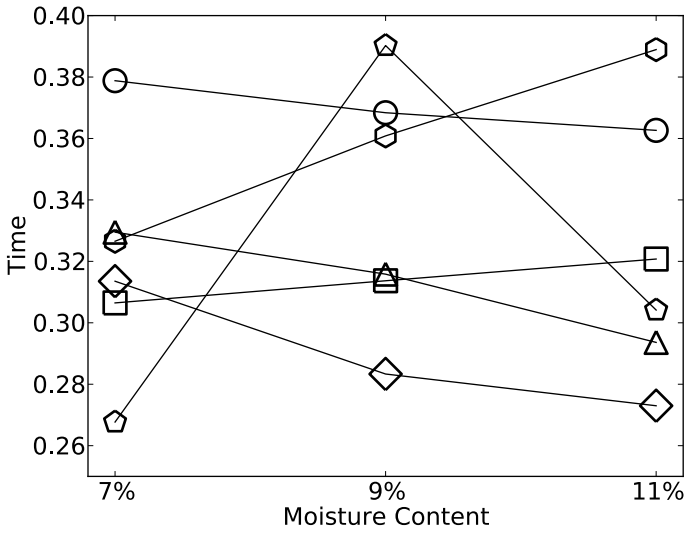

Figure 2.9: Temporal centroid of all notes at different MC levels. Different notes are denoted by markers as follows: E2 (○), A2 (△), D3 (⬡), G3 (◇), B3 (□), and E4(⬠).

2.4.3 Vibration Analysis

Modal analysis of the guitar's soundboard and impedance measurements at the bridge at each MC level were also conducted in order to draw connections to the subject testing. Modal analysis was completed using a roving impact hammer and fixed accelerometer method[1]. Two sets of measurements were completed for each MC level with different fixed accelerometer placements to avoid measuring at a node and potentially missing a vibration mode. The results reported are the averaged values from the two tests. Figure 2.10 illustrates the mode shapes and table 2.2 gives the associated modal frequency and damping coefficient. Vibration modes have a role in sound production, so examining these modal parameters for connections to the subject results is considered to be useful.

In all three modes a decrease in modal frequency is seen with increasing MC. This result is expected as increasing MC will reduce the stiffness of the soundboard plate and add mass to the system, both of which are things that should reduce these values. The damping coefficient, however, did not follow this trend, with the highest values measured at the 9% MC level for all three modes. Similarly to some of the psychoacoustical signal analysis parameters discussed earlier, this non-linear trend gives evidence to the complexity of the guitar as a vibratory system and requires further investigation.

The impedance measurements also present a somewhat murky picture. To mea-

[1]Geometry and measurement data were entered into the B&K Pulse system [45] and MEScope [46] was used to post process the data and to extract the modal parameters.

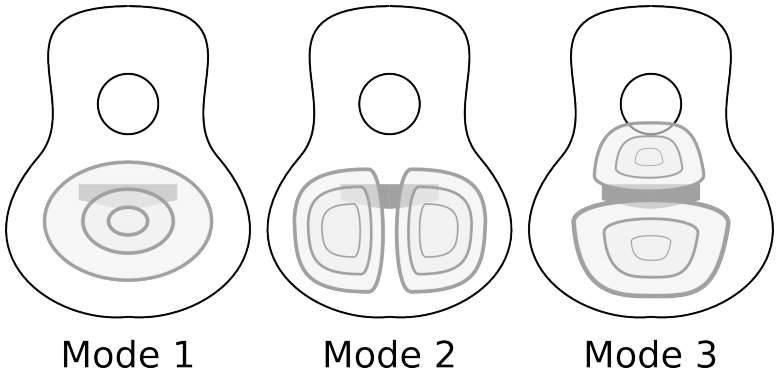

Figure 2.10: Graphical representation of the first three vibration mode shapes of the guitar soundboard.

Table 2.2: Modal parameters of the guitar soundboard.

Modal Frequency (Hz)			
Mode	7%	9%	11%
1	194	192	191
2	375	372	370
3	387	384	381
Damping Coefficient			
Mode	7%	9%	11%
1	2.95	3.26	2.15
2	0.87	1.01	0.92
3	0.98	1.06	0.91

sure impedance an impact hammer [47] and laser doppler velocimeter [48] were used. This method avoids mass loading the soundboard, but also places limitations on the frequency range of the results. At each MC level two sets of measurements were completed: one on the left (bass) side of the guitar bridge and one on the right (treble) side of the bridge. The impedance measurements presented in figure 2.11 show significant differences in the 400 to 1400 Hz region. At 600 Hz a stepwise decrease in impedance can be seen that aligns with increasing MC, but this trend is not consistent throughout for impedance at the bass end of the bridge. It can also be seen that the treble end of the bridge shows even less agreement or consistency with the MC trend. Changing the MC level of the wood in a real instrument clearly does not have the simple effect of increasing or decreasing the mechanical impedance, although some trends in specific frequency bands can be observed.

2.5 Conclusion

The primary result of this study is the demonstration that changes in moisture content are perceptible as changes in the tone of a musical instrument. If a participant were to randomly guess during the 3AFC task their expected hit rate would be 0.33, but it was found that the hit rate for any block or grouping of tests was well above the random response case even with small differences in MC (2%). At 0.76, the hit rate for all users in all tests clearly indicates that the participants could successfully perceive the difference in tone between guitar sounds recorded at different moisture levels. These MC levels are typical of indoor extremes experienced in North America during the summer and winter months [3] and validate the idea that under normal conditions these kinds of changes are perceptible.

When examining the psychoacoustical signal analysis parameters some trends in levels are visible, but are not consistent across all strings. The majority of results for a particular string do tend to either increase or decrease incrementally with increasing MC, but only when examining the modal frequencies of the guitar top are the measured values all in agreement with the trend of increasing MC. All of this speaks to the complexity of the response of a real musical instrument and the importance of the examination of a wide range of frequency components in the signal.

Another basic hypothesis was that tests that compared sounds with larger differences in MC would be more readily identified than those with smaller MC differences. The results indicated that participants performed significantly better on the 4% difference test than either of the 2% difference tests (0.85 versus 0.72 and 0.72). This strongly supports the idea that MC changes are perceptible and that larger MC changes are more perceptible than small changes in MC.

Finally, several groupings of participant test data were considered. Pitch did appear to have an effect on the hit rate for participants, with a trend towards higher notes being more easily distinguished. More careful examination is required

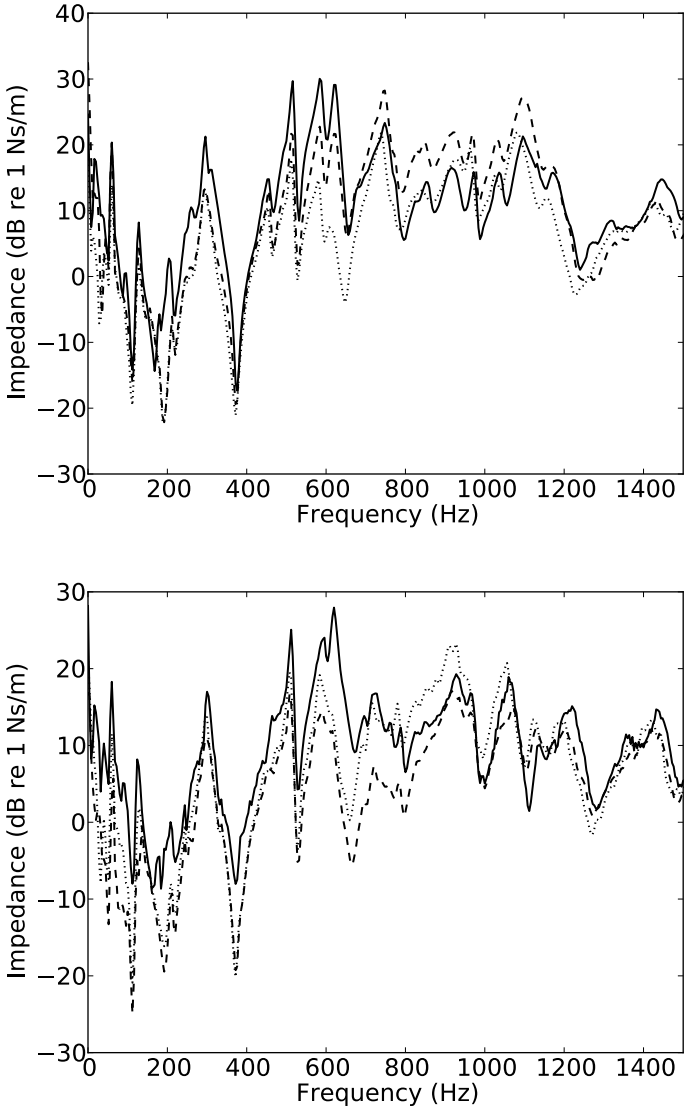

Figure 2.11: Impedance measured at bass side (top figure) and at treble side (bottom figure) of guitar bridge for 7% MC (solid), 9% MC (dashed), 11% MC (dotted).

to completely understand this effect, but one hypothesis to explain this would be that notes with higher pitches would have more low order harmonics in the 400-1400 Hz region where the most significant impedance changes were observed at the bridge of the guitar. An example would be the difference between notes E2, with a fundamental of 82 Hz, and E4, with a fundamental of 330 Hz. Note E2 would have its first four harmonic peaks at 82, 164, 246, and 328Hz, all below the frequency range where the most significant impedance differences are observed. Note E4, on the other hand, would have its first four peaks at 330, 660, 990, and 1320 Hz, right in the middle of this frequency range.

It was also observed that participants with musical experience also had higher hit rates than those without musical experience. Whether the musically experienced participants had 'better ears' or perhaps just had more motivation to perform well on the 3AFC task would take more experimentation to determine. A statistically significant difference between the 'plucked' and 'windowed' was also observed and could be interpreted as the differences in the 'windowed' tests being more readily perceived than in the 'plucked' tests. An explanation for this could be that the initial plucking pulse is creating a perceptual masking effect that interferes with the subject hearing the periodic portion of the signal. Further testing would be needed to test this hypothesis.

The results indicate that the basic hypothesis that even small humidity changes can create perceptible differences in the tone of a guitar is well defended. Due to the practical limitation of not having a large number of different guitars to include in the sample pool the conclusions cannot be extended to apply to all guitars, but should be considered to be limited to the particular instrument tested. That said, given the significance of the average correct identification rate, 76%, and the anecdotal evidence of audible differences, it is likely that these results could be generalized to other instruments. Further testing would be required to prove this in a statistically significant way.

A similar methodology could be used to examine the differences between the different types of woods used in musical instrument construction as changes in material properties due to changes in moisture content present a similar range of variation to changes in the wood species used in the construction of an instrument. There is little consensus among builders which particular wood species are best suited for soundboard materials, but the materials that have historically been used do fall into a small range of material properties [1]. Finding the perceptible limit of changes in instrument tone (the just noticeable difference level) in terms of material property differences is an obvious next step and will be the focus of the next chapter.

Chapter 3

Perceptual Evaluation of Moisture Content Using Simulated Sounds

3.1 Introduction

With the perceptibility of changes in MC established under normal indoor variations in humidity the next step in this project was to establish a just-noticeable difference level (JND) in terms of variations in humidity. To do this an orthotropic thin plate model was created using the finite-difference method. The advantage of using a model to create the sound samples instead of using recorded sounds of a real instrument is that it allows for precisely controlling MC in a way that is not possible in the real world. A study was conducted to psychoacoustically verify the performance of the model against the previous guitar tests, and once verified the model was used to create the sample sounds for an adaptive 3AFC listening test used to establish the JND level with regards to MC.

3.2 Model

The purpose of the finite-difference model is to allow fine control of the MC property; as controlling this in real samples is somewhat difficult not only to achieve, but also to measure and ensure consistency of in musical instruments that cannot be destructively tested. The model consists of three parts: a stiff string with frequency dependent damping, an orthotropic thin-plate model with frequency dependent damping, and a sound field approximated by the Rayleigh integral. A basic schematic of the system is provided in figure 3.1.

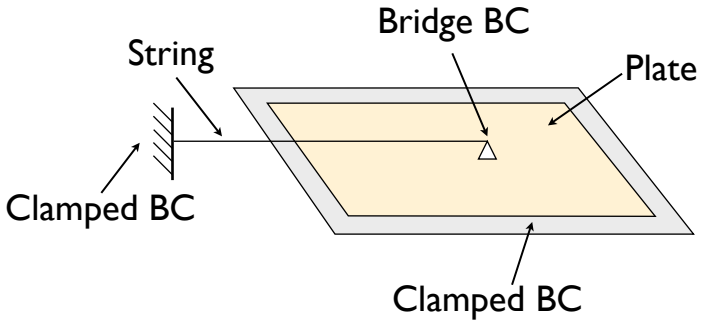

Figure 3.1: Simplified schematic of the orthotropic thin plate and stiff string system being modelled.

3.2.1 Stiff String

The spatially-scaled stiff string equation is defined using the finite difference approach following Bilbao's method [13] as a combination of the wave equation:

$$w_{tt} = \gamma^2 w_{xx} \tag{3.1}$$

and the ideal bar equation:

$$w_{tt} = -\kappa^2 w_{xxxx} \tag{3.2}$$

giving the stiff string equation with added damping terms:

$$w_{tt} = \gamma^2 w_{xx} - \kappa^2 w_{xxxx} - 2\sigma_0 w_t + 2\sigma_1 w_{txx} \tag{3.3}$$

where $w(x,t)$ is transverse displacement at a point x along the string, γ is wave speed relating speed of sound, c, and length, κ is a stiffness parameter, and σ_0 and σ_1 are damping constants. The string displacement, $w(x,t)$, is assumed to be real-valued, linear, and continuous. String tension is then included in the definition of the speed of sound, c, of the string and is held constant (i.e. there is no change in string tension with change in displacement). Subscripts denote derivatives, i.e. w_{tt} is equivalent to $\frac{\partial^2 w}{\partial t^2}$. The string is modelled as having one end with a clamped boundary condition and the other with a free boundary condition constrained to the transverse displacement of the attachment point of the string to the plate at the bridge.

A finite-difference scheme can then be created for the string with the basic equations defining the behaviour of the system described by equation 3.3. An implicit formulation of the string equation is:

$$\delta_{tt} w = \gamma^2 \delta_{xx} w - \kappa^2 \delta_{xxxx} w - 2\sigma_0 \delta_{t\cdot} w + 2\sigma_1 \delta_{t\cdot} \delta_{xx} w \tag{3.4}$$

where the difference operators are defined as:

$$\delta_{xx} w_l^n = \frac{1}{h^2}(w_{l+1}^n - 2w_l^n + w_{l-1}^n) \tag{3.5}$$

$$\delta_{xxxx} w_l^n = \frac{1}{h^4}(w_{l+2}^n - 4w_{l+1}^n + 6w_l^n - 4w_{l-1}^n + w_{l-2}^n) \tag{3.6}$$

$$\delta_{t\cdot} w_l^n = \frac{1}{2k}(w_l^{n+1} - w_l^{n-1}) \tag{3.7}$$

$$\delta_{t\cdot}\delta_{xx} w_l^n = \frac{1}{2kh^2}(w_{l+1}^{n+1} - 2w_l^{n+1} + w_{l-1}^{n+1} - w_{l+1}^{n-1} + 2w_l^{n-1} - w_{l-1}^{n-1}) \tag{3.8}$$

$$\delta_{tt} w_l^n = \frac{1}{k^2}(w_l^{n+1} - 2w_l^n + w_l^{n-1}) \tag{3.9}$$

and subscripts on w denote spatial location and superscripts indicate the discrete time, h is the grid spacing, and k is the time step. The operator $\delta_{t\cdot}$ is the centered time difference, which leads to the implicit formulation of the problem. These discretizations can be considered to be consistent because the truncation error of the discretized equation tends to zero as the discretization becomes finer. An example is provide for the forward difference δ_{t+}:

$$\delta_{t+} u(t) = \frac{1}{k}(u(t+k) - u(t)) \tag{3.10}$$

where k is the time step and t is the current time index. Expanding $u(t+k)$ in Taylor series about t gives[13]:

$$\delta_{t+} u(t) = \frac{du}{dt} + \frac{k}{2}\frac{d^2u}{dt^2} + \dots \tag{3.11}$$

and when k tends to zero it can be seen that the truncation error also tends to zero and the discretization is consistent.

Equation 3.4 can then be rearranged in term of time steps and written in matrix form as:

$$\mathbf{A}\mathbf{w}^{n+1} + \mathbf{B}\mathbf{w}^n + \mathbf{C}\mathbf{w}^{n-1} = 0 \tag{3.12}$$

with

$$\mathbf{A} = (1 + \sigma_0 k)\mathbf{I} - \sigma_1 k \mathbf{D}_{xx} \tag{3.13}$$

$$\mathbf{B} = -2\mathbf{I} - \gamma^2 k^2 \mathbf{D}_{xx} + \kappa^2 k^2 \mathbf{D}_{xxxx} \tag{3.14}$$

$$\mathbf{C} = (1 - \sigma_0 k)\mathbf{I} + \sigma_1 k \mathbf{D}_{xx} \tag{3.15}$$

where $\mathbf{D}_{xx}$ and $\mathbf{D}_{xxxx}$ are sparse matrix representations of the spatial difference operators and $\mathbf{I}$ is the identity matrix. The solution for the next time step at all locations, $\mathbf{w}^{n+1}$, can then be solved using a sparse matrix solver for the equation:

$$\mathbf{w}^{n+1} = -\mathbf{A}^{-1}(\mathbf{B}\mathbf{w}^n + \mathbf{C}\mathbf{w}^{n-1}) \tag{3.16}$$

Now that the basic equations and finite difference scheme are established the boundary conditions of the string need to be set. The string is modelled as having one end clamped and one end constrained to the transverse displacement at its attachment point to the plate.

$$\begin{array}{ll} \text{Clamped BC} & \text{Bridge BC} \\ w(0,t) = 0 & w(l,t) = u(x,y,t) \\ w_x(0,t) = 0 & \end{array} \tag{3.17}$$

The 'Bridge BC' is enforced by updating the value of $w(l,t)$ at every time step of the solution with the value of $u(x,y,t)$, the plate displacement at point $(x,y) on the plate$. To implement the clamped boundary condition at the other end of the string the difference matrices, $\mathbf{D}_{xx}$ and $\mathbf{D}_{xxxx}$, need to be modified for the boundary nodes. With the difference operators defined in equations 3.5 and 3.6 the kernels of the difference matrix operating on the string vector, w, can be seen to be:

$$\mathbf{D}_{xx} = \frac{1}{h_x^2} \begin{array}{|c|c|c|} \hline 1 & -2 & 1 \\ \hline \end{array} \qquad \mathbf{D}_{xxxx} = \frac{1}{h_x^4} \begin{array}{|c|c|c|c|c|} \hline 1 & -4 & 6 & -4 & 1 \\ \hline \end{array} \tag{3.18}$$

where the kernels relate to equations 3.5 and 3.6 respectively. The centre element of the kernel is applied at the desired node on the discretized string and the difference is calculated from adjacent nodes with appropriate coefficients from the difference operators. This is essentially a shorthand notation of equations 3.5 and 3.6 that will be useful once the 2D operators are introduced.

With clamped BC's, $w(0,t) = 0$ and $w_x(0,t) = 0$ we can apply this difference operator concept to solve for a virtual grid point [13] that is required when applying equations 3.5 and 3.6 at $w(0,t)$. This virtual grid point is required because the difference operator will contain a term for a non-existent grid point at $w(-1,t)$ that is not included in the model, but is required for the difference calculation. An example of this virtual grid point technique for $\mathbf{D}_{xx}$ is derived from the basic boundary condition definition, $w_x(0,t)$ and the definition of a centred difference as:

$$\begin{aligned} &\delta_x . w(0,t) = 0 \\ &\frac{1}{2h}(w(1,t) - w(-1,t)) = 0 \\ &w(1,t) = w(-1,t) \end{aligned} \tag{3.19}$$

which can then be substituted into $\mathbf{D}_{xx}$:

$$\mathbf{D}_{xx}|_{x=0} = \frac{1}{h_x^2}(-2w(0,t) + 2w(1,t)) \tag{3.20}$$

giving the appropriate difference matrix coefficients for the end point of the string calculation.

A similar method can then be used to solve the virtual grid points for $\mathbf{D}_{xxxx}$ and the boundary conditions of the string can be fully established. The next aspect of the string model that needs to be defined is the initial condition. Instead of introducing a complex excitation model the initial condition of the string was instead set at an initial displacement with zero initial velocity. Several different initial positions were tried with the goal of reproducing the sound of a guitar pluck. A 1D cubic spline function was eventually chosen for use in the model, referred to as 'Spline Pluck', and is illustrated alongside the ideal definition of an ideal plucked initial condition below where the string is given an initial position that goes directly from the boundary to the pluck point with a sharp discontinuity at the excitation point. The initial conditions of the string are as follows:

$$w(x,0) = s_{fit}(\mathrm{IP}(x)) \tag{3.21}$$

$$w_t(x,0) = 0 \tag{3.22}$$

where x is the position along the string and $s_{fit}(x)$ is a cubic spline fit to the ideal pluck $\mathrm{IP}(x)$ which is a straight line from $\mathrm{IP}(h) = 0$ at $x = h$ to the pluck point $\mathrm{IP}(x_{pp}) = 1$, and back again to the bridge boundary condition $\mathrm{IP}(1) = 0$ at $x = 1$.

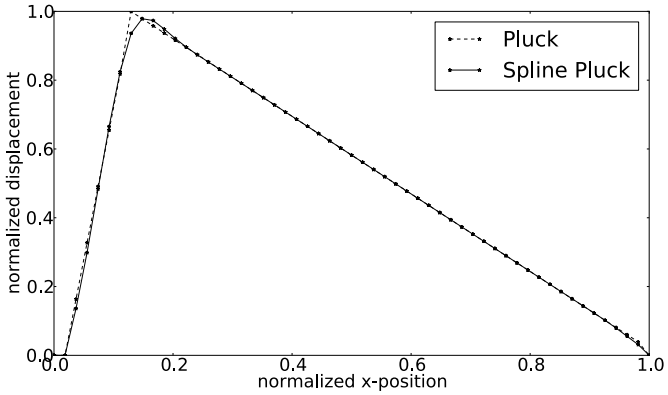

Figure 3.2: Initial position of the string showing the ideal pluck (Pluck) and the smoothed spline pluck (Spline Pluck).

The 'Spline Pluck' was chosen as it did not introduce unrealistic high frequency energy that was a result of the sharp discontinuity in the basic 'Pluck' at the pluck point. By smoothing over the pluck point a more realistic sound was created. The basic definition of the string PDE also precludes the ideal pluck as bending stiffness in the string would not allow a sharp discontinuity in the string as seen above in the ideal case.

In terms of model stability a von Neumann energy analysis method is used. The characteristic equation for the string then becomes:

$$h^4 - \gamma^2 k^2 h^2 - 4\kappa^2 k^2 \geq 0 \tag{3.23}$$

The time step (k), wave speed (γ), and stiffness parameter (κ) are all set to desired values, so the only free variable is the grid spacing (h). Rearranging equation 3.23 in terms of a minimum h value that ensures stability we get:

$$h \geq h_{min} = \sqrt{\frac{\gamma^2 k^2 + \sqrt{\gamma^4 k^4 + 16\kappa^2 k^2}}{2}} \tag{3.24}$$

Choosing an h value closer to the stability limit will reduce dispersion and increase the accuracy of the results of the model, but will increase model complexity and the number of calculation nodes by reducing the grid spacing. For simulation purposes the grid spacing used in the string model is set at the stability limit defined by equation 3.24.

Finally, the material properties of the string are input to the model with an attempt made to mimic the properties of steel guitar strings. The string properties required by the model include length, density, and diameter. To do this an appropriate string diameter and length were chosen based on the pitch of the note being simulated. This meant six different string diameters were chosen, representative of the six different strings of the guitar, and ranged from 1.4 mm for the string with the lowest pitch on a guitar, E2 - 82.4 Hz, to 0.3m̈m for the note with the highest pitch, E4 - 329.6 Hz. The density of steel was set at 8000 $\mathrm{kg/m^3}$ as the main goal was to evaluate changes in wood, not changes in sound to due variations in the properties of steel, and the strings were modelled as unwound, solid core strings. With these model parameters set the stiff string model is complete.

3.2.2 Orthotropic Plate

The spatially-scaled Kirchhoff orthotropic plate equation used in the model is then defined, following Bilbao's method [13], as:

$$u_{tt} = -\kappa_x^2 u_{xxxx} - \kappa_y^2 u_{yyyy} - \kappa_{xy}^2 u_{xxyy} - 2\sigma_0 u_t + 2\sigma_1 \Delta u_t + J_p F \tag{3.25}$$

where $u(x, y, t)$ is transverse displacement at time t at point (x, y) on the plate, J_p is a spreading function, F is a force applied by the string, σ_0 and σ_1 are damping constants, and Δ is the spatial gradient, with stiffness parameters:

$$\kappa_x^2 = D_x/\rho H L^4 \tag{3.26}$$
$$\kappa_y^2 = D_y/\rho H L^4 \tag{3.27}$$
$$\kappa_{xy}^2 = D_{xy}/\rho H L^4 \tag{3.28}$$
$$\tag{3.29}$$

and stiffness constants:

$$D_x = \frac{E_x H^3}{12(1 - \upsilon_{xy}\upsilon_{yx})} \tag{3.30}$$

$$D_y = \frac{E_y H^3}{12(1 - \upsilon_{xy}\upsilon_{yx})} \tag{3.31}$$

$$D_{xy} = \upsilon_{yx} D_x + \upsilon_{xy} D_y + \frac{G_{xy} H^3}{3} \tag{3.32}$$

where E_x and E_y are Young's modulus values in the respective coordinate directions, G_{xy} is the shear modulus, υ_{xy} and υ_{yx} are Poisson's ratios, H is the plate thickness, ρ is density, and $L = \sqrt{L_x L_y}$. The finite difference scheme can then be expressed as:

$$\delta_{tt} u = -\kappa_x^2 \delta_{xxxx} u - \kappa_y^2 \delta_{yyyy} u - \kappa_{xy}^2 \delta_{xxyy} u - 2\sigma_0 \delta t \cdot u + 2\sigma_1 (\delta_{xx} + \delta_{yy}) \delta_{t\cdot} u + J_p F \tag{3.33}$$

where the difference operators are defined as:

$$\delta_{xx} u_{l,m}^n = \frac{1}{h_x^2}(u_{l+1,m}^n - 2u_{l,m}^n + u_{l-1,m}^n) \tag{3.34}$$

$$\delta_{yy} u_{l,m}^n = \frac{1}{h_y^2}(u_{l,m+1}^n - 2u_{l,m}^n + u_{l,m-1}^n) \tag{3.35}$$

$$\begin{aligned} \delta_{xxyy} u_{l,m}^n = \frac{1}{h_x^2 h_y^2}(&u_{l+1,m+1}^n - 2u_{l,m+1}^n + u_{l-1,m+1}^n \\ &- 2u_{l+1,m}^n + 4u_{l,m}^n - 2u_{l-1,m}^n \\ &+ u_{l+1,m-1}^n - 2u_{l,m-1}^n + u_{l-1,m-1}^n) \end{aligned} \tag{3.36}$$

$$\delta_{xxxx} u_{l,m}^n = \frac{1}{h_x^4}(u_{l+2,m}^n - 4u_{l+1,m}^n + 6u_{l,m}^n - 4u_{l-1,m}^n + u_{l-2,m}^n) \tag{3.37}$$

$$\delta_{yyyy} u_{l,m}^n = \frac{1}{h_y^4}(u_{l,m+2}^n - 4u_{l,m+1}^n + 6u_{l,m}^n - 4u_{l,m-1}^n + u_{l,m-2}^n) \tag{3.38}$$

$$\delta_{t\cdot} u_{l,m}^n = \frac{1}{2k}(u_{l,m}^{n+1} - u_{l,m}^{n-1}) \tag{3.39}$$

$$\delta_{tt} u_{l,m}^n = \frac{1}{k^2}(u_{l,m}^{n+1} - 2u_{l,m}^n + u_{l,m}^{n-1}) \tag{3.40}$$

where subscripts on u denote spatial location and superscripts indicate the discrete time, h_x and h_y are the grid spacings in the x and y directions respectively, and k is the time step. It should be noted that the coordinate system for the plate is different than the co-ordinate system of the string. The operator $\delta_{t\cdot}$ is the centered time difference, which again leads to an implicit formulation of the problem. To provide a more computationally efficient solution method the 2D nodes of the plate

model are vectorized and in a similar manner to the string equation, the plate equation 3.33 can be rearranged in term of time steps and written in matrix form as:

$$\mathbf{A}\mathbf{u}^{n+1} + \mathbf{B}\mathbf{u}^{n} + \mathbf{C}\mathbf{u}^{n-1} - J_p F = 0 \tag{3.41}$$

with

$$\mathbf{A} = 1 + \sigma_0 k\mathbf{I} - \sigma_1 k(\mathbf{D}_{xx} + \mathbf{D}_{yy}) \tag{3.42}$$
$$\mathbf{B} = -2\mathbf{I} + k^2\kappa_x^2\mathbf{D}_{xxxx}k^2\kappa_y^2\mathbf{D}_{yyyy}k^2\kappa_{xy}^2\mathbf{D}_{xxyy} \tag{3.43}$$
$$\mathbf{C} = 1 - \sigma_0 k\mathbf{I} + \sigma_1 k(\mathbf{D}_{xx} + \mathbf{D}_{yy}) \tag{3.44}$$

where $\mathbf{D}_{xx}$, $\mathbf{D}_{yy}$, $\mathbf{D}_{xxyy}$, $\mathbf{D}_{xxxx}$, and $\mathbf{D}_{yyyy}$ are sparse matrix representations of the spatial difference operators and $\mathbf{I}$ is the identity matrix. The solution for the next time step at all locations, $\mathbf{u}^{n+1}$, can then be solved using a sparse matrix solver for the equation:

$$\mathbf{u}^{n+1} = -\mathbf{A}^{-1}(\mathbf{B}\mathbf{u}^{n} + \mathbf{C}\mathbf{u}^{n-1} - J_p F) \tag{3.45}$$

The boundary conditions for the plate are then set in a similar manner to the string, by modifying the matrix forms of the difference operators using the virtual grid point concept. The plate is modelled with clamped boundary conditions on all edges, that is:

$$u(x, 0, t) = u(x, 1, t) = u(0, y, t) = u(1, y, t) = 0 \tag{3.46}$$
$$u_x(0, y, t) = u_x(1, y, t) = u_y(x, 0, t) = u_y(x, 1, t) = 0 \tag{3.47}$$

In terms of the kernel of the matrix form of the difference operator $\mathbf{D}_{xxyy}$ this looks like:

$$\mathbf{D}_{xxyy} = \frac{1}{h_x^2 h_y^2} \begin{array}{|c|c|c|} \hline 1 & -2 & 1 \\ \hline -2 & 4 & -2 \\ \hline 1 & -2 & 1 \\ \hline \end{array} \tag{3.48}$$

corresponding to equation 3.36 where the center of the kernel is applied at the desired location on the plate and the difference is calculated from adjacent nodes with the appropriate coefficients from the kernel. Applying the virtual grid point method described above the difference operator for corner, edge, and interior nodes

will then become:

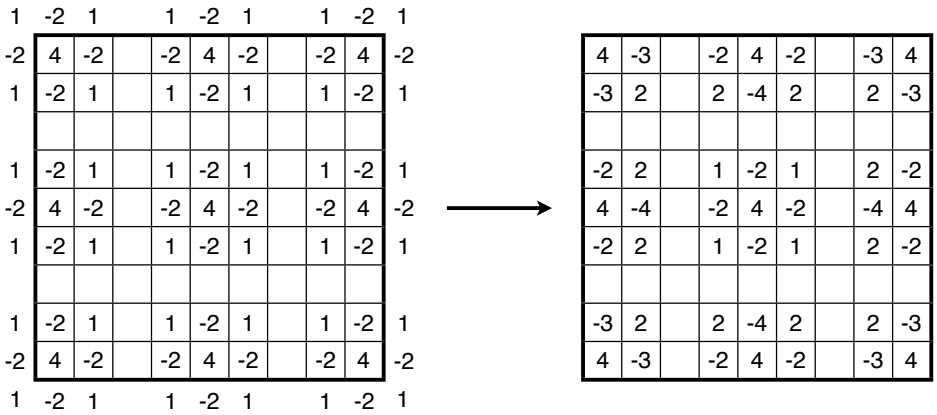

(3.49)

A similar approach can be applied to the other difference operators to derive appropriate boundary conditions using the virtual grid point concept.

The stability criterion is again found using the von Neumann energy analysis method in terms of the grid spacing in the x direction, h_x:

$$h_x \geq (4k^2(\kappa_x^2 + \kappa_y^2/r^4 + \kappa_{xy}^2/r^2))^{1/4} \tag{3.50}$$

where r relates the ratio of the grid spacings h_x and h_y:

$$r = h_y/h_x \tag{3.51}$$

By choosing the value of r carefully the effect of stiffness can be made symmetric in the two coordinate directions. For materials like wood that are strongly anisotropic this will increase the accuracy of the results with r set as:

$$r = \sqrt{\frac{\kappa_x}{\kappa_y}} \tag{3.52}$$

Initial conditions for the plate are simply defined as zero displacement and zero velocity at all grid points:

$$u(x, y, 0) = 0 \tag{3.53}$$

$$u_t(x, y, 0) = 0 \tag{3.54}$$

3.2.3 Plate Geometry and Material Properties

The plate simulation aimed to reproduce the performance of a guitar so the dimensions were chosen to be similar to the soundboard size of the guitar used in the 3AFC testing of chapter 2. A rectangular plate was modelled with a thickness of 3 mm, a length of 50 cm in the x-direction (longitudinal), and a width of 35.5 cm in the y-direction (radial).

To determine the material properties used as inputs to the model a study by Pérez et. al. [4] was used. In this work experimentally derived values for the material properties of a thin quarter sawn plate of Norway Spruce at various MC levels were established using a combination of modal and FEM analysis. The results of their experiments can be seen in figure 3.3.

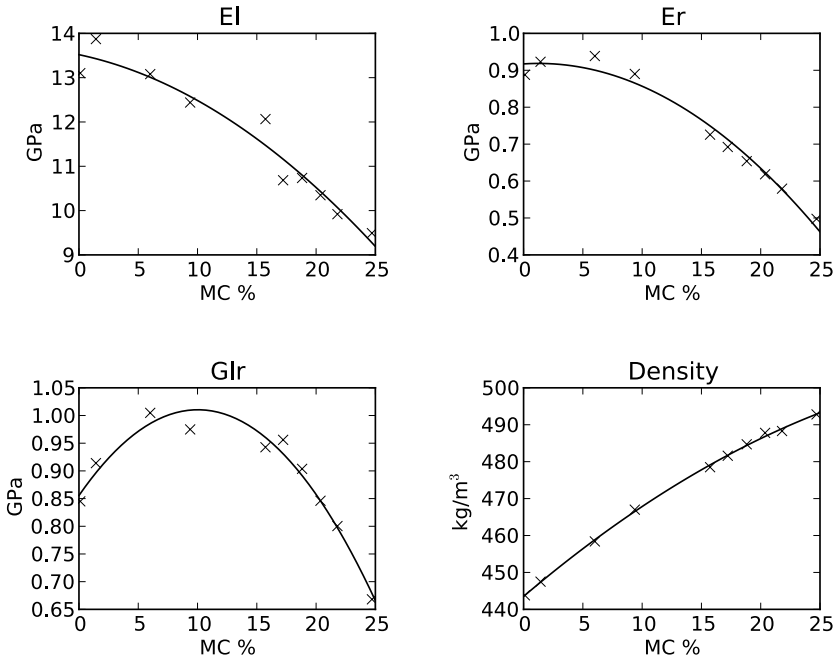

Figure 3.3: Polynomial fit and experimentally determined material properties as a function of moisture content replotted from Pérez et. al. for Picea Abies (Norway Spruce) [4].

Young's modulus in the longitudinal grain direction and in the radial grain direction show a general decreasing trend with increasing MC. Shear modulus exhibits more of a parabolic shape, with a maximum value at approximately 9% MC and density of the plate follows the expected behaviour of increasing density with increased MC. The data from these experimental results provides the basis for the parameters of the model. Data points are provided by Pérez et. al and a polynomial fit was calculated for the material properties seen in figure 3.3. Input values for material properties are then calculated from these polynomial fits for the specific MC value being simulated.

3.2.4 Sound Field

To calculate sound pressure at a point in the sound field, $L(x, y, z, t)$, the Rayleigh integral is then applied to the transverse plate acceleration, $u_{tt}(t)$, of the plate as:

$$p(x, y, z, t) = \rho_0 \int_S u_{tt} \frac{(x_p, y_p, t - R/c_0)}{2\pi R} dS \tag{3.55}$$

where:

$$R = \sqrt{(x - x_p)^2 + (y - y_p)^2 + z^2} \tag{3.56}$$

and x, y, and z are coordinates in the sound field, x_p and y_p are coordinates on the plate, ρ_0 is the density of the acoustic medium, c_0 is the speed of sound in the acoustic medium [49], and S is the surface of the vibrating plate. This is obviously not the most complex way to model the sound field, as it simulates a free field without reverberations, but for the purpose of this study that kind of detail is considered unnecessary for the analysis being conducted. The point of the model is to see if differences in the MC of the wood plate being modelled are perceptible and adding in more complex acoustical modelling would not help towards this goal. Chaigne et al. [15] followed a similar method when developing their thin plate models to reduce unnecessary computational costs associated with fully modelling the sound field when creating simulated sounds.

3.2.5 Simulated Sounds

The result of calculating the Rayleigh integral is a pressure vector used to create the simulated audio files for subsequent psychoacoustical testing. An example waveform for a real Norway spruce plate and guitar string replicating the geometry and dimensions of the model is provided in figure 3.4 along with a simulated sound for note E2. A similar comparison can also be made in the frequency domain as seen in figure 3.5.

In direct comparison the overall waveform and FFT shapes are seen to be similar between the simulated and real sounds. Probably the most important point of comparison is the decay rate, which is similar in the simulation and real recording. It should be noted that the purpose of the simulation is to produce 'guitar-like' sounds, not exactly duplicate the performance of any particular guitar or recording. One major exclusion from the model is air resonance modes, that contribute significantly to the sound of a guitar. The purpose of this study is to examine material property changes as a function of MC, not air properties, and was considered acceptable. As a first pass the model provides an acceptable level of performance in approximating the sound of a real guitar string and wooden plate, but the more important aspect of model validation will be conducted in the next section: showing that changes in MC are perceived in similar ways for the real and simulated sounds.

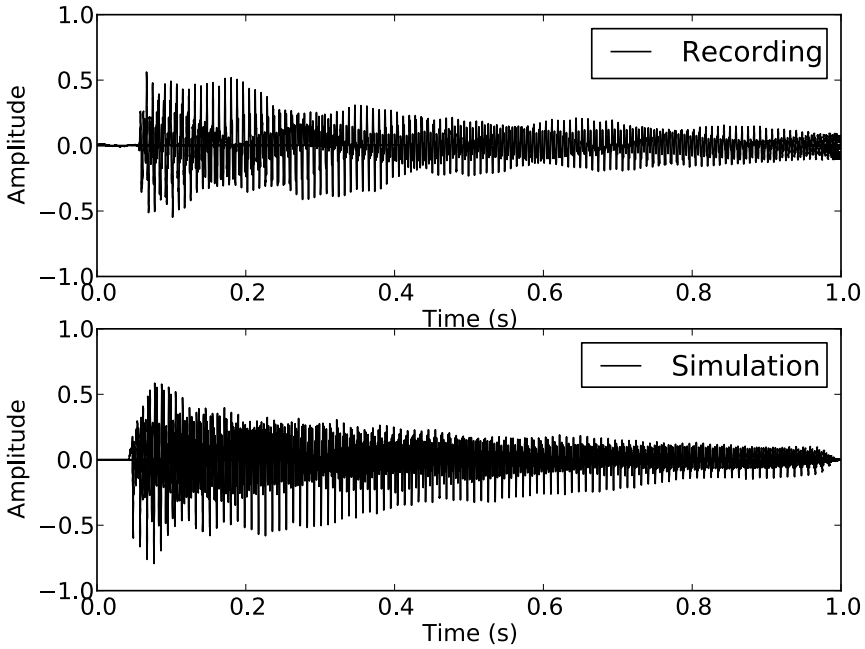

Figure 3.4: Waveforms of a recording of note E2 for a real Norway spruce plate and guitar string of the same dimension as the modelled string-plate system; and a simulated sound from the orthotropic plate and stiff string model.

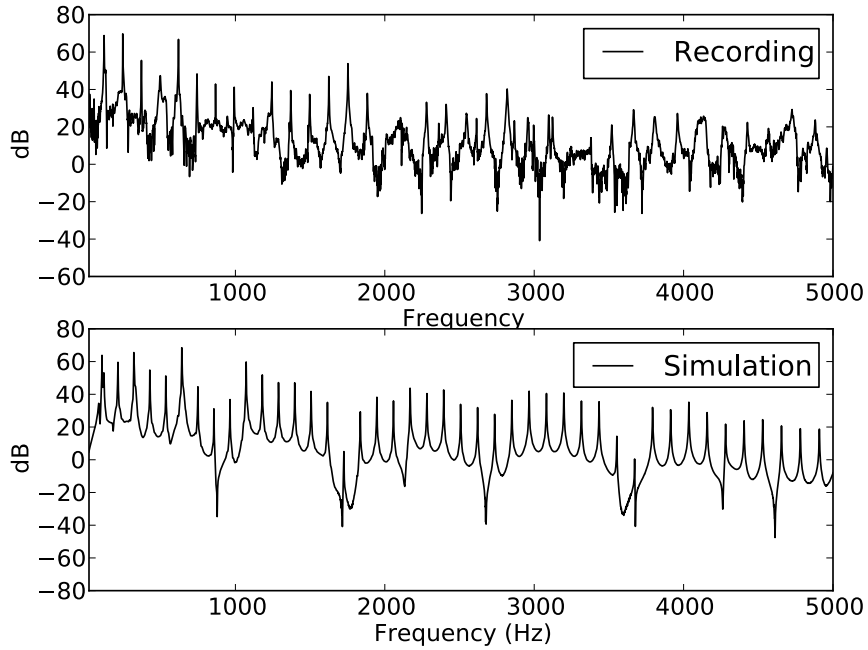

Figure 3.5: FFT of a recording of note E2 for a real Norway spruce plate and guitar string of the same dimension as the modelled string-plate system; and a simulated sound from the orthotropic plate and stiff string model.

3.3 Psychoacoustical Testing of Simulated Sounds

Two different listening test approaches are used to achieve two goals: to validate the behaviour of the wood-plate model; and then to use the model to establish a just-noticeable difference (JND) level indicating the limit of perceptibility of a change in moisture content by a listener.

3.3.1 Model Validation

Experimental protocols for the 3AFC testing used to validate the model were identical to those of the previous chapter. In total there were 54 possible combinations of notes E2, A2, D3, G3, B3, and E4, at MC levels of, 7%, 9%, and 11% that were repeated twice for a total of 108 comparisons per subject. Test subjects were selected from a university population and varied in age from 17 to 22 years old. In total 21 subjects completed the 3AFC test, with one subject being excluded because they did not follow the provided instructions while completing the test. Subjects had the right to withdraw without penalty and were remunerated with course credit for their participation.

The main purpose of the 3AFC experimental component of the experiment is to verify the performance of the model against previous results obtained from testing a guitar under various humidity conditions. Figures 3.6 and 3.8 provide the experimental results from the guitar testing and provide a comparison point for the results presented in figures 3.7 and 3.9 for the simulated sounds tested in the current study.

Figure 3.6 provides a histogram showing an average hit rate of 0.73 with a standard deviation of 0.1 and a distribution that is approximately normal for all tests of the real recordings of guitar sounds under different humidity conditions. These results compare favourably to the results of figure 3.7 where a similar experimental protocol was followed, only with simulated sounds instead of real sounds.

For the simulated sounds a mean hit rate of 0.76 was observed, with a standard deviation of 0.1 and a distribution that, again, is approximately normal. As these values are for overall comparisons a further breakdown can be made by comparison type for both the real and simulated sounds. The three comparisons used in the 3AFC testing were 7-9% MC, 9-11%MC, and 7-11%MC and box plots for the observed performance of the test subjects are provided in figures 3.8 and 3.9.

In the testing of the real sounds no statistically significant difference was observed between the 7-9%MC and 9-11%MC tests (both tests with a 2% MC difference), but the 7-11% (a 4% MC difference) was found to be significantly different, with a higher correct identification rate, than both the 7-9%MC and 9-11%MC tests using a t-test method of comparison. In a similar manner to the results in chapter 2 an adjusted p-value of 0.01 will be the criteria for statistical significance using the Bonferonni adjustment.

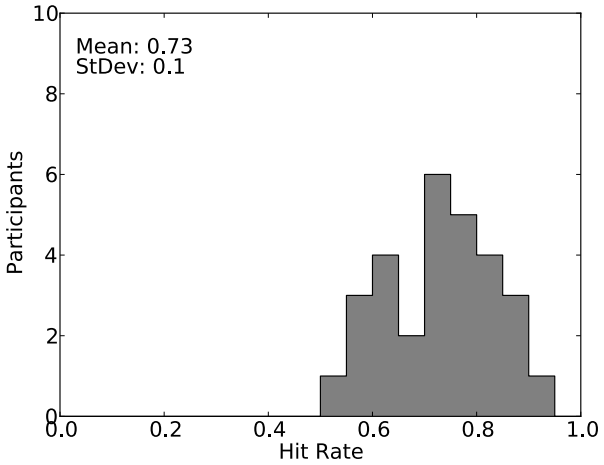

Figure 3.6: Histogram of the average hit rate for all participants for plucked guitar sounds from chapter 2 using a real instrument to create sample recordings. A mean hit rate of 0.73 indicates that on average participants correctly responded 73% of the time with a standard deviation of 0.1.

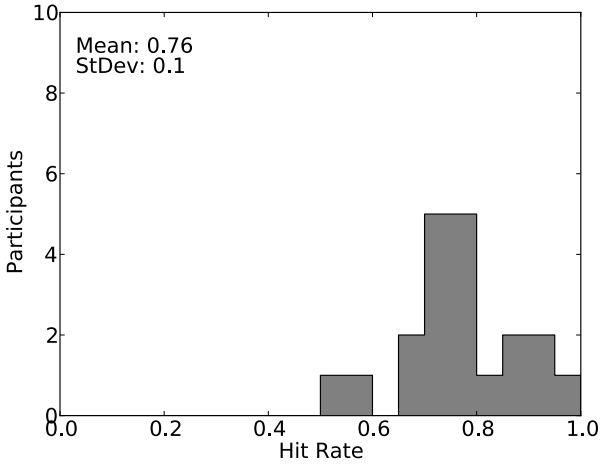

Figure 3.7: Histogram of the average hit rate for all participants for all types of simulated sounds created from the model described above. A mean hit rate of 0.76 indicates that on average participants correctly responded 76% of the time with a standard deviation of 0.1.

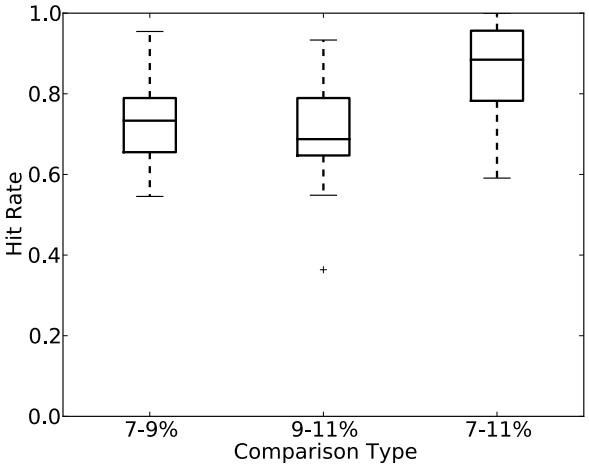

Figure 3.8: Box plot of the three test combinations, 7-9%, 9-11%, and 7-11%, for plucked guitar sounds from chapter 2 using a real instrument with whiskers indicating maximum and minimum values, a box outlining quartiles, a line indicating mean value, and a cross indicating any outliers.

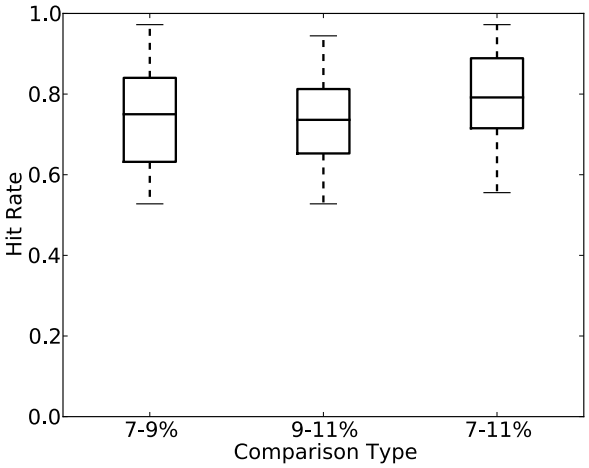

Figure 3.9: Box plot of the three test combinations, 7-9%, 9-11%, and 7-11%, for simulated sounds created from the model described above with whiskers indicating maximum and minimum values, a box outlining quartiles, a line indicating mean value, and a cross indicating any outliers.

The performance of the test subjects with simulated sounds shows a similar behaviour, with no statistically significant difference between the 7-9%MC and 9-11%MC tests (both tests with a 2% MC difference). The 7-11%, however, was not found to be significantly different, but had a higher correct identification rate than both the 7-9%MC and 9-11%MC tests using a t-test method of comparison.

The favourable comparisons observed between the performance of test subjects' response to both the real and simulated sounds and the general similarity of the waveforms and FFT allows the model to be considered to be accurately reproducing the behaviour of a real orthotropic thin plate, at least with regards to the perceptibility of tonal differences due to changes in MC. With the model verified the establishment of JND MC levels can proceed.

3.3.2 Just-Noticeable Difference

An adaptive 3AFC approach was used to establish a just-noticeable difference (JND) level for change in MC. This method was used to reduce the number of samples that would be required to determine JND level using a non-adaptive comparison method, something that helps to eliminate the issue of subject fatigue. This JND level indicates the perceptible limit of differences in MC in the wood-plate model. The adaptive 3AFC approach was chosen as it has been used previously for sound discrimination tasks[21] and is easily extended from the previous tests. An initial 4% MC difference was presented (i.e. a 7-11% MC comparison) for the first 3AFC test sample and a correct response reduced the difference in MC presented in the subsequent test sample. An incorrect identification in the 3AFC test sample caused an increase in the MC difference of the subsequent 3AFC test sample. Ultimately, the goal of this testing method is to approach a limit at which subjects are randomly guessing, corresponding to an average hit rate of 0.33. When randomly guessing the subject should get 2 incorrect responses for every correct response, thus the adjustments need to be set to ensure the overall effect of the adjustments is equal to multiplying by 1 at this point. The previous MC difference was multiplied by 0.8 after a correct response to get the new MC difference for a subsequent test. Misses caused a similar adjustment, but this time the MC difference of the subsequent test was increased by $\sqrt{1/0.8} = 1.118$. Subjects were then allowed to respond until they reach the random guessing phase and were stopped after approximately 10 responses without significant overall increase or decrease in the MC difference between the test samples. Sound samples were synthesized to allow as small a difference as 0.1 MC% (i.e. 7.0 and 7.1 MC% could be tested).

Notes E2, E3, and E4 were examined using this method to allow a comparison across pitch and samples were presented in random order (i.e. one of b-a-a, a-b-a, or a-a-b). This reduced set of notes was chosen to allow a similar of pitches to be examined, while reducing the overall length of testing required as the adaptive 3AFC task needed to be repeated for each note. The subject was instructed to indicate which sample they believe to be different with adjustments made to MC

in the samples of subsequent tests. Subjects could listen to the sound samples as many times as they wanted and there was no time limit for the test. A Python script and computer interface was used to present the data and Sennheiser HD 280 Pro headphones [42] were used for playback with an M-Audio soundcard [43] while subjects were seated in an Industrial Acoustics Company sound isolation chamber [44]. A new set of test subjects were selected from a university population and varied in age from 17 to 23 years old. In total 20 subjects completed the 3AFC test, with no exclusions. Subjects in the JND testing were different from those that completed the 3AFC testing used to verify the performance of the model and subjects had the right to withdraw without penalty and were remunerated with course credit for their participation. Results for note E2 are presented in figure 3.10.

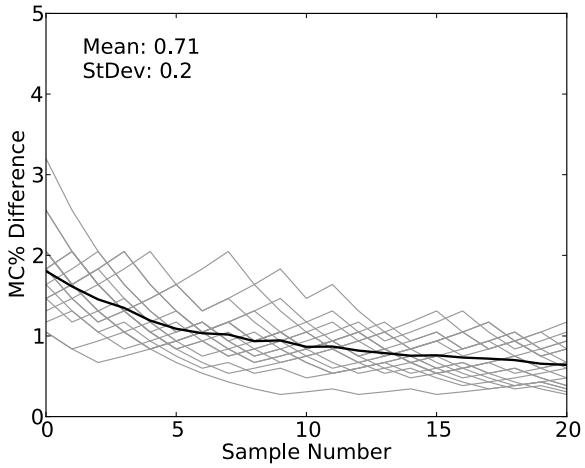

Figure 3.10: Averaged behaviour of subjects on their last 20 responses in the JND test for note E2 (82.4 Hz). Mean value of 0.71% MC difference and standard deviation of 0.2 on the final response. The solid black line is the average response and the grey lines are the individual responses of the test subjects.

The final average value that the subjects reached for note E2 was a 0.71 MC% difference, that is, subjects began guessing when they compared sounds simulated with 7.0% MC and 7.71% MC. This change in MC is roughly equivalent to a change in relative humidity of 10%, which in the context of typical changes in RH due to weather patterns is quite small. As an example the RH measured in Waterloo, Ontario, Canada on August 20th, 2013, varied from a high of 99% at 07:00 to a low of 48% at 16:00 [50]. Indoor variations in RH would be smaller than outdoor variations, but the effect of MC on wood in musical instruments can clearly be an issue not just from season to season, but even within a shorter time period if weather patterns are changing rapidly. the guitar studied in this experiment was reaching equilibrium after 30% MC differences in approximately 24 hours. Subject data for notes E3 and E4 showing a similar response to that of note E2 are provided

in figures 3.11 and 3.12.

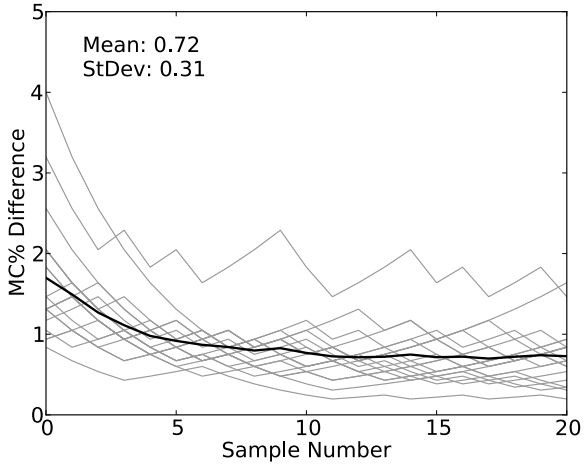

Figure 3.11: Averaged behaviour of subjects on their last 20 responses in the JND test for note E3 (164.8 Hz). Mean value of 0.72% MC difference and standard deviation of 0.31 on the final response. The solid black line is the average response and the grey lines are the individual responses of the test subjects.

The final averaged response value for note E3 is observed to be 0.72% MC and for note E4 is observed to be 0.70%MC. All three tests exhibit approximately normal distributions and subjects converged upon a final value after approximately 25-30 individual comparisons. Box plots for the responses of all three notes can be seen in figure 3.13 to illustrate the comparison between the three notes and the effect of pitch on the results. One hypothesis in the context of previous results in chapter 2, is that notes with higher pitch should have a smaller JND level because they were more easily distinguished in 3AFC testing of the real guitar sounds. This behaviour, however, was not observed in the JND testing as no statistically significant difference between the responses for the three different notes was found.

One anecdotal observation of interest was that several subjects described the simulated sounds as 'guitar' sounds, but in the participant induction process no label was given describing the sounds as simulating a guitar, just that they were musical instrument sounds.

Another important factor to keep in mind is the relatively young age of the test subject pool. It is likely that these results would not generalize to more elderly subjects who are known to typically suffer from hearing loss with age[51]. Further testing with a more diverse testing pool would be required to explore the perceptual effects of MC in these kinds of groups.

An interesting way to view these overall results is to use them as a design criterion. If a 0.7% change in MC is considered to be imperceptible then the variation in the mechanical properties established by Pérez et. al. [4] associated

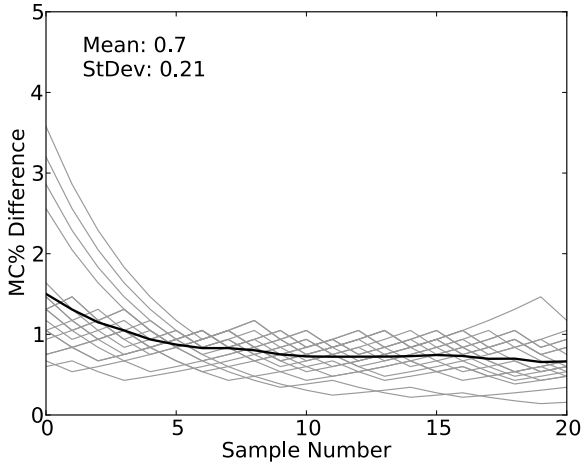

Figure 3.12: Averaged behaviour of subjects on their last 20 responses in the JND test for note E4 (329.6 Hz). Mean value of 0.70% MC difference and standard deviation of 0.21 on the final response. The solid black line is the average response and the grey lines are the individual responses of the test subjects.

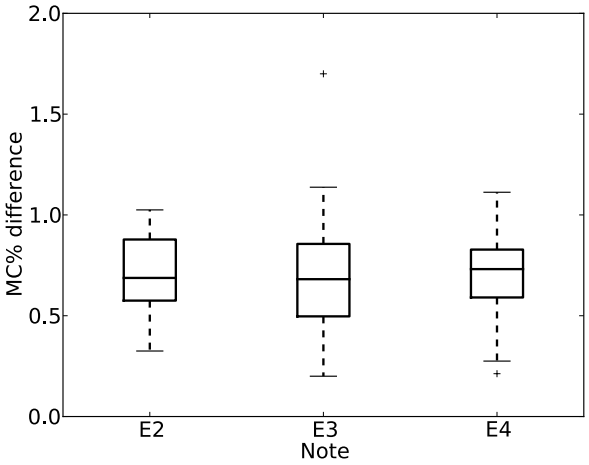

Figure 3.13: Box plots of subjects' final value of MC% for notes E2, E3, and E4 with whiskers indicating maximum and minimum values, a box outlining quartiles, a line indicating mean value, and a cross indicating any outliers.

Table 3.1: Moduli and Density at 9%MC and 9.7%MC

Parameter	9%MC	9.7%MC	Units	% Change
E_l	12.63	12.53	GPa	-0.8%
E_r	0.87	0.86	GPa	-1.1%
G_{lr}	1.008	1.010	GPa	+0.1%
ρ	465.7	467.2	kg/m^3	+0.3%

with this change in MC can also be considered to be imperceptible. Considering an example case of a plate at 9% MC and 9.7% MC one can calculate values for various moduli and density that can be seen in table 3.1.

With a 0.7% change in MC it can be seen that the variation in material properties is really quite small, about 1% or less. Materials used to replace wood in musical instruments could vary within these limits and need not be completely anhygroscopic. Given that to be considered imperceptibly stable a new material would have to vary less than 1% in these properties across all moisture conditions, not just from 9%-9.7% MC, the material would need to be very nearly anhygroscopic. This of course is assuming that the goal of the wood replacement is perfect stability, but a compromise is likely required given the challenges of retaining a traditional 'wood' sound and aesthetic while achieving this kind of stability. The question of replacement materials for wood will be discussed further in chapter 6.

It should also be noted that the natural variability within an individual species of wood is significantly larger than the values listed in table 3.1. Hoadley reports that for most species the strongest piece will be twice as strong as the weakest due to differences in growth rate and density [3], which implies that the natural variation of the wood used in musical instruments is likely to be highly perceptible.

3.4 Conclusions

An orthotropic thin plate model was combined with a stiff string model and experimentally determined material properties, as a function of MC, to produce a simulation capable of accurately producing sound samples at any desired MC level. The basic behaviour of the modelled system was verified by a psychoacoustical listening test that compared well with the results of listening tests, conducted in chapter 2, of a guitar acclimatized under different moisture conditions.

JND levels were then established for MC differences in a simulated plate replicating the dimensions of a typical guitar soundboard. It can be concluded that even small variations in RH can be perceived as changes in tone in a musical instrument as the JND level was established to be approximately a 0.7% MC difference. Any material used to replace traditional soundboard woods, like sitka spruce, would

need to have less variability with relative humidity than the equivalent material property changes for this 0.7% MC difference. Two main approaches are possible: using stabilized wood products like acetylated wood, or finding alternative materials that are anhygroscopic like carbon fiber. It is clear, however, that the goal of this replacement must be well-defined; to either accurately replicate the sound of the existing wood instrument or to provide a stable instrument with timbral characteristics unique from the original using new materials with different vibrational properties.

Chapter 4

Wavelets and Psychoacoustical Signal Parameters

4.1 Introduction

Traditionally the development of psychoacoustics has been highly dependent on the use of a Fourier domain representation of audio signals to relate the frequency content of a sound to the way we perceive that sound. One of the issues that the Fourier transform struggles with is the representation of short, impactive components of sounds because it works under the assumption that the sound signal is purely periodic in nature, which in many cases it is not. Wavelet analysis is a powerful alternative to traditional Fourier analysis that can be used to address this problem of representing short, aperiodic events more accurately. The application of wavelet methods to psychoacoustical signal analysis is shown in this study to provide a new perspective to the field of psychoacoustics.

The motivation for this work comes from the need to analyze musical instrument sounds for their psychoacoustical properties in order to quantify timbral differences. For example, the perceptibility of small changes in physical design properties that affect their output sound can be evaluated. These small differences are often hard to quantify using standard methods, especially with the complex nature of musical instrument sounds that have many partials, inharmonicity, and longitudinal string vibrations. Another aspect that complicates the analysis is that pianos and guitars (among many others) exhibit attack transients that have been shown to be important in classification studies [52], but are poorly represented using Fourier methods. Developing perceptual models of musical instrument tone requires signal processing techniques that can accurately represent these transient components of the sound. This provides an interesting avenue for the application of wavelets in psychoacoustics.

Historically the application of wavelets in signal analysis tasks has yielded positive results in various fields. Farge's application in fluid dynamic analysis [53],

Daubechies in image processing [54], and a number of researchers in seismology [55, 56], have added significantly to their fields. A benefit of wavelet analysis is that its use of finite length wavelets instead of periodic sinusoids as the decomposing signal allows finite length transient signals to be more accurately represented than when using the FFT. It is also able to have increases in time and frequency resolution simultaneously, whereas Fourier methods suffer from an inverse relationship in this regard.

An overview by Peeters [7] provides a large set of established psychoacoustical signal parameters in the temporal and Fourier domain that includes spectral centroid, effective duration, and spectral slope, among many others. These parameters have been used by researchers to provide quantitative descriptions of sounds and in the comparison of these sounds in subsequent analyses. Using these signal processing techniques allows percussive sounds to be distinguished from sustained sounds, the rating of the brightness of a sound, or the assessment of the noisiness of a sound. By modifying conventional psychoacoustical signal parameters to incorporate the wavelet transform a better representation of sounds that include short impactive components is possible and a comparison will be made in this chapter to show the difference between the Fourier and wavelet methods with regards to these parameters.

4.2 Background

Psychoacoustics is a broad and diverse field that studies the perception of sound. One of the primary signal processing tasks in psychoacoustics is to extract parameters from a sound signal to be incorporated into a perceptual model. A classic example of one of these kinds of signal parameters is spectral centroid, or the centre of mass of the frequency spectrum of a time signal. An increase in perceived brightness has been related to an increase in spectral centroid of a particular set of similar sounds [35, 57] and provides a basic model for this perception of brightness.

Psychoacoustical parameters of sound signals are generally divided into four fundamental types: *temporal shape*, *temporal features*, *energy features*, and *spectral shape* features [7]. *Temporal shape* parameters quantify the envelope of the time signal and extract features like attack time, effective duration, and temporal increase/decrease. *Temporal features* are parameters that are not related to the shape of the time signal, but are still calculated in the time domain. An example is zero-crossing rate which is an indicator of the noisiness of the signal. *Energy features* are calculated in the time or frequency domain and are related to the energy content of a signal, be it in terms of harmonic, noise, or global energy. Finally, *spectral shape features* are signal parameters calculated in the frequency domain, typically from a fast Fourier transform (FFT) of the time domain signal. Spectral centroid, slope, skewness, and kurtosis are all examples of spectral shape features. Higher level signal parameters can in turn be calculated from the fundamental parameters and are labelled as perceptual features. Typically these perceptual features are

based on a model of auditory perception and include parameters such as sharpness and relative loudness [7]. The thing all of these parameters have in common is that they are calculated in either the time or frequency domains, something that will be expanded upon by introducing the wavelet transform and its associated scale and time domains as a basis for the calculation of signal parameters. Some of these features can be seen in figure 4.3.

Wavelet methods have already been successfully incorporated in several aspects of psychoacoustics including speech modelling [58, 59], music classification [24, 60], and audio compression [61, 62]. In all of these research areas the wavelet transform's ability to compactly represent both short, finite length, and periodic signals accurately is harnessed to improve performance. Extending psychoacoustical signal parameters to incorporate wavelets can give researchers a new perspective on their datasets, particularly for sounds with impactive components like those created by percussive instruments.

Many musical instrument sounds are characterized by a short, transient attack that is followed by a sustained tonal component. In percussive instruments, like the piano, the attack component is related to a hammer striking the string which is then left to vibrate and produce the steady tone of the instrument [23]. Other factors like the sound of the key striking the keybed and longitudinal waves in the piano string have also been shown to contribute to the transient sound of the piano. Askenfelt [23] observed a touch precursor of approximately 20-30 ms followed by a key bottom sound that also lasts approximately 20-30 ms; both of these would be difficult to analyze in the Fourier domain with any sort of specific frequency resolution due to their short temporal length and the inverse nature of frequency and time resolution in the discrete Fourier transform. For this reason piano and other instrument sounds that contain a mixture of transient and tonal components may be ideally suited to wavelet analysis[63]. Other instrument sounds like that of the harpsichord or guitar also contain an initial transient component due to the plucking of the string [64, 65] that would be well suited to wavelet methods.

4.3 Wavelet Theory

A brief overview of wavelet theory will be provided here; a thorough treatment of the wavelet transform is provided by Daubechies [54]. A more accessible introduction is provided by Torrence and Compos [22] and the application of the wavelet transform in the analysis of piano sounds is discussed by Wang [63].

The basic concept behind the wavelet transform is to decompose a signal into components of different scale length using a particular 'mother wavelet'. This is similar to the idea of the Fourier transform breaking down a signal into a combination of sinusoidal components, but with the important difference being that the wavelets are chosen to have a finite length (and are thus non-periodic). Two example mother wavelets that are used in this chapter are the Morlet wavelet: [22]

$$\Psi(\eta) = \pi^{-1/4} e^{i\omega_0 \eta} e^{-\eta^2/2} \tag{4.1}$$

and the Paul wavelet: [22]

$$\Psi(\eta) = \frac{2^m i^m m!}{\sqrt{\pi(2m)!}} (1 - i\eta)^{-(m+1)} \tag{4.2}$$

where ω_0 is the frequency of the Morlet Wavelet, m is the order of the Paul wavelet, and η is a non-dimensional time parameter such that $\eta = t/s$, or time per second. Graphical representations for equations 4.1 and 4.2 are found in figure 4.1.

Wavelets come in many different types, with orthogonal wavelets being required for the discrete wavelet transform (DWT), and both orthogonal and non-orthogonal wavelets being acceptable for the continuous wavelet transform (CWT) [22]. By allowing the use of non-orthogonal wavelets the CWT is much less restrictive than the DWT, but this comes at the cost of returning redundant information and added computation time. For the present purposes only the CWT is used, and as such is defined for a discretized signal, x_n, as the convolution of x_n with a scaled and translated version of the mother wavelet, $\Psi_0(\eta)$:

$$\mathrm{W}_n(s) = \sum_{n'=0}^{N-1} x_{n'} \overline{\Psi} \left[\frac{(n' - n)\delta t}{s} \right] \tag{4.3}$$

where s is the wavelet scale, $\overline{\Psi}$ is the complex conjugate of Ψ, and n is the local time index. This convolution is somewhat computationally costly in the time domain, so most implementations perform this operation in the Fourier domain where the CWT can be calculated at all n simultaneously [22].

As mentioned previously, there are two main advantages of the wavelet approach to signal decomposition. Due to the finite length of the decomposing wavelets used a wavelet transform can better approximate short, aperiodic events in a signal. One of the major assumptions of the Fourier transform is that the signal being analyzed is periodic, something that is not true for most musical signals which have an impactive attack portion followed by a decaying steady state section. Secondly, the wavelet transform provides a choice of many different wavelet types that may be better suited to the decomposition of the particular signal being analyzed. The wavelet transform is often used in signal compression where the choice of mother wavelet can be better suited to particular types of data [66] or in image processing where different types of image structure can be revealed with different mother wavelet templates [67].

The main disadvantage of the wavelet transform is that a direct interpretation of each transformed component as a specific frequency is not possible because the

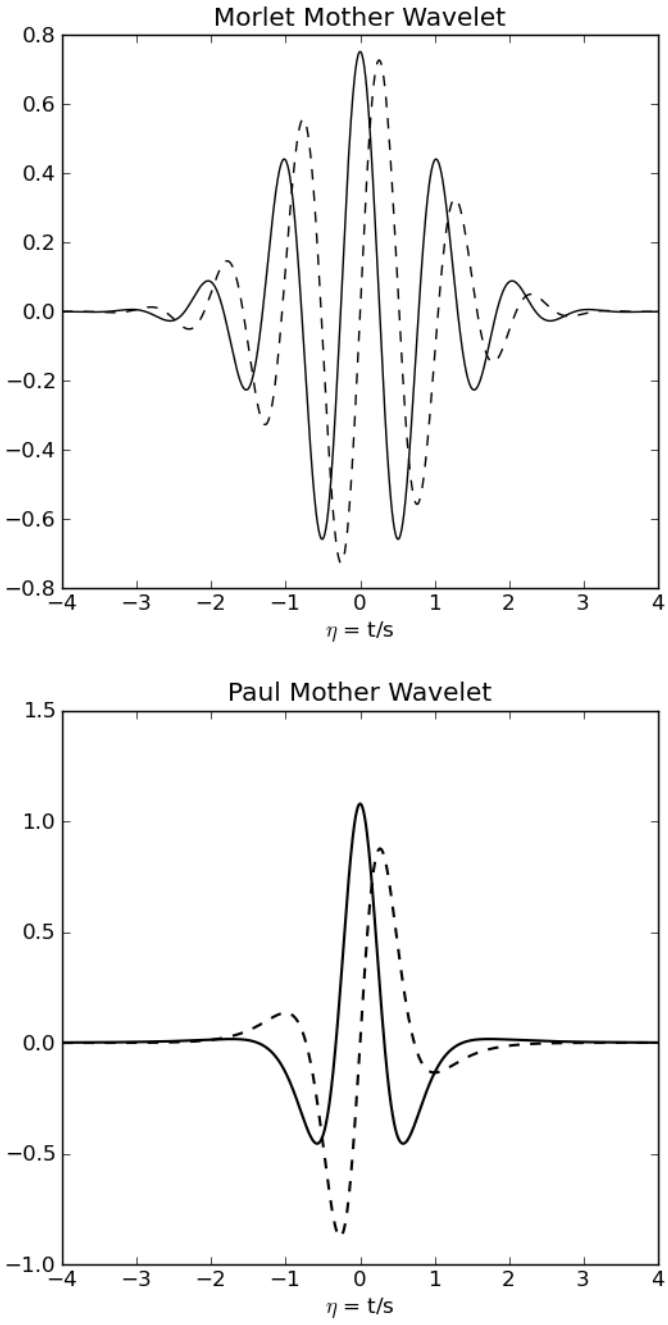

Figure 4.1: Morlet and Paul wavelets showing real (solid lines) and imaginary (dashed lines) parts. The Morlet wavelet is plotted with $\omega_0 = 6$ and the Paul wavelet is of order $m = 4$.

wavelet used in the transform is not a pure sinusoid. Typically when discussing the results of a wavelet transform the scale (or period) of the wavelet is used, but a method for determining an equivalent Fourier frequency is possible [22] and is referred to as the Fourier scale. The other issue that the wavelet method creates is that it turns a 1D time signal into a 2D wavelet domain representation of that signal in the form of a scalogram. The interpretation of such a 2D scalogram signal can be challenging at first, but ultimately provides more potential to represent the fine details of a signal. An example of a scalogram is seen in figure 4.2. Each (t, s) (time and scale axes respectively) coordinate value of the scalogram, σ, is calculated as follows from the wavelet transform data.

$$\sigma(t, s) = \frac{\mathrm{WP} - \min(\mathrm{WP})}{\max(\mathrm{WP}) - \min(\mathrm{WP})} \tag{4.4}$$

$$\mathrm{WP}(t, s) = 20 \log_{10}(|\mathrm{W}(t, s)|) \tag{4.5}$$

where W is the CWT, and WP is *wavelet power*. From equation 4.4 it is clear that the values in a scalogram range between 0 and 1. It should be noted that if a complex wavelet is used in the DWT or CWT, the wavelet transform values will also be complex, and $|\mathrm{W}(t, s)|$ is the complex modulus.

4.4 Conventional Psychoacoustical Parameters

Traditionally psychoacoustical signal parameters have been calculated in the time and Fourier domains, with a focus on frequency content being representative of perceptual effects [7]. There are a large number of possible parameters that could be translated into the wavelet domain, but five common parameters are selected in this chapter for illustrative purposes.

Temporal Centroid

The *temporal centroid* (TC) is defined as the centroid of the energy envelope of the time signal of the sound [7]:

$$\mathrm{TC} = \frac{\sum_{t=0}^{t_w} e(t) \cdot t}{\sum_{t=0}^{t_w} e(t)} \tag{4.6}$$

where $e(t) = (y(t))^2$ is the energy envelope, y is the signal amplitude, and t is the time. The time window, t_w, used in this calculation may be selected as appropriate and in the calculations in this section is set to be t_w =1 s. This signal parameter is typically used to distinguish between percussive and sustained sounds and can be thought to relate to the decay properties of a sound [7].

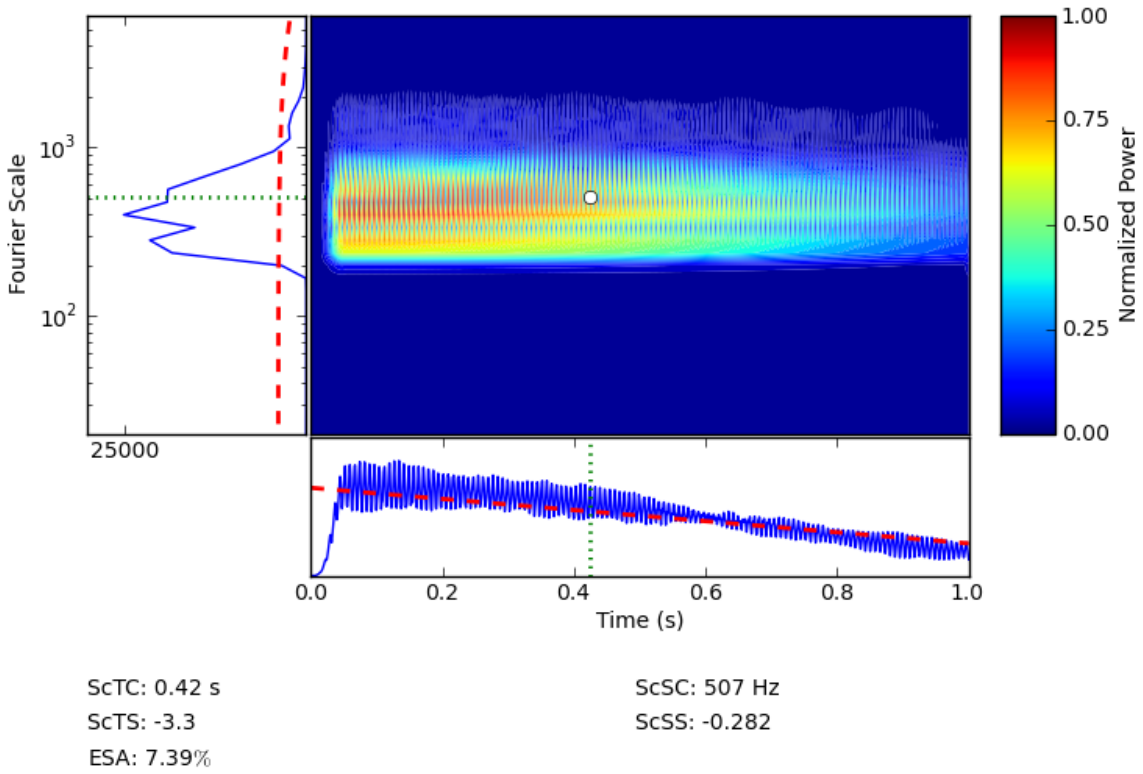

Figure 4.2: Scalogram of the CWT with Morlet wavelet of the unmodified synthesized sample sound. The sample signal consists of a fundamental and 29 partials with inharmonicity intended to synthesize the harmonic structure typically found in piano sounds. Dotted lines represent the location of centroid values and dashed lines indicate slope values.

Spectral Centroid

The *spectral centroid* (SC) is equivalent to the temporal centroid, but instead of calculating the centroid of the time signal, the centroid of the frequency spectrum is used. The spectral centroid has been linked to the perception of brightness, with higher SC values corresponding to brighter sounds [35, 57].

$$\mathrm{SC} = \frac{\sum f(x) \cdot x}{\sum f(x)} \tag{4.7}$$

where x is the frequency bin of the FFT of the time signal and $f(x)$ is the magnitude of the FFT, and the sum is over all relevant x (i.e. for an appropriate frequency band).

Effective Duration

The *effective duration* (ED) of a sound quantifies the amount of the signal that is perceptually prominent. It is useful in differentiating percussive and sustained sounds and is calculated from the portion of the energy envelope, $e(t)$, that exceeds 40% of the maximum energy of the signal [7]. It is essentially the amount of time that the 40% threshold is exceeded:

$$\mathrm{ED} = \sum t \text{ where } e(t) \geq 0.4 \cdot \max(e(t)) \tag{4.8}$$

Spectral Slope

The *spectral slope* (SS) is defined as the slope of frequency spectrum found by a first order least squares linear regression model [1].

Temporal Slope

The *temporal slope* (TS) is defined as the slope of the time domain amplitude found by a first order least squares linear regression model.

[1] The linear regression function 'linregress' in the SciPy software package was used to calculate this value. 'Scientific tools for python', (2012), URL http://www.scipy.org (date last viewed 1/1/13).

4.5 Wavelet Domain Psychoacoustical Parameters

In this section novel reformulations of psychoacoustical parameters described above will be calculated in the wavelet domain.

Scalogram Centroid

In the wavelet domain a scale and time axis are present in a 2D scalogram representation of the signal. Calculating the *scalogram centroid* is similar to combining both the TC and SC parameters from the previous section. The scale and time coordinates of the scalogram centroid would then be related to the SC and TC respectively. The t-coordinate, or time axis centroid is calculated as:

$$\text{ScTC} = \frac{\sum \sigma(t,s) \cdot t}{\sum \sigma(t,s)} \tag{4.9}$$

and the s-coordinate, or scale axis centroid:

$$\text{ScSC} = \frac{\sum \sigma(t,s) \cdot s}{\sum \sigma(t,s)} \tag{4.10}$$

where $\sigma(t,s)$ is the value of the scalogram at coordinates (t,s).

Effective Scalogram Area

The *effective scalogram area* (ESA) is related to the effective duration (ED) defined earlier in the time domain. In this case ESA is defined as the total area of the scalogram that exceeds 40% of maximum scalogram level. In the discrete scalogram each (x,y) value could be considered to be a 'bin', where the actual area is $dx \cdot dy$, but to simplify the calculation each bin is considered to have an area $a = 1$. This also avoids issues of uneven scale divisions that could affect the area calculation when using a logarithmic division of the scale axis. The 'area' value is then normalized by the total area of the scalogram to determine the final ESA value.

$$\text{ESA} = \text{A}/\text{Total Scalogram Area} \tag{4.11}$$

$$\text{A} = \sum a \text{ with } \sigma(t,s) \geq 0.4 \cdot \max(\sigma(t,s)) \tag{4.12}$$

where $\sigma(t,s)$ is the value of the scalogram at coordinates (t,s).

Scalogram Slope

Summing the scalogram across either time or scale creates a time spectrum or scale spectrum, as seen in figure 4.2. A linear regression mode can then be applied to these spectra in the same manner used in the FFT and time domains. The scalogram slope in the time axis, ScTS, and in the scale axis, ScSS, are defined as before by the slope value from a linear regression model.

Figure 4.2 visually represents these parameters with dotted lines indicating the location of centroids (ScTC and ScSC) and dashed lines indicating the slope parameters (ScTS and ScSS). In the case of the ScSS value the slope is calculated on the linear data, but is plotted on a logarithmic axis and is thus distorted in the figure. The white dot in the figure is the intersection point of the two centroid values and represents the overall centroid of the scalogram.

4.6 Application Examples

To demonstrate the differences between the Fourier and wavelet approaches a set of sample sounds was synthesized to create piano-like test data. Inharmonicity was included with a fundamental frequency of 130.8 Hz (C3) and 29 partials comprising the test signal. An envelope was applied to the time signal to simulate the decay characteristics found in piano tones. This signal is referred to as the unmodified sample.

Two types of impactive sounds were also added to create variations of the signal: a Hanning pulse and a square pulse. These signals were added as ideal representations of impactive sound components like a pluck or hammer strike, but do not contain the noise components of those kinds of excitations. Two samples for each type of pulse were created with a magnitude of 0.15 and 0.3 relative to a maximum possible magnitude of 1.0, with the largest possible magnitude of any particular partial being 0.3 (i.e. the largest pulse is similar in magnitude to the largest harmonic component in terms of amplitude) and temporal length of 0.01 s. Example waveforms for the original signal and signals with the added Hanning pulse are shown in figures 4.3 and 4.4 respectively. Each sound was analyzed using the conventional psychoacoustical parameters as well as the corresponding wavelet versions described in section 4.5. The results are presented in table 4.1 for further discussion.

Theoretically it is expected that a short pulse being added to a time signal would result in a broadband energy bump in the Fourier domain. Ideally a Dirac type pulse should add equal energy at all frequencies, but with a longer impulse less high frequency energy would be expected. This effect can be seen when comparing figures 4.3 and 4.4, with a large energy bump in the low frequencies that decreases with increasing frequency value. In the wavelet domain a pulse is represented more accurately due to the finite length of the wavelets used to decompose the signal. Impulses are seen as expanding cones at low Fourier scale [2] as seen in figures 4.5.

[2] Low 'Fourier scale' is equivalent to a low sinusoidal frequency, which in wavelet terms would

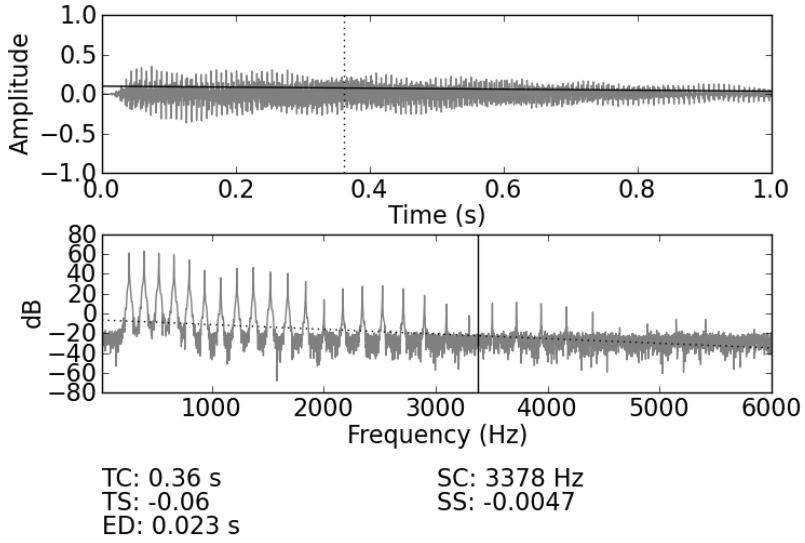

Figure 4.3: FFT and time domain representation of the synthesized sample sound. Vertical dotted lines represent the location of centroid values and dashed lines indicate slope values.

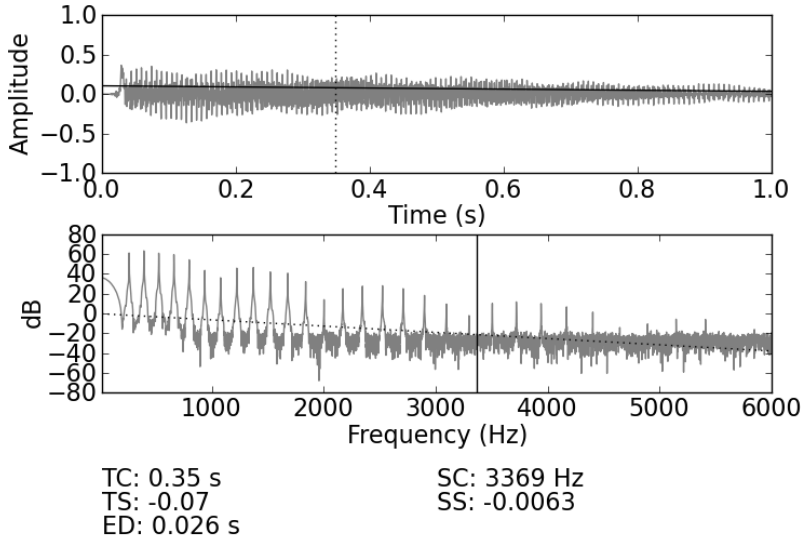

Figure 4.4: FFT and time domain representation of the synthesized sample sound with a 0.30 magnitude Hanning pulse added. Vertical dotted lines represent the location of centroid values and dashed lines indicate slope values.

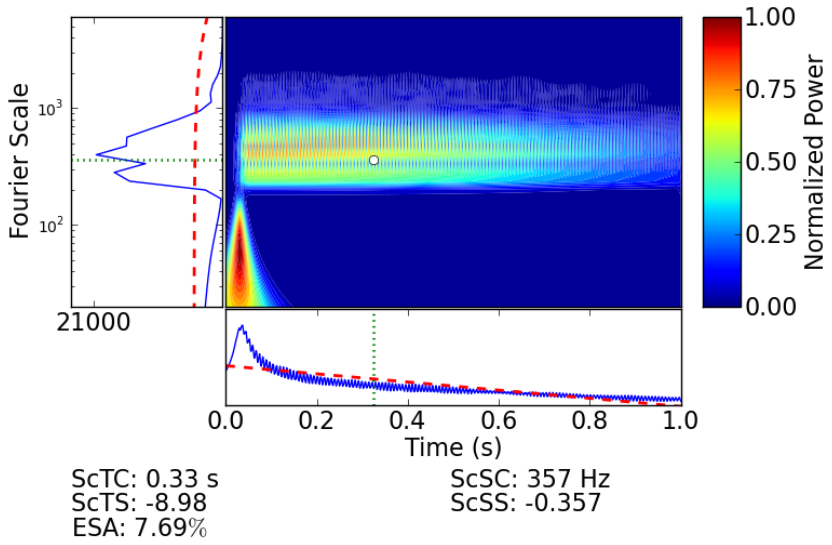

Figure 4.5: Scalogram of the CWT of the synthesized sample sound with a 0.30 magnitude Hanning pulse added. A Morlet wavelet is used in the CWT with dotted lines representing the centroids and dashed lines representing slopes.

Table 4.1: Psychoacoustical parameter values for synthesized sample sounds

	Spectral Centroid			Temporal Centroid		
Sample	FFT	Morlet	Paul	FFT	Morlet	Paul
Unmodified	3378	507	540	0.36	0.42	0.42
0.15 Hanning	3398	419	471	0.36	0.37	0.37
0.30 Hanning	3369	357	417	0.35	0.33	0.34
Unmodified	3378	507	540	0.36	0.42	0.42
0.15 Square	2788	366	423	0.35	0.33	0.34
0.30 Square	1844	288	349	0.33	0.28	0.29

	Spectral Slope			Temporal Slope			Effective Dur/Area		
Sample	FFT	M	Pl	FFT	M	P	FFT	M	P
Unmodified	-0.0047	-0.28	-0.24	-0.063	-3.3	-3.1	0.023	0.074	0.046
0.15 Hanning	-0.006	-0.36	-0.29	-0.066	-7.1	-5.8	0.024	0.081	0.052
0.30 Hanning	-0.0063	-0.36	-0.23	-0.07	-9	-5.9	0.026	0.077	0.027
Unmodified	-0.0047	-0.28	-0.24	-0.063	-3.3	-3.1	0.023	0.074	0.046
0.15 Square	-0.0052	-0.42	-0.29	-0.069	-10	-7.2	0.024	0.1	0.051
0.30 Square	-0.0048	-0.3	-0.18	-0.077	-9	-5.8	0.02	0.039	0.02

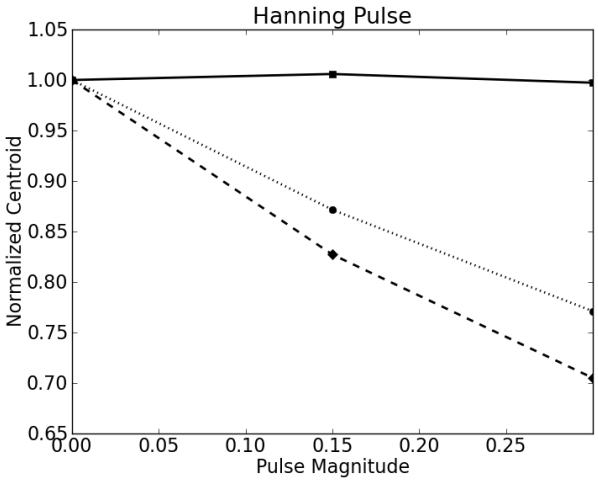

Figure 4.6: Spectral centroid and scalogram spectral centroid comparison for the addition of different magnitude Hanning pulses to the synthesized sound. Values for the conventional FFT based techniques (solid), the wavelet method using a Morlet wavelet (dashed), and the wavelet method using a Paul wavelet (dotted) are shown.

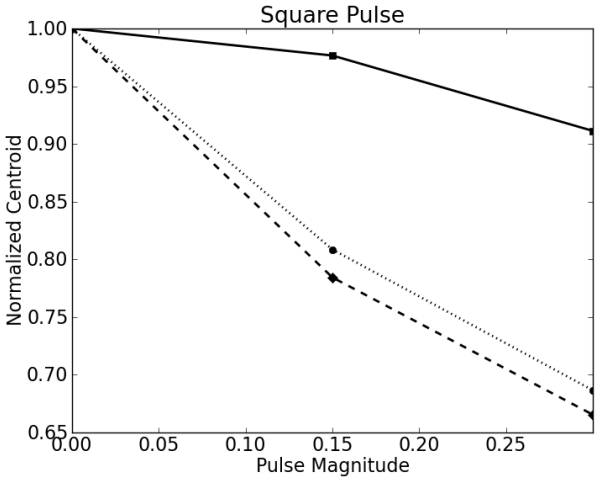

Figure 4.7: Temporal centroid and scalogram temporal centroid comparison for the addition of different magnitude square pulses to the synthesized sound. Values for the conventional FFT based techniques (solid), the wavelet method using a Morlet wavelet (dashed), and the wavelet method using a Paul wavelet (dotted) are shown.

4.7 Psychoacoustical Signal Parameters

From table 4.1 it is clear that, when compared to the results using a traditional FFT method, the wavelet transform is better able to represent impactive events from the original time signal and incorporate them into the calculation of psychoacoustical signal parameters. In the majority of cases with increasing pulse magnitude a larger change in the associated parameter is seen for the wavelet domain versus the Fourier domain.

Figures 4.6 and 4.7 illustrate the differences in performance between the wavelet and Fourier methods. In both cases the centroid values change much more significantly with the addition of the Hanning and square pulses for the wavelet approach, with the Morlet wavelet calculating slightly larger differences than the Paul wavelet. The spectral centroid (ScSC) values decrease by 30% relative to the unmodified sample sound in the case of the 0.3 magnitude Hanning pulse and the Morlet wavelet CWT, whereas the traditional Fourier method shows almost no change for the analogous parameter (SC). Comparable results are found for the 0.3 magnitude square pulse modification, an example of which is seen in figure 4.7 where the Morlet wavelet CWT method calculates a decrease in temporal centroid (ScTC) of 34%, with the analogous Fourier value (TC) decreasing by only 9% relative to the unmodified sound.

A case in table 4.1 where the change in parameter value for the two different approaches is not as large is seen in the spectral centroid values for the 0.3 magnitude square pulse test sample. The wavelet methods see a decrease in ScSC of 43% and 36% for the Morlet and Paul wavelets respectively, while the Fourier value, SC, decreases by 55%. An explanation for this result compared to the similar case discussed above for the Hanning type pulse of the same magnitude can be found when examining the Fourier domain representation of each pulse shown in figure 4.8. The square pulse has a higher magnitude Fourier representation in a broader frequency band than the Hanning pulse, and as a result affects the calculation of the spectral centroid in a more significant way. The Hanning pulse has a smaller effect in the Fourier domain, but in the wavelet domain the change in scale centroid (ScSC) is similar for both square and Hanning pulses. These results illustrate two important points: (i) that certain types of transient sound in the signal may be better suited to using wavelet methods, and (ii) for a more natural (i.e. continuous) impulsive sound like the Hanning pulse the wavelet approach is able to reveal significantly larger differences than the traditional Fourier methods do.

---

be considered to be large scale (i.e. at low Fourier frequencies a larger scale wavelet is used to decompose the signal).

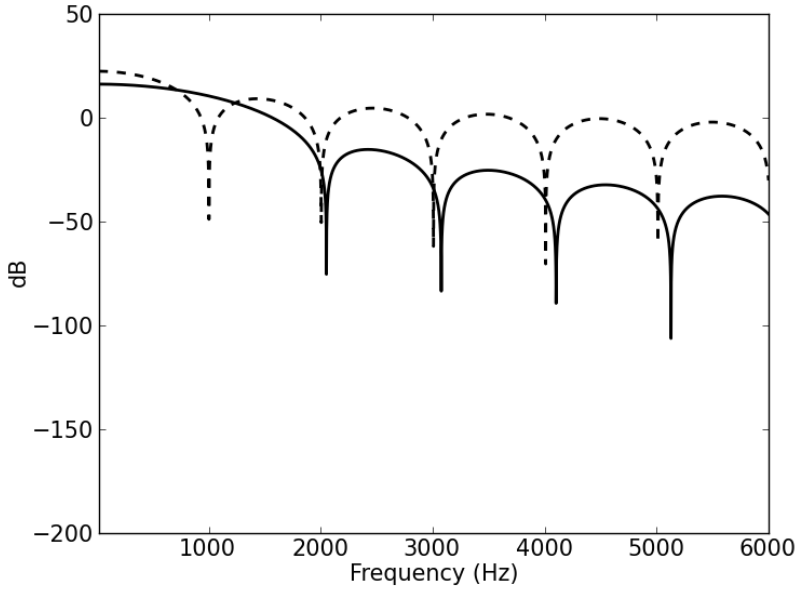

Figure 4.8: Fourier domain representation of Hanning (solid) and square (dashed) pulses.

4.8 Choice of Mother Wavelet

Another interesting aspect of this analysis is to examine the effect of the choice of mother wavelet by comparing results with the same sound using scalograms with the Paul (figure 4.9) and Morlet (figure 4.5) wavelets. The Morlet wavelet produces a broader spike associated with the added Hanning pulse and the overall structure of each is visibly quite different. The Paul wavelet produces a less well defined, or perhaps more smoothed, result than the Morlet wavelet. It can also be seen in table 4.1 that the choice of a Morlet wavelet generally creates larger differences compared to the Paul wavelet.

It is also important to note that although the Morlet wavelet marginally outperforms the Paul wavelet in this instance, both produce significantly bigger differences than the Fourier approach in most cases. The impactive events have a larger magnitude in the wavelet domain than the Fourier domain and thus have a larger contribution in the final calculation of the psychoacoustical signal parameters. The flexibility of the wavelet method is also emphasized, as the choice of wavelet can be fine tuned to suit the particular type of signal analysis task desired. That said, in the samples analyzed in this study the actual differences were probably insignificant. A similar result has been found in image compression where an ideal wavelet representation is sought for a particular image. Mandal et al [66] concluded that trying to find an optimal wavelet representation is warranted for some specific types of images with low signal activity, but in most cases an optimization

of wavelet choice yielded little benefit. Applying this result to the analysis of audio signals suggests that the actual choice of mother wavelet is in most cases unimportant, but in certain circumstances an optimal choice may be possible for specific tasks. An example application for which it would be advantageous to have several wavelets to choose from is an identification task for a specific kind of impactive noise in a complex sound with several different transient components.

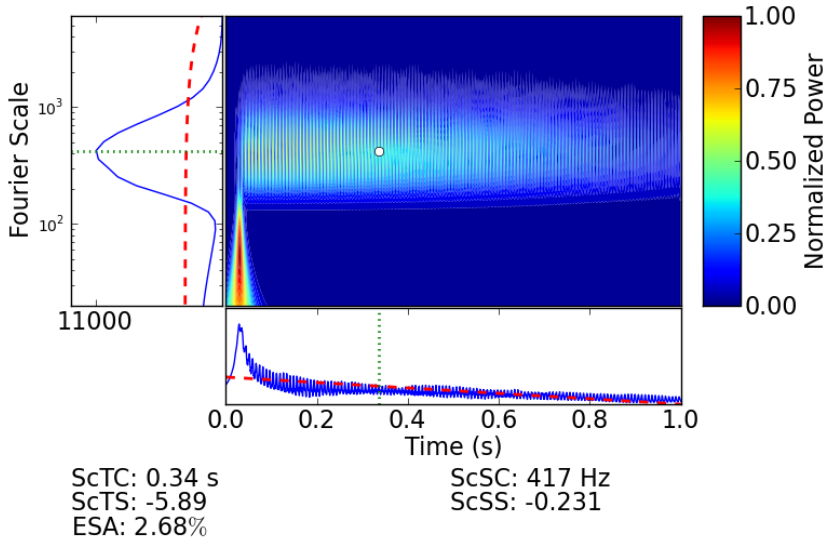

Figure 4.9: CWT scalogram with Paul wavelet and a 0.30 magnitude Hanning pulse added to the base signal.

4.9 Real Piano Sounds

The simulated sounds with abstract impulses examined in the previous sections illustrate the idealized case, but when analyzing real sounds the picture becomes more complicated. A scalogram of the time signal of a recorded piano note, C4-261.6 Hz, is shown in figure 4.10 and illustrates the typical structure of this kind of sound in the wavelet domain. A strong fundamental along with harmonic bands and significant phasing of energy in and out are all visible. The scalogram of the real piano sound does not have as strongly defined low Fourier scale energy compared to the ideal cases seen earlier in figures 4.5 and 4.9, but instead has a less predominant region of low Fourier scale energy with an extended duration. This difference is explained by the characteristics of the real 'knock' sound of a piano compared to the ideal square or Hanning pulse which create an idealized representation in the scalogram.

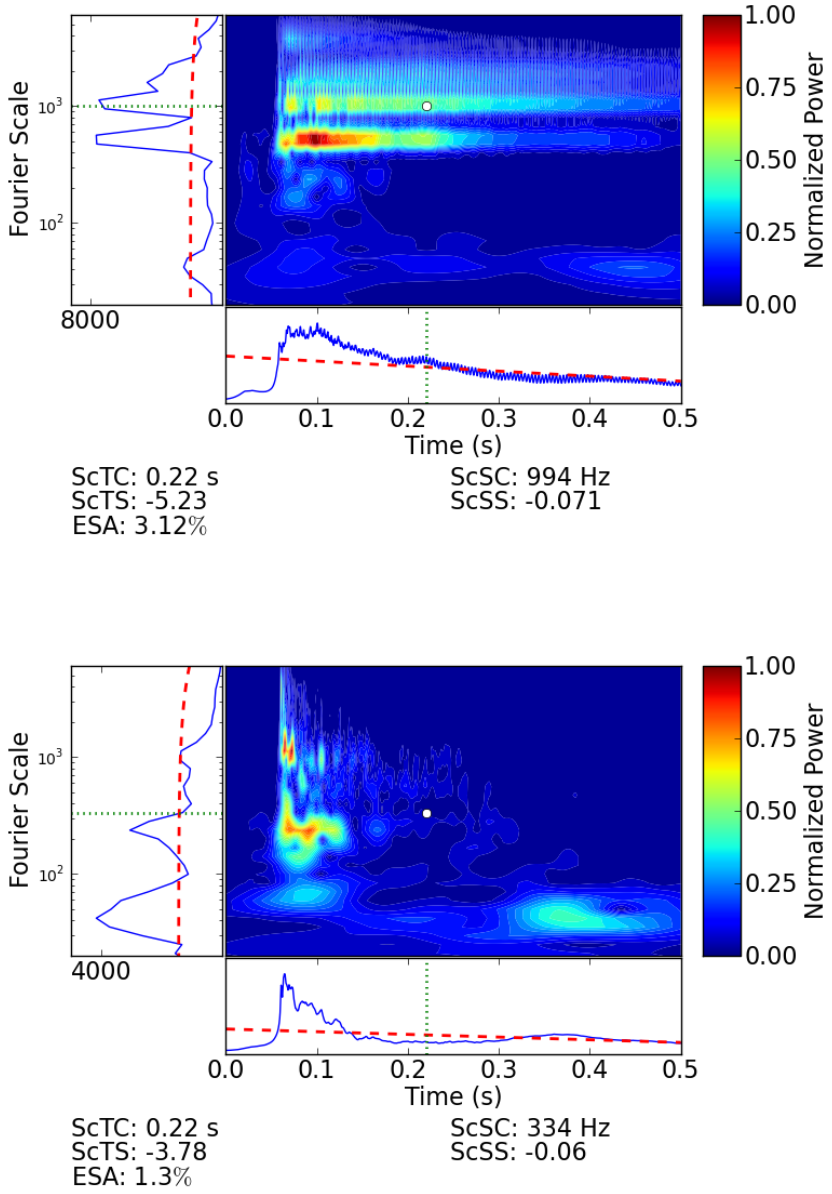

Figure 4.10: CWT scalogram of a recorded piano note C4 (top) and the CWT scalogram of the same note played with the string damped (bottom). A Morlet wavelet is used in the CWT with dotted lines representing the centroids and dashed lines representing slopes. In both cases a 0.05 s period of silence is recorded before the keystroke is initiated.

Another recording of the same note was made with the string damped in an attempt to provide a sound sample that represents the typical 'knock' sound of a piano. This sound includes the hammer striking the strings, the motion of the piano action, and the striking of the keybed. A noticeable phasing of the knock energy at low scale is observed in the bottom scalogram of figure 4.10 after the initiation of the 'knock' at approximately t = 0.05 s. The overall effect of the 'knock' in terms of psychoacoustical signal parameters is to lower spectral centroid and temporal centroid, and to increase the magnitude of spectral and temporal slope compared to a similar sound that is lacking a 'knock' component. An overlay of the 'knock' sound on the undamped sound is provided in figure 4.11 that further illustrates the contribution of the 'knock' to the overall undamped sound of note C4.

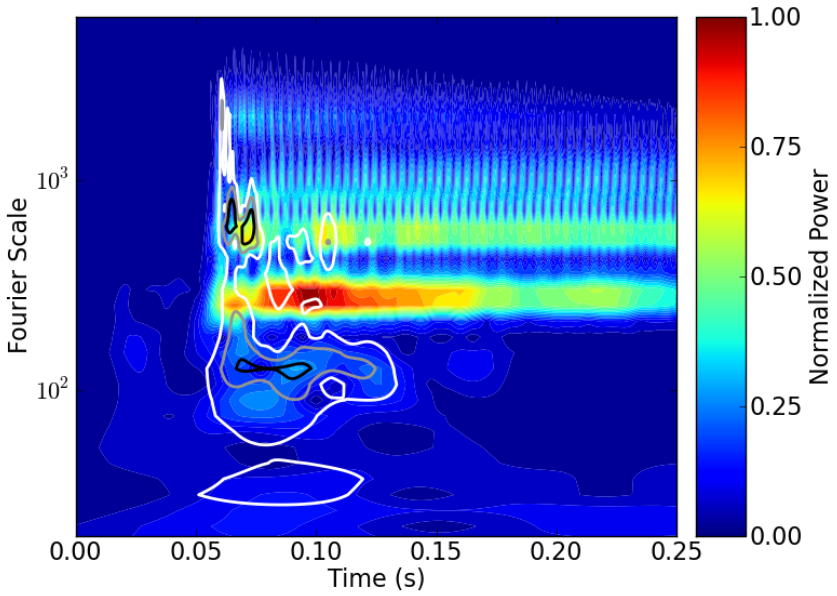

Figure 4.11: CWT scalogram of a recorded piano note C4 with the scalogram of recorded C4 'knock' noise overlaid as contour lines to emphasize the 'knock' contribution.

The complexity of the time response is completely lost when examining the same 'knock' sound as a spectrogram, seen in figure 4.12. In the spectrogram the 'knock' becomes a continuous addition of energy at all frequencies, with more temporal extent at low frequencies. The Fourier domain spectrogram method also requires a limit on frequency resolution to gain temporal resolution, something that is not ideal for musical psychoacoustics where small changes in frequency content are perceptually important, however, some techniques may apply like decreasing hop-size and more zero-padding that could increase spectrogram resolution. By using wavelet methods a more accurate temporal description is achieved compared to Fourier methods, particularly for knock components of the sound, while at the same time retaining temporal resolution. It is reasonable to hypothesize that the

more accurate representations of our test signals provided by wavelet methods will help researchers achieve more accurate models of the perception of those sounds.

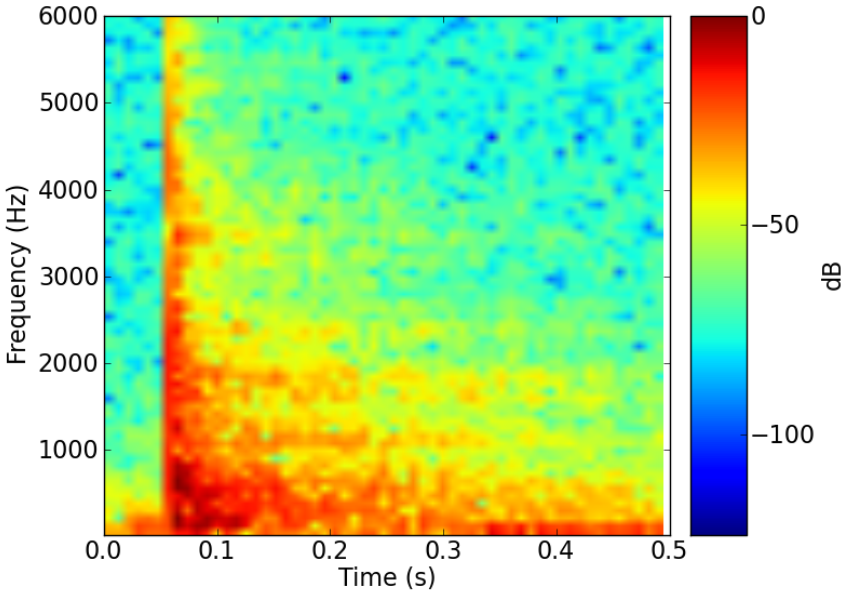

Figure 4.12: Spectrogram of note C4 played with the string damped corresponding to the bottom scalogram of figure 4.10.

4.10 Wavelets and Moisture Content

Wavelet PSPs are also well suited to analyzing the subtle change in tone that occurs due to varying MC demonstrated in chapters 2 and 3. An analysis of note G3 from the guitar testing of chapter 2 is provided in figures 4.13 and 4.14 to illustrate the sensitivity of the wavelet method in comparison to the traditional FFT-based methods.

From the scalograms of figure 4.13 a general trend of decreasing high frequency energy is observed as MC increases, something that is explained by the general increase of damping and loss of stiffness that occurs with increasing MC demonstrated earlier. The direct comparison of spectral centroid (SC) and scalogram scale centroid (ScSC) seen in figure 4.14 further illustrates the improved sensitivity of the wavelet method. Normalized values are presented, as the two different approaches are not directly relatable in terms of the frequency/scale axis, with the important concept being the amount of relative change calculated by each the parameters as a function of MC. The SC value is seen to increase by only 1.2% from 7-11% MC, whereas the wavelet version, ScSC, increases by close to 15% for both types of mother wavelet. Both approaches show the same general increasing trend with MC, but the wavelet method is clearly much more sensitive in this case.

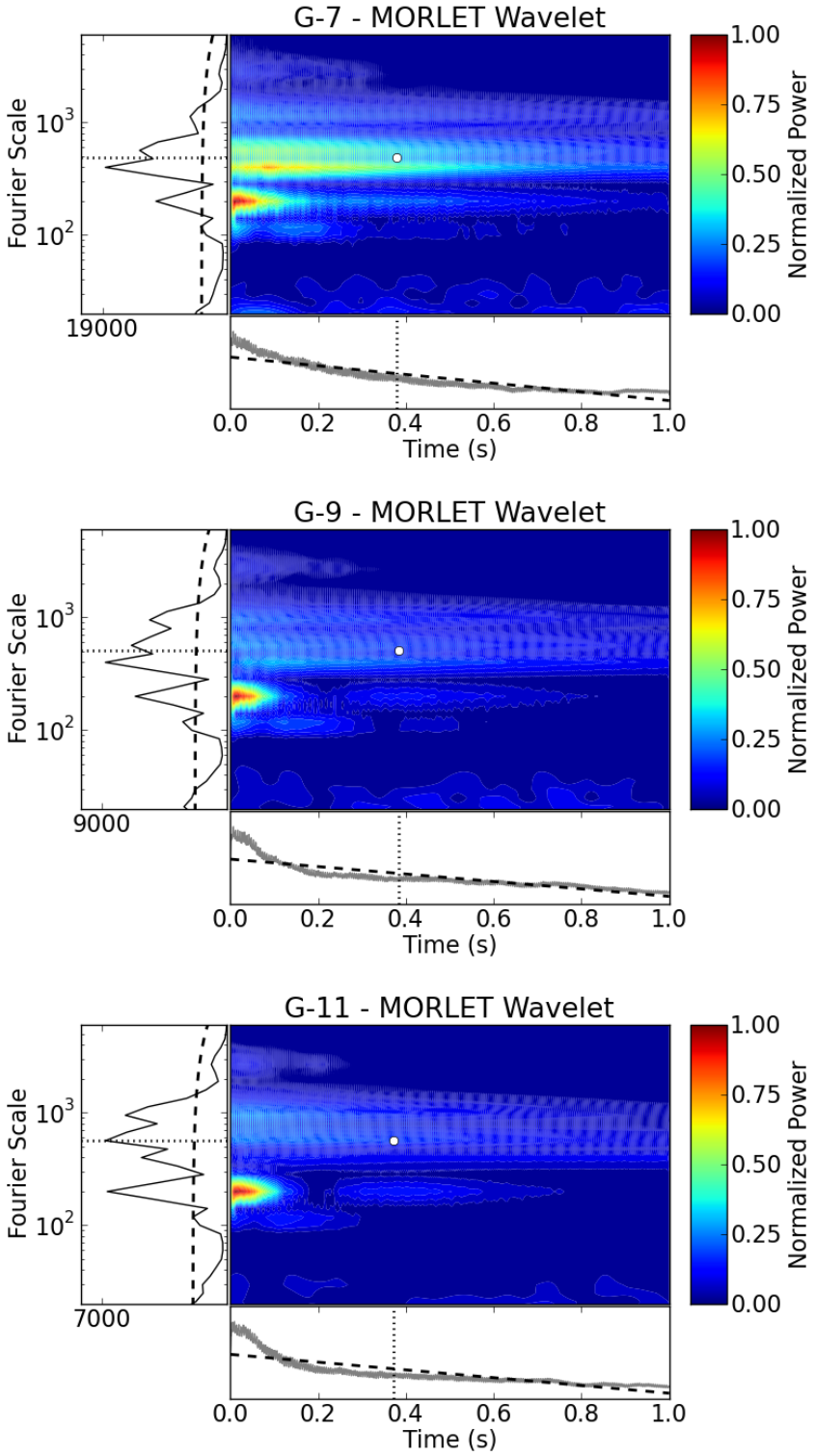

Figure 4.13: Scalograms of the CWT using a Morlet wavelet of note G3 recorded at 7% (Top), 9% (Middle), and 11% MC (Bottom).

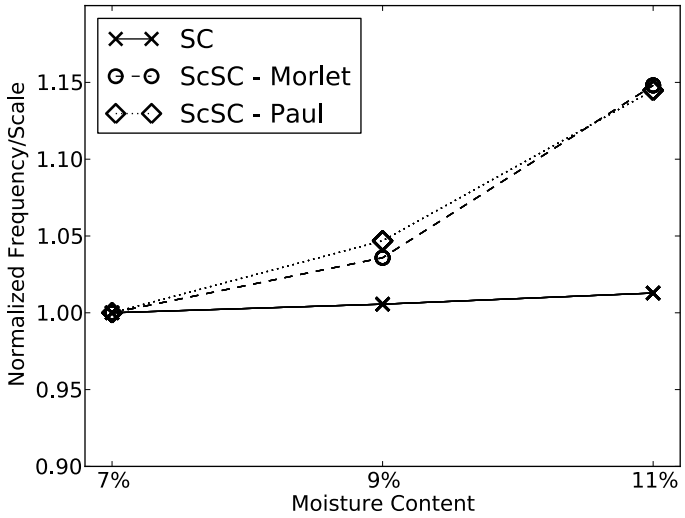

Figure 4.14: Spectral centroid (SC) and scalogram scale centroid (ScSC) values of note G3 at 7, 9, and 11% MC. Values have been normalized by their respective 7% MC datapoint to allow for direct comparison. SC is calculated from the FFT, while ScSC is reported for both Morlet (ScSC-Morlet) and Paul (ScSC-Paul) mother wavelet versions.

4.11 Conclusions

Several novel formulations of psychoacoustical signal parameters in the wavelet domain have been presented and have been shown to be suited to the analysis of signals which have both periodic and aperiodic components. The application of the wavelet transform has been successful in many different scientific fields [53, 66, 54, 68] and the field of musical psychoacoustics will likely also benefit from the improved ability of the wavelet transform to better characterize these types of real musical signals. Tonal differences due to changes in MC were also shown to be suited to analysis by wavelet PSPs where improved sensitivity was observed in comparison to the conventional methods. A comparison between the changes in different portions of sounds may also be applicable to the work presented in chapters 2 and 3.

Extending the results obtained herein to other conventional signal parameters, along with the development of new psychoacoustically relevant parameters provides a significant possibility to improve the efficacy of methods currently relying on the traditional FFT approach. That is not to say that FFT methods are inferior in all cases, but that a wavelet approach gives a different, and sometimes more appropriate, perspective on the same dataset. Using both methods will likely provide researchers with the most complete understanding of their data.

Future work could include implementing auditory perceptual models using the wavelet transform in order to see if the increased representational accuracy of the

wavelet method correlates with observation.

Chapter 5

The Evolution of Piano Design

5.1 Introduction

As the design of the piano has evolved, so has its tone and the performance techniques used to play it. In this section a range of historic pianos are analyzed using the piano tone mapping technique [69], standard psychoacoustical signal parameters [7], and novel wavelet based psychoacoustical signal parameters, along with impedance measurements. The objectives of this chapter are to explore the development of piano tone and its relation to design changes, to provide an example application of PSPs with a comparison between conventional and wavelet formulations, and to discuss the relationship between quantitative measurements of piano properties and subjective interpretations of playing style related to pianos from different musical eras.

The majority of pianos used in this study were recorded at the home of David Breitman [70], a Professor of music at Oberlin college in Oberlin, Ohio. The instruments consisted of a Dulcken (1790), Walter (1800), Graf (1830), and Bösendorfer (1860) piano. A Steinway B (1920) grand piano was also recorded as a point of comparison in the home of Jan Narveson in Waterloo Ontario. A modern style Hardman (1890) grand piano studied in the Piano Design Lab at the University of Waterloo is also presented, as well as a clavichord recorded at the home David Breitman.

In discussing the contrast between the modern grand pianos (Steinway and Hardman) and historic early pianos (Graf, Dulcken, Walter) Breitman made several comments. Modern pianos, he felt, saw composers and performers placing more emphasis on a single line as they have a 'more muddled, less clear sound'. In general he believes when performing on a modern piano unpedalled playing is avoided. Historic early pianos, however, he felt produced a sound with more clarity when playing several notes together. The emphasis of counterpoint in the music composed during the time period that these historic instruments were constructed is one hypothesis for this difference. Overall Breitman characterizes these historic pianos

as having a sound that allows all components (in terms of notes) to be heard equally [70].

As the modern piano developed it underwent a number of significant changes that affect the way it sounds and plays. The introduction of thicker soundboards, wound strings, felt hammers, the cast iron frame and over stringing, and thicker, longer strings under greatly increased tension all contribute to these differences. A more detailed description of each of the pianos is provided in chronological order:

Clavichord

The clavichord is a precursor to the early piano that allowed the player to have some control of the dynamics with which the instrument was played in comparison to a harpsichord which affords very little control in terms of loudness. This desire for significant dynamic control was not possible on the harpsichord due to the method of excitation and led to the development of the early piano (pianoforte - soft loud) and the modern grand piano in order to provide the player with more expressive control. The clavichord studied has a limited range of notes compared to a modern piano, only notes 15-69 of the 1-88 that are available on standard modern keyboards. A clavichord also has a unique method of exciting the strings; when the key is pressed a stop is raised to act as the string termination (similar to the role of a fret on a guitar), often with several notes played with the same string. This instrument, seen in figure 5.1, has a very small soundboard and limited volume in terms of loudness.

Figure 5.1: Clavichord

Dulcken

The Dulcken piano represents an early piano with a playing range of notes 9-71. The keyboard is attached by a simplified mechanical action to leather wrapped hammers used to strike the strings. Dulcken's design allows for a small amount of dynamic control, but was hindered in the bass range by the small size of the soundboard in comparison to modern grand pianos. This instrument, seen in figure 5.2 was tuned at A4-430 Hz and has 20 pairs (one pair per note) of brass strings in the bass, with the other strings made of steel also in pairs.

Figure 5.2: Dulcken

Walter

The Walter piano is quite similar in design and construction to the Dulcken. It has the same playing range, notes 9-71, and is also excited by the same kind of leather wrapped hammers. Soundboard area is approximately the same, as well as the tuning and types of strings. The design similarities can be seen in figure 5.3

Figure 5.3: Walter

Graf

The Graf style piano, (a modern replica), represents the next generation of piano design. The playing range is expanded to include notes 4-81 and, most significantly, the soundboard area is increased. The piano is straight strung and has one continuous bridge for both the bass and tenor notes and the hammers are leather wrapped, providing a small amount of dynamic control. The stringing is arranged with 5 pairs of brass in the low bass, followed by 11 brass tri-chords, with the remaining notes strung with tri-chords of steel.

Figure 5.4: Graf

Bösendorfer

The Bösendorfer piano continues the evolution of the piano and could be considered as being more of a modern grand piano than an early piano in terms of construction. The playing range of this instrument includes notes 1-85 and the action and hammers are of a more modern style, with the important change from leather wrapped hammers to felt wrapped hammers. Strings are divided between a bass and tenor bridge and the instrument is straight strung. The bass stringing consists of 3 individual wound strings, followed by 5 wound pairs, and then 10 tri-chords. All notes on the tenor bridge have tri-chords made of unwound steel strings. The area of the soundboard has increased from earlier pianos and the change in hammer materials and the use of wound strings are the most significant differences. This piano is shown in figure 5.5.

Figure 5.5: Bösendorfer

Hardman

With the Hardman grand piano the full set of features common to most modern grand pianos are seen. The playing range has been expanded to include all notes 1-88 and the action and hammers are of the current modern style with felt wrapping. The soundboard area has increased slightly from the Bösendorfer, and is representative of a 'normal' modern grand piano. Notes are divided between a bass and tenor bridge, with 7 individual wound strings, 8 pairs of wound strings, and 7 tri-chords of wound strings on the bass. The tenor notes are all unwound tri-chords. A final design difference of note is the use of an overstrung string arrangement, where the bass strings cross over top of the tenor strings. This is a design feature that eventually became an industry standard when used by the Steinway company in their pianos. The Hardman piano is seen in figure 5.6

Figure 5.6: Hardman

Steinway

The final instrument examined is a modern Steinway B grand piano. It is similar in size and construction to the Hardman and features a full playing range of notes 1-88, modern action with felt hammers, and a relatively large soundboard area. The piano is overstrung with 8 individual wound strings and 12 pairs of wound strings attached to the bass bridge and the remaining notes on the tenor bridge all tri-chords of unwound steel strings.

General trends in piano design can be seen to include the increase in size of the soundboard, the increase in the range of notes that can be played, the splitting of the bass and tenor bridges, and the introduction of wound strings for bass notes that also create the potential for increased loudness. These changes in design act primarily to improve the low frequency acoustic behaviour of the piano by increasing the mass and dimension of the soundboard, but also aim to allow more expressive playing. What expressive playing actually is is a rather subjective term, so it perhaps is best to interpret the evolution of the piano in the context of moving towards a desired sound quality relevant to a particular time-period, as opposed to moving towards some sort of 'ideal' tone.

Figure 5.7: Steinway

5.2 Tone Mapping

The structure of the partials of a piano tone is known to be an important psychoacoustical property of sound [35], and by extracting the partials structure of each note a surface plot can be made that illustrates the entire partial structure of a piano in one image. This technique is referred to as piano tone mapping [69], and is used to provide a visual comparison between the partial structure of the previously mentioned pianos. In this method sound recordings of all the notes playable by an instrument are recorded and analyzed to extract the magnitudes of their partial components. These magnitudes are then plotted to form a pseudocolor plot representing their relationship within and across notes. Noticeable features of the maps can then be related to design aspects of the pianos they are visualizing as seen figure 5.8. Tone maps for each of the instruments can be found in figure 5.9.

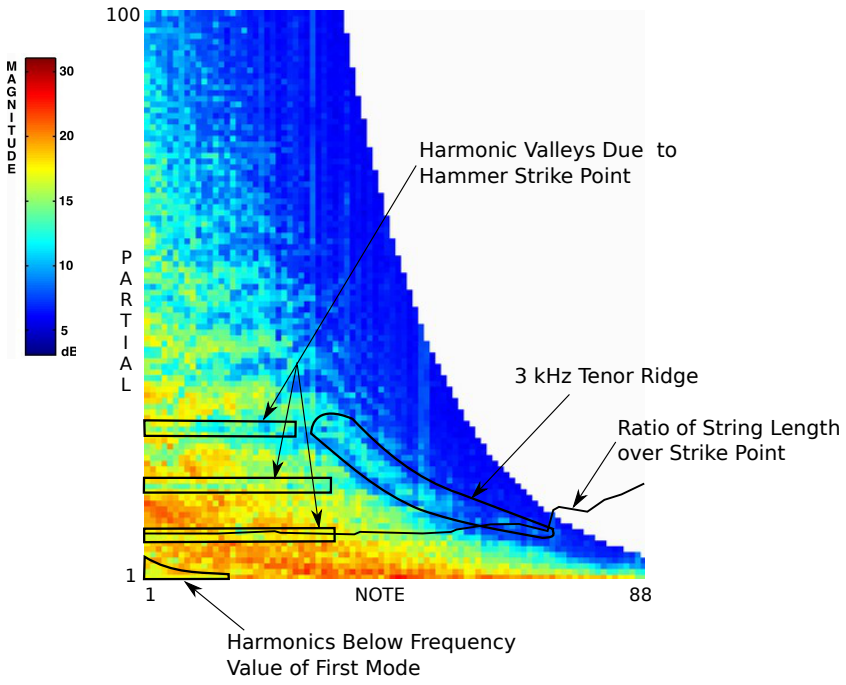

Figure 5.8: Typical partial structures of a modern grand piano. The strike point is approximately 1/8th of the speaking length of the string for most of the notes and the frequency of the first vibration mode of the soundboard is approximately 75 Hz.

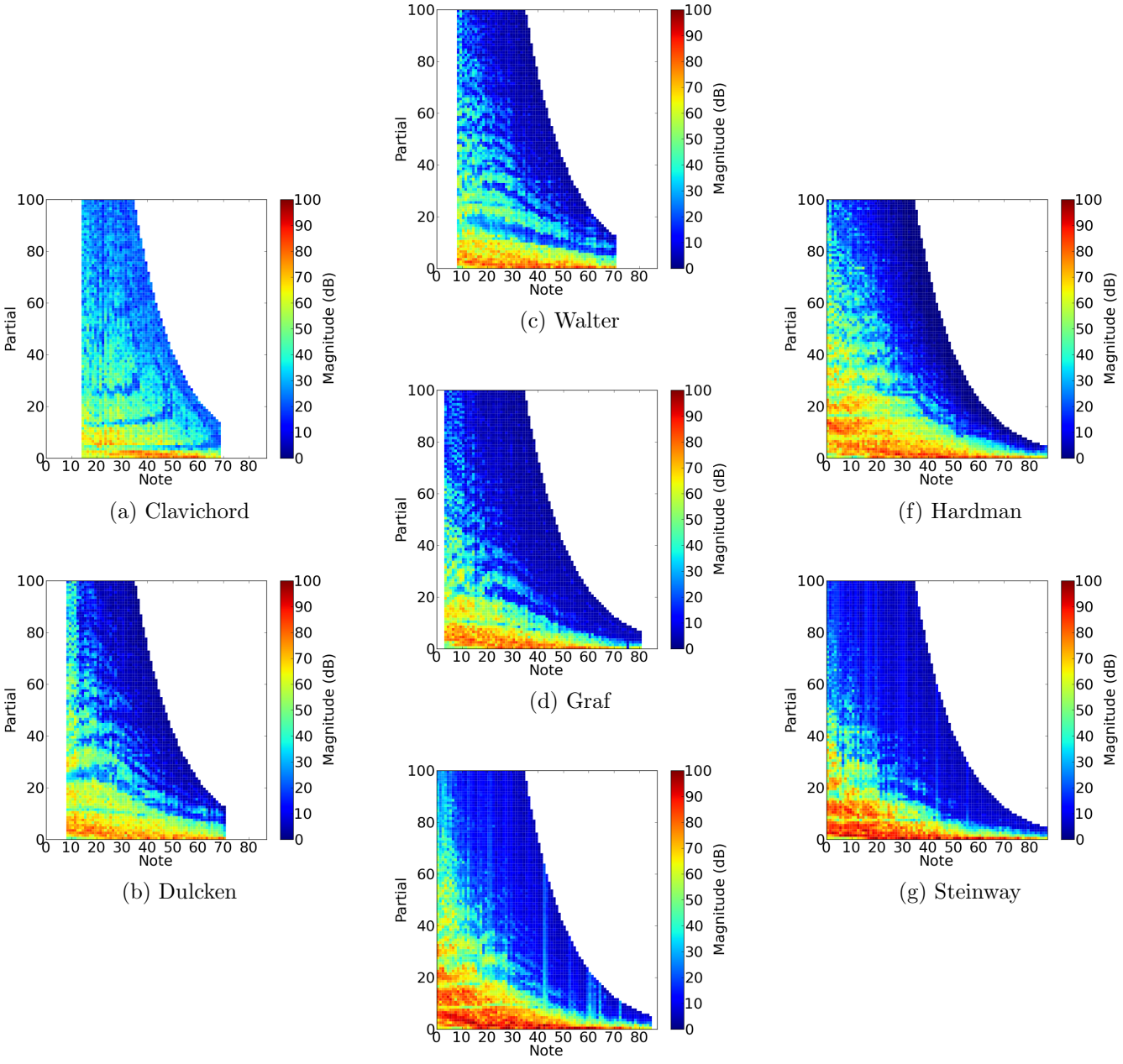

(a) Clavichord

(b) Dulcken

(c) Walter

(d) Graf

(e) Bösendorfer

(f) Hardman

(g) Steinway

Figure 5.9: Tone maps of a group of historic pianos.

The clavichord, as a precursor to the piano, represents the most significant difference in this group of instruments in terms of tone. Key features of the clavichord tone map are the presence of significant upper partial content in all notes and limited fundamental response before note 24. The presence of significant upper partial energy is attributable to the method of excitation of the clavichord where force is applied at the string termination. Theoretically exciting a string at the termination should provide excitation of all partials, and in comparison to the subsequent piano maps this kind of excitation is evident. For notes 15-20 it can be seen that the magnitude of the fundamental is less than the other higher partials. In the modern grand piano this behaviour is also evident and is attributed to the dimension of the soundboard and the frequency value of its first vibration mode [69]. The limited bass response of the clavichord is likely due to the same effect, but modal analysis would need to be conducted to verify this.

Moving forward from the clavichord we head into the early piano era. The Dulcken and Walter pianos represent a significant step towards modern grand piano design, with leather wrapped hammers creating the excitation force and an expanded range of notes similar to that of the harpsichord, but with a smaller soundboard and shorter scale lengths than those of a modern grand piano. In both of these maps the structure of the bass partials is less developed in the upper partials when compared to modern grand pianos where more energy is present at these higher partials. A 3 kHz tenor ridge found in modern grand pianos [69] is not as visible in these pianos. Specific PSPs will be discussed in a more quantitative manner later, but the overall partial structure provides an initial point of comparison.

The next progression in piano development is represented by the Graf piano where the most significant changes are the expanded bass note range, larger soundboard, larger scale length, and consequently, a more complex bass response. In the tone map this is seen as the presence of more energy in the high partials, particularly of the bass notes.

Entering the modern piano era we examine the 1880's Bösendorfer which has felt hammers, wound strings, and a large soundboard. The final two instruments, the Hardman and Steinway grand pianos, are representative of fully modern grand piano designs. They are both overstrung with wound strings and felt hammers and have large soundboards in comparison to earlier pianos. Both of their tone maps share the characteristics illustrated in figure 5.8, with significant energy in the higher partials of the bass notes and more well defined structures. These differences would correspond to a harmonically rich and more complex sound in the bass notes, with a general increase in the precision of scale design (string length and hammer strike point) resulting in the increased definition of map structures. The use of wound strings and higher tension are also important factors. One question that arises is how consistent these maps would be for several identical pianos made by one manufacturer, unfortunately access to a group of pianos like this was not possible. A more quantitative description of these concepts in relation to the evolution of piano design is provided in the next section using PSPs.

5.3 Psychoacoustical Signal Parameters

Two of the psychoacoustical parameters presented in Peeters [7] work are employed in the analysis of the set of pianos described above. These parameters are calculated in the time or frequency domain, and represent standard analysis methods. Each piano was analyzed for spectral centroid and temporal centroid as defined in equations 4.7 and 4.6 respectively. An overview of all the pianos with regards to these PSPs is plotted in figures 5.10 and 5.11 showing trend lines for each parameter.

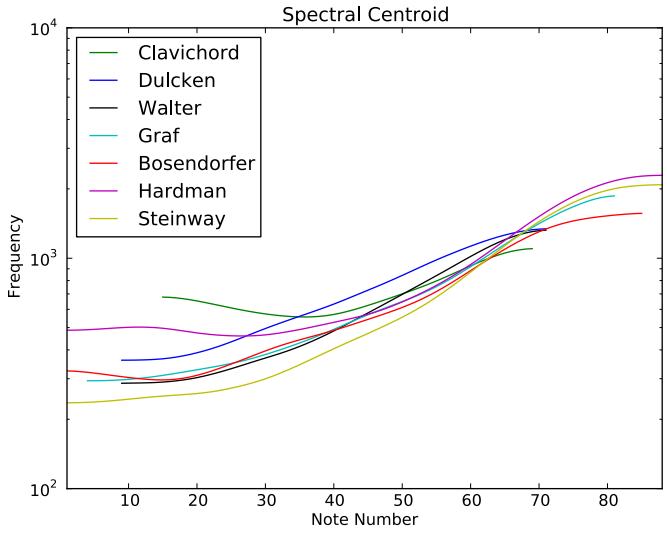

Figure 5.10: Spectral centroid trend lines for a set of historic pianos. The legend lists instruments in chronological order with a cubic spline curve fit applied to the raw data.

In terms of spectral centroid trends the most visible differences can be seen in the lower half of the piano keyboard, notes 1-40. The response of the clavichord has the highest SC values of any instrument below note 30, something that can be explained by the small size of the clavichord's soundboard. Because the clavichord has such a small soundboard it likely has high impedance at the low frequencies that are present in the fundamental and low order partials of notes 15-30. As a result the clavichord's SC values will be shifted up as the upper partials of higher frequency will then play a more prominent role in the SC calculation. Similarly, the larger soundboard and improved bass response of the Steinway piano sees a larger emphasis on the fundamental and lower frequency partials in the SC calculation which brings those values down. Excluding the Hardman, a general decreasing trend is observed with the development of the piano through time, as larger soundboards and an improved bass response were built into more modern instruments.

In contrast to the bass notes the behaviour in the top half of the piano keyboard, notes 40-88, is observed to be fairly similar for all instruments in terms

of SC. This is due to the fact that as notes increase in pitch there is a stronger emphasis on the fundamental frequency with fewer partials present in the signal. With the fundamental dominating the SC calculation there would be little difference expected between the different instruments in terms of SC, and that is exactly what is observed.

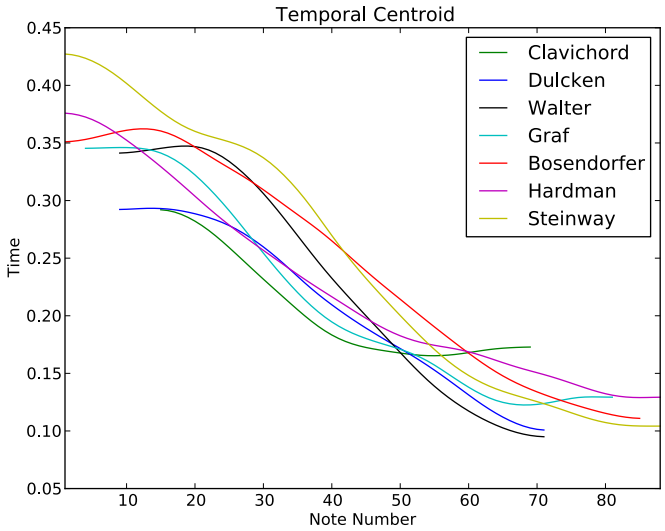

Figure 5.11: Temporal centroid trend lines for a set of historic pianos. The legend lists instruments in chronological order with a cubic spline curve fit applied to the raw data.

The plot of temporal centroid trends in figure 5.11 presents a similar result. In general the more modern instruments are seen to have larger TC values indicating that they have more sustain than the earlier instruments. These changes are attributable to the larger soundboards and vibrating mass of the more modern designs. Specifically looking at notes 1-20 we can see the chronological development of the increased sustain characteristic of the modern piano as a general increasing trend in TC values.

When looking beyond just the general trend lines for SC and TC the raw data itself appears to be quite noisy, with sudden fluctuations in SC and TC noted for all instruments. Examples of this data can be seen in figure 5.12 with a seemingly large amount of variation, or 'noise', from note to note where a smooth transition might have been expected.

To investigate this apparent 'noise' further studies of the Hardman grand piano were conducted to determine if any genuine physical attributes of the piano contribute to this effect. A simplified version of figure 5.12 is presented for just the Hardman piano's data in figure 5.13. Close ups of notes 20-30 are shown in figure 5.14 and of notes 40-50 are shown in figure 5.15.

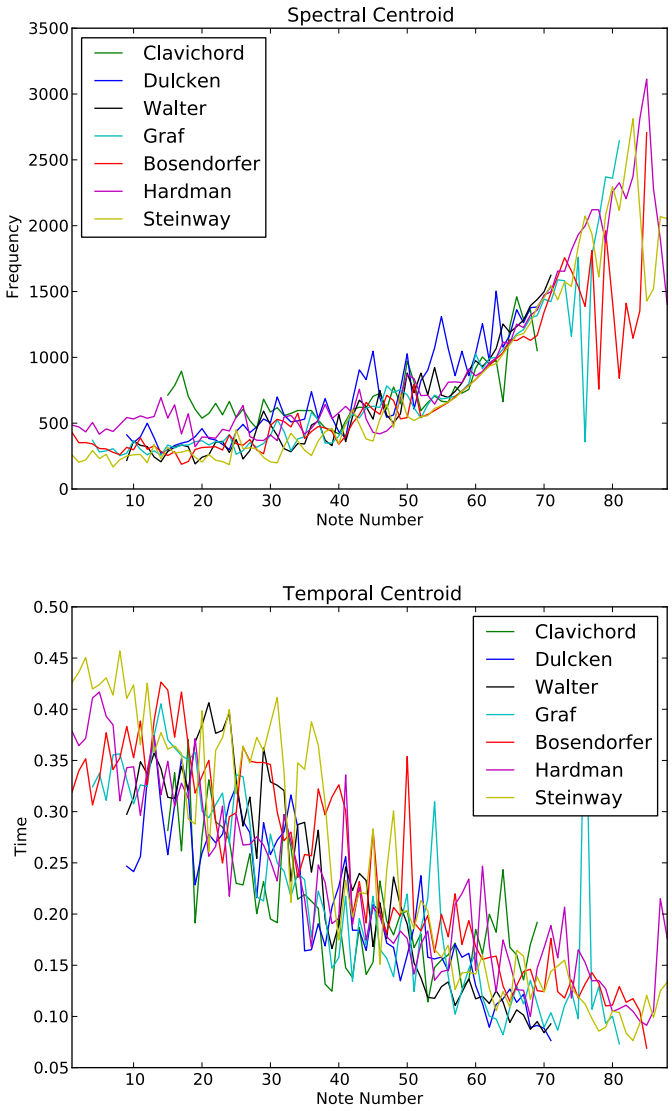

Figure 5.12: Spectral and Temporal centroid data for a set of historic pianos. The legend lists instruments in chronological order.

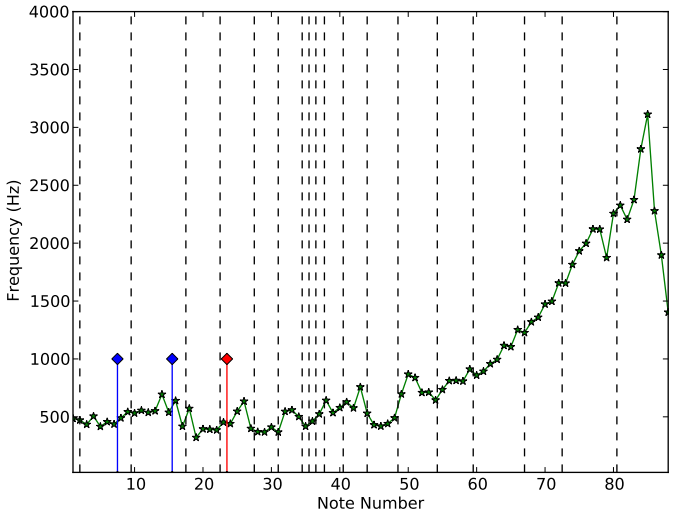

Figure 5.13: Spectral centroid values for the modern Hardman grand piano. Black dashed vertical lines represent bridge-rib intersections, solid blue vertical lines indicate string transitions, and the solid red vertical line represents transition from bass bridge to tenor bridge.

Alongside the spectral centroid values on these plots are vertical lines that represent the bridge-rib intersections, string transitions (wound single, wound double, wound triple, and unwound triple), and the transition from the last note on the bass bridge to the first note on the tenor bridge. All of these points represent situations that might explain the sudden fluctuations seen in the SC data as variations in vibration properties are likely to occur at these locations.

The most common type of transition can be seen to occur at the bridge-rib intersection points. These intersections occur because the ribs of a piano soundboard run approximately perpendicular to the bridge, and at several points they intersect. With the strings transferring energy through their attachment point at the bridge, it is hypothesized that differences in impedance could be affecting the output sound of the piano where some notes are attached to the bridge on or near a rib, and others are attached to the bridge in-between ribs. From figure 5.13 it can be observed that this explanation of the fluctuations in SC value has some support. Clear patterns or sudden changes in value do seem to exist at most transitions, although there is not perfect alignment throughout. Another mechanism that could contribute to this variability is the coupling of vibration modes and the different frequency components present in different notes which could cause fluctuations in decay time and spectral centroid.

Examining figures 5.14 and 5.15 provides more support for the role of ribs in the changes in SC observed. To further test this hypothesis impedance measurements at these transitions points would be able to demonstrate if any significant

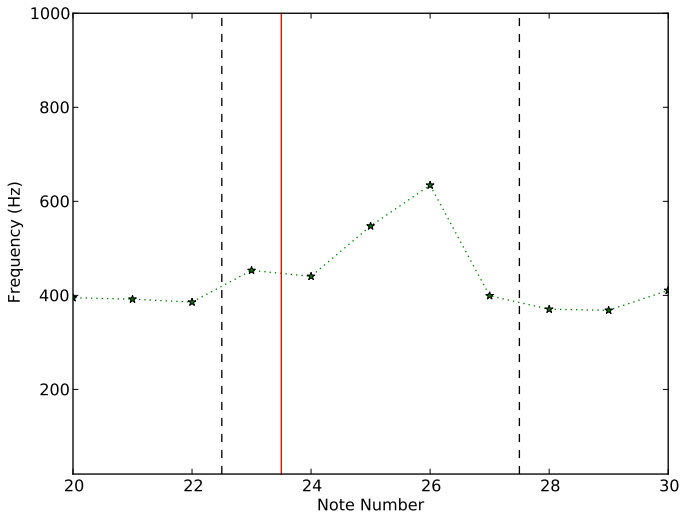

Figure 5.14: Spectral centroid values for notes 20-30 of the modern Hardman grand piano. Black vertical lines represent bridge-rib intersections and the solid red vertical line represents transition from bass bridge to tenor bridge.

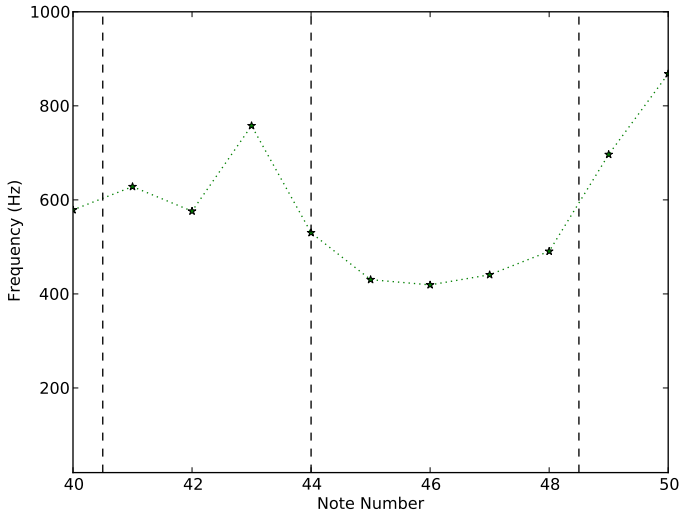

Figure 5.15: Spectral centroid values for the modern Hardman grand piano. Black vertical lines represent bridge-rib intersections.

changes are occurring. Unfortunately, not all bridge and rib intersection points are accessible enough in a fully strung piano to conduct this impedance testing. In one case, notes 26 and 27, measurements were completed to determine if any impedance changes could be related to the sudden jump in SC observed at these particular notes. Note 26 has a fundamental frequency of 116.5 Hz and note 27 has a fundamental frequency of 123.47 Hz. Both notes could also have frequency components below their fundamentals due to impactive noise due to key and hammer strike. Impedance curves for a large frequency band are plotted in figure 5.16 and in a narrower band in figure 5.17.

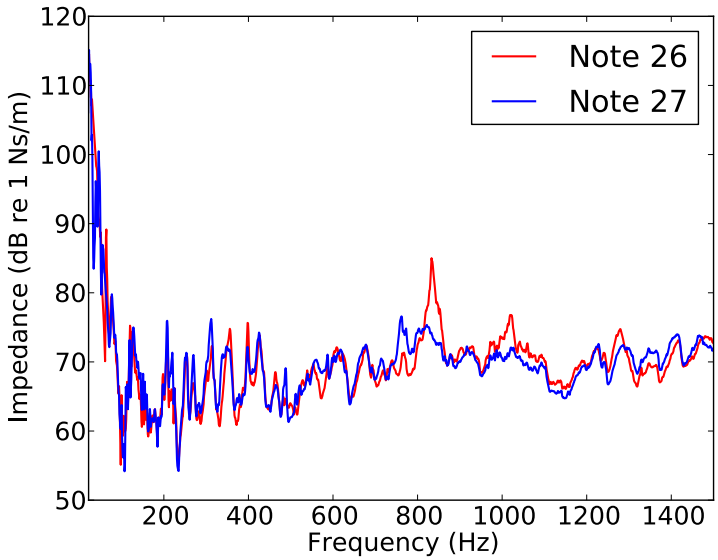

Figure 5.16: Impedance values from 20-1500 Hz for note 26 and note 27. Note 26 is located in-between two adjacent bridge-rib intersections and note 27 is located near to a bridge-rib intersection.

The general behaviour observed in figure 5.16 for 20-1500 Hz shows that for the most part the notes are quite similar, but when examining just the low frequency region, 20-200 Hz in figure 5.17, a more relevant difference is observed. The attachment point of note 27 to the bridge is located adjacent to a rib, whereas, for note 26 the attachment point is located farther way from this rib, somewhat in-between the rib associated with note 27 and the rib associated with note 23. The decrease in impedance below 40Hz observed for note 27 in comparison to note 26 means that note 27 can more readily vibrate at frequencies below 40 Hz. This aligns with the observed decrease in SC from note 26 to 27. Further examination, with perhaps a complete mapping of impedance at all string attachment points, could reveal more insight into the effect of piano ribs on output sound, but would be very difficult for practical reasons due to a lack of accessibility to the required measurement locations. Conklin [71] did perform a set of measurements like this, but was only able to do so with an unstrung piano. The loading and tension cre-

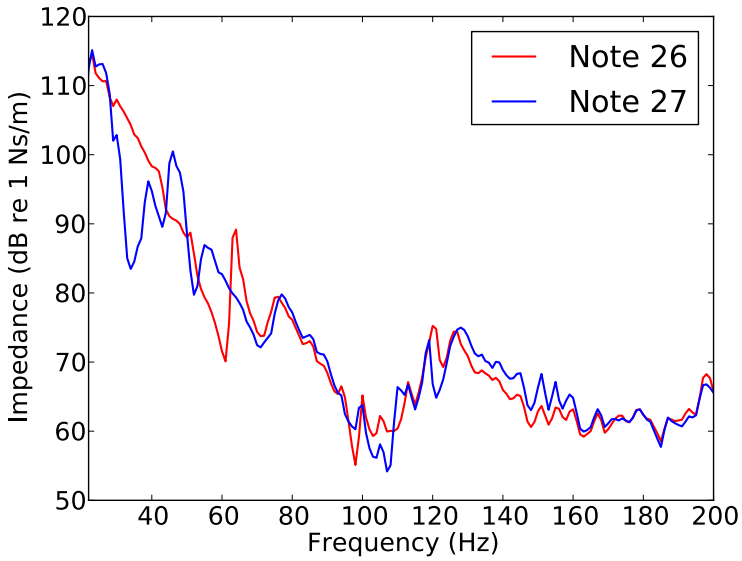

Figure 5.17: Impedance values from 20-200 Hz for note 26 and note 27. Note 26 is located in-between two adjacent bridge-rib intersections and note 27 is located near to a bridge-rib intersection.

ated by the strings is obviously an important aspect of soundboard vibration, but unfortunately the manner in which a piano is strung restricts the access required to do accurate measurements.

In a similar manner to SC, it is possible to plot the same bridge-rib intersections on the TC data for the Hardman grand piano to look for any visible trends or explanation for the observed fluctuations from note to note. Figure 5.18 shows TC plotted with these intersection points.

Once again patterns do seem to appear at the transition and intersection points for TC, with large variations, or direction changes occurring at these locations. In general, the TC data appears to be have more variation than the SC data, but there does seem to be some weight to the hypothesis that the structural variations in the soundboard and bridge due to rib intersections could be influencing these PSPs in the manner described above. More testing and comparison among several different instruments would be needed to fully support this hypothesis.

5.4 Wavelet PSP Analysis

Finally, to give another perspective on this data the wavelet formulations introduced in equations 4.9 and 4.10 for scalogram scale centroid (ScSC) and scalogram time centroid (ScTC) is presented in figures 5.19 and 5.20.

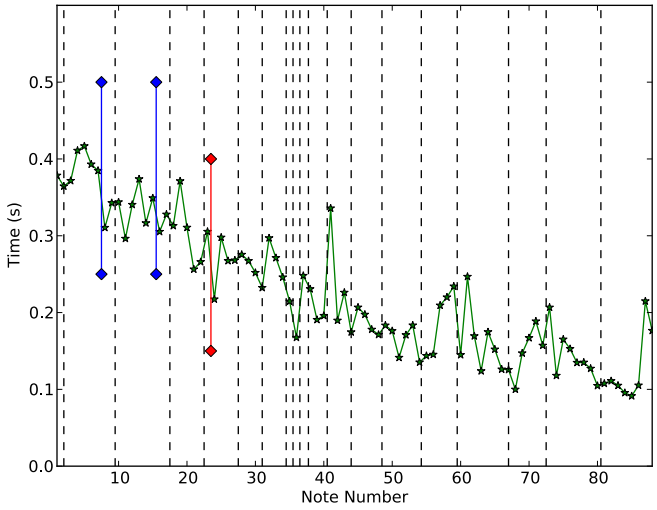

Figure 5.18: Temporal centroid values for the modern Hardman grand piano. Black dashed vertical lines represent bridge-rib intersections, solid blue vertical lines indicate string transitions, and the solid red vertical line represents transition from bass bridge to tenor bridge.

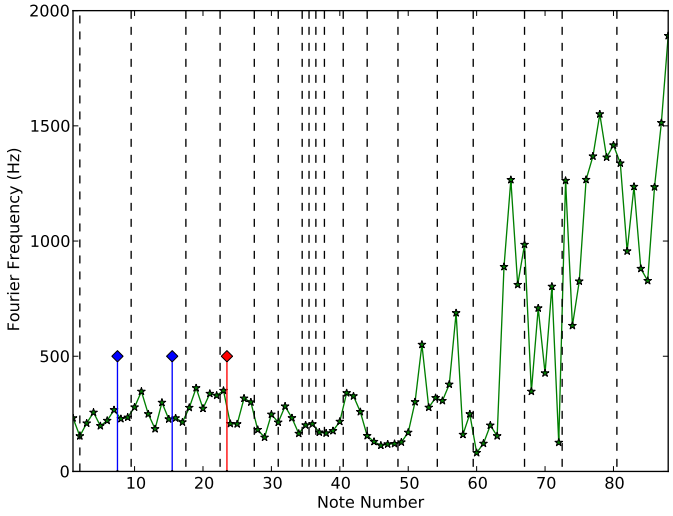

Figure 5.19: Wavelet domain scale centroid values for the modern Hardman grand piano. Black vertical lines represent bridge-rib intersections, blue vertical lines indicate string transitions, and the red vertical line represents transition from bass bridge to tenor bridge.

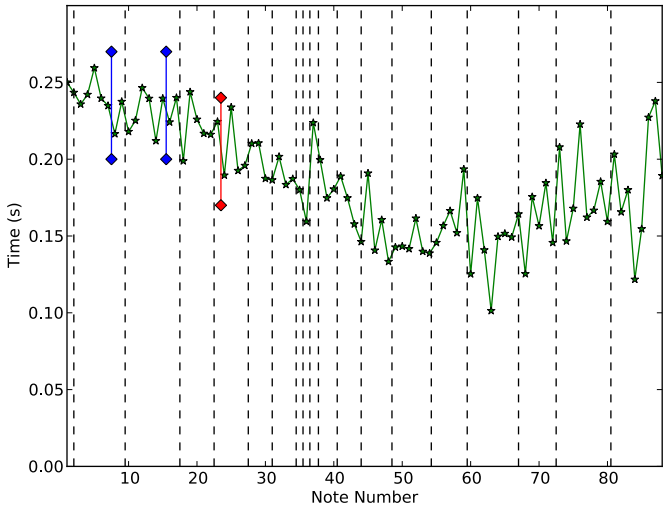

Figure 5.20: Wavelet domain time centroid values for the modern Hardman grand piano. Black vertical lines represent bridge-rib intersections, blue vertical lines indicate string transitions, and the red vertical line represents transition from bass bridge to tenor bridge.

In both of these figures the same general trends can be observed as seen in their Fourier and time domain analogues, but for the high notes (60-88), a much larger amount of variation is witnessed. This is explained by the percussive nature of those high notes of the piano which have very little sustain and a significant impactive component. The wavelet method includes these effects more prominently than the conventional method, but the question remains whether this is perceptually valid. The high notes of the piano are known to be less consistent than the middle and low notes, but this wavelet perspective may also allow us to reemphasize the role of excitation in our perception of these kinds of properties of musical instrument sounds. Perceptual studies would be required to further explore the application of wavelets in this kind of application.

5.5 Conclusions

A number of design features can be seen to have developed corresponding tonal features during the development from the early piano to the modern grand piano. An improved bass response and the presence of more energy in the upper partials, particularly in these bass notes, are due to an increase in soundboard area, the introduction of longer string lengths, and the use of wound strings for bass notes.

More specific studies of the instruments would be required to fully support Breitman's hypotheses [70] that early pianos have a sound with more clarity and

are less 'muddled', but the results of the PSP analysis do lend some support. In particular, the increased temporal centroid in the bass range of the modern grand piano versus the early piano would indicate that these notes, in general, have more sustain. Spectral centroid also trends toward lower values for more modern instruments due to their increased bass response. This is something that is likely due to their larger soundboards and the development of wound strings for bass notes. Improving the bass response of the modern instruments could be considered to have given them a more complex sound that might be interpreted as being more 'muddled' when directly compared to early pianos. The challenges of linguistically describing instrument tone are evident here and emphasize the value of quantitative signal parameters that can be used to describe the properties of sounds.

Sudden localized changes in SC from note to note were also examined for the Hardman grand piano and were observed to possibly relate to the intersection of the soundboard ribs and the bridge near note attachment points. Impedance measurements at notes 26 and 27 indicated that note 27, which is close to a rib, saw a decrease in impedance below 40ż in comparison to note 26. This decrease in impedance means note 27 can more readily vibrate at frequencies below 40 Hz and this aligns with the observed decrease in SC from note 26 to 27. Similar trends are observed near other bridge-rib intersections in terms of SC, but further impedance measurements were not feasible with a fully strung instrument to further support this hypothesis.

The role of MC in piano tone was not investigated directly in this chapter, but it is clear that the effects observed in guitars should also be observed in pianos. The guitar's small size makes it more suitable for this kind of analysis, but if the resources and equipment were available a detailed study of the piano under varying ambient humidity conditions would be a worthwhile direction for future research.

Chapter 6

The Application of Stabilized Wood in Musical Instrument Construction

6.1 Introduction

What is the motivation for using stabilized wood products in musical instruments? For thousands of years musical instruments have been built without stabilized wood technology and, for the most part, have been able to produce exceptional tone when built by the best craftsmen. These instruments represent a compromise, however, as accommodations must be made to ensure that the unavoidable dimensional changes are allowed for when they are built. A perfect example comes from the piano soundboard which is prone to cracking due to expansion and contraction and also suffers from the variations in tone demonstrated earlier in this thesis that occurs with changes in relative humidity.

A stabilized wooden soundboard should do two things: it should stabilize the elastic moduli, damping, and density of the soundboard; and it should also stabilize the structural geometry of the soundboard. The first point is important because changes in elastic moduli, damping, and density, have been shown earlier to affect the tone of an instrument. If these properties can be stabilized then so can the tone of the instrument. The second point, geometric stability, is important because of the way instrument soundboards like those of the guitar and piano are constructed; pre-stressed with a slight curvature. This curvature is used to turn the flat plate into more of a shell element which provides an increase in effective stiffness without adding mass (i.e. stiffening achieved by increasing the thickness of the top will add mass, where arching does not). This curvature is highly important to the sound of both guitars, and even more so, pianos. With geometric stability this soundboard arching (in guitar terms) or crowning (in piano terms) should stay consistent and provide for more consistent tone. With both these kinds of stability the guitar or piano builder would then be able to fine tune the sound of their instruments

knowing that the tone will not be significantly affected by changes in humidity, something which is currently not possible using untreated woods.

To achieve this stability while still retaining a traditional sound we need a process that does not significantly alter wood properties and reduces the effects of moisture transfer. Several methods of stabilization have been explored in the literature, such as saligenin treatment [26], and plasticizing wood, but the acetylation technique is selected and investigated herein because of its long research history and because it has recently become a commercially viable process [27]. Acetylation is a process by which the hydroxyl groups in wood are occupied by a permanently bonded acetyl group. By effectively blocking the sites where moisture transfer can occur the acetylation process can significantly reduce the expansion and contraction due to moisture transfer and also stabilize the mechanical properties of wood. Testing has shown that acetylation is non-toxic, provides long term results (20+ year studies), and has many other secondary benefits aside from stability such as rot-resistance [27]. The Yamaha corporation has also investigated its application in piano construction [25], but the conclusions of the research with regards to the sound of the instruments were limited to qualitative listening tests by a small group of 'experts' who concluded that the test instruments were 'highly evaluated with respect to volume, sound, and expression'. This evaluation may be good enough to be included in a patent application, but has no real objective value.

6.2 Experimental Procedures

A number of tests were conducted to quantify the performance of acetylated wood in comparison to that of the untreated samples. The ultimate goal of these tests is to illustrate the improved stability of the acetylated plate and to hopefully show that the properties of an acetylated soundboard panel are similar to those of an untreated panel. If the acetylated wood can achieve both goals then it can be considered a suitable replacement for untreated woods that can still retain the traditional tone of musical instruments made of untreated wood.

6.2.1 Test Panels

Two book matched sets of Norway spruce guitar soundboard quality wood were procured from a luthier for the purposes of this study. An acetylated panel made from one of the sets was prepared by Accsys Technologies plc., a European wood technology company that has commercialized the acetylation process under the trade name 'Accoya' [28]. The other panel was left untreated and can be considered to be typical of the wood used in guitar soundboard construction. The panels were both made to have a width of 0.4 m in the radial direction, 0.55 m in the longitudinal direction, and a thickness of 4 mm in the tangential grain direction.

The acetylated board was calculated to have a weight percentage gain (WPG) of approximately 20%, a value generally agreed upon as being an ideal WPG in terms of stabilization [27, 29]. The panels were then acclimatized in a small humidity chamber which used silica-gel packs to reduce the relative humidity level present in the chamber. An example of the acclimatization cycle for one test is provided in figure 6.1.

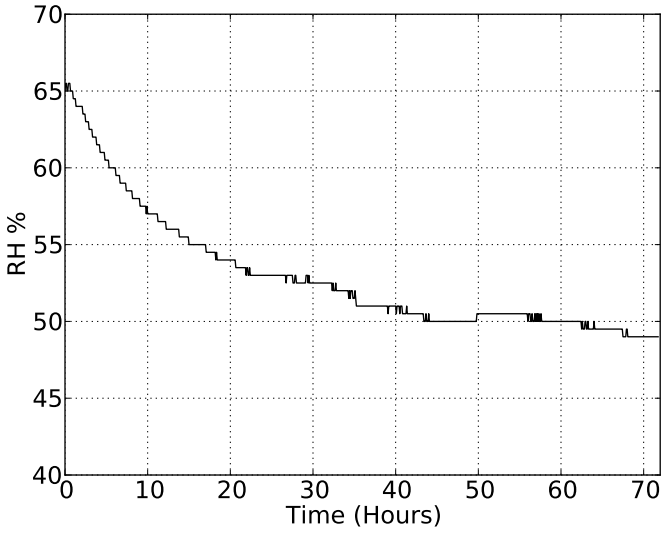

Figure 6.1: Relative humidity in acclimatization chamber. The small fluctuations in RH seen as the curve approaches steady state are due to changes in room temperature, for instance from day to night.

6.2.2 Dimension and Mass

The dimensions and mass of the soundboard panels were measured during testing and used to determine the moisture content of each board. The relative humidity that the boards were acclimatized at was recorded, along with the mass and overall dimensions of the plate. A tape measure was used to measure length and width, and a micrometer was used to measure thickness. Eliminating dimensional change, particularly in the radial direction, is a major goal of this testing as improved dimensional stability implies improved geometric stability.

6.2.3 Modal and Impedance Testing

Modal and impedance tests were conducted on the test panels, which were considered to be orthotropic as they were quartersawn, using a similar analysis package, equipment, and methodology as described in chapter 2. In the current plate testing procedure a fixed shaker/roving accelerometer method was used and the plates

were clamped in a rigid steel frame seen in figure 6.2. The plate was excited with a white noise signal and measurements were taken at 35 distributed grid points on the plate. The shaker method introduces the possibility of mass loading the plate, but since the relative performance was considered the most important the use of the shaker method allowed for improved accuracy in terms of coherence.

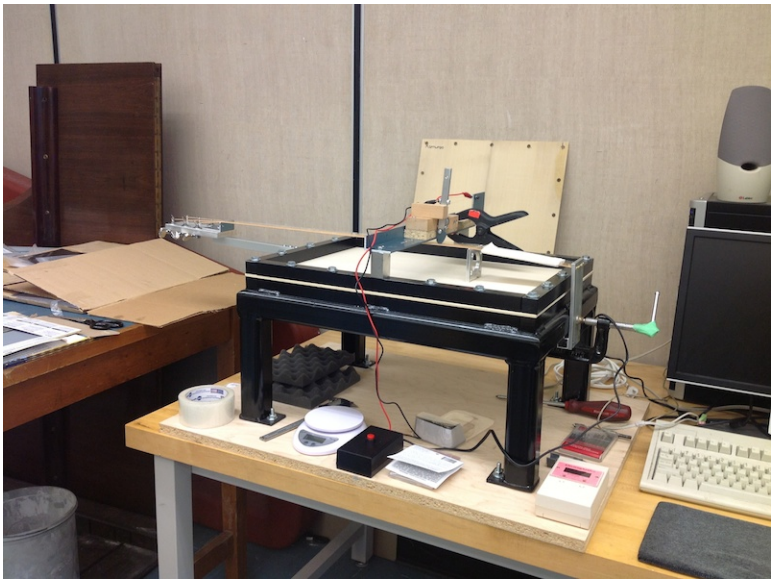

Figure 6.2: Test apparatus used for vibration testing of acetylated and untreated plates.

Another free boundary condition test was also conducted to calculate Young's modulus using the approach of Larsson [72]. In this method the value of Young's modulus is determined from the first bending mode in the longitudinal direction from the equation:

$$E = f_{(2\,0)}^2 \rho \frac{19L^4}{2\pi^2 h^2} \tag{6.1}$$

where $f_{(2\,0)}$ indicates the frequency of the (2 0) bending mode for free boundary conditions. A schematic of the mode shapes and naming conventions for the modes presented herein can be seen in figure 6.3. Modal testing was repeated at two different locations, MP1 and MP2, to ensure modes were not missed.

Impedance was measured using an accelerometer with a force sensor attached to the shaker. The impedance measurements were made at MP2 as shown on the schematic seen in figure 6.4.

6.2.4 Wood Classification

Wegst [1] and Yoshikawa [5] both present schemes that aim to provide a typical range of acceptable material properties used in the soundboards of musical instruments calculated from the values of woods traditionally used for this purpose. To

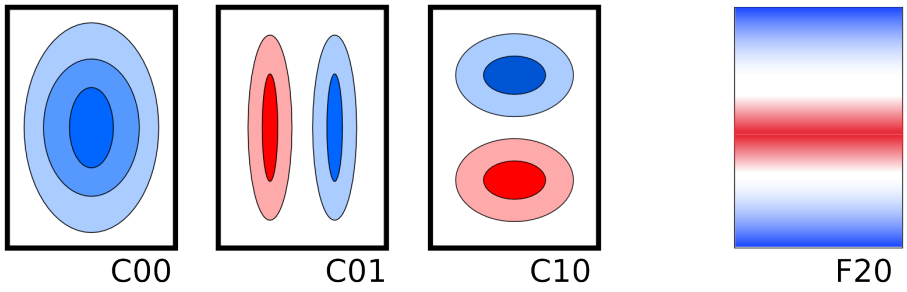

Figure 6.3: Modes shapes and naming conventions for transverse bending modes for both free (F20) and clamped boundary conditions (C00, C01, C10)

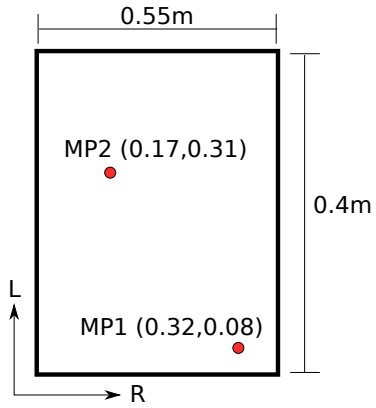

Figure 6.4: Schematic representation of the modal and impedance measurements with MP1 and MP2 indicated.

determine these ranges they use the results of modal analysis, Young's modulus, and mass/dimension properties to calculate derived parameters. For Wegst these parameters are loss coefficient:

$$\eta = \frac{1}{Q} = \frac{\Delta f}{f} = \text{Damping Percentage} \tag{6.2}$$

and sound radiation coefficient:

$$R = \frac{c}{\rho} = \sqrt{\frac{E}{\rho^3}} \tag{6.3}$$

where f is the frequency value of a modal peak,Δf is the -3 dB width of that peak, E is Young's modulus, c is speed of sound, and ρ is density. Yoshikawa defines two parameters using the same material properties, the anti-vibration parameter and the transmission parameter:

$$\text{AVP} = \rho/c \tag{6.4}$$

$$\text{TP} = cQ \tag{6.5}$$

By comparing the performance of the acetylated and untreated plates with regards to these parameters their suitability as soundboard materials can be assessed. It should be noted that none of these parameters are non-dimensionalized, something that might be useful if comparisons between systems of different dimension are being made. Wegst and Yoshikawa examine 'soundboard woods', without qualifying the woods by instrument size or construction. The much larger size of a piano in comparison to that of a guitar might be an example where a non-dimensionalized parameter would be more appropriate to allow a better comparison between the materials used in the two different instruments. Despite the advantage of non-dimensionalized parameters these dimensional parameters are used to provide context in terms of the observed properties of the two test plates in relation to properties reported in above-mentioned studies.

It should also be noted that no indication is given of the MC or the method of determining damping in the Wegst paper and Yoshikawa's material property values are selected from a variety of sources with no indication of MC. The experimental results obtained with the acetylated and untreated plates will be plotted against these schemes to see how they perform in comparison to each other and to traditional soundboard materials.

6.3 Results and Discussion

6.3.1 Dimension and Mass

The primary motivation for the development of wood stabilization techniques is to provide dimensional stability. As expected the acetylated board had significantly

less dimensional change, particularly in the radial direction of the plates. Results for the length, width and thickness are presented in figure 6.5.

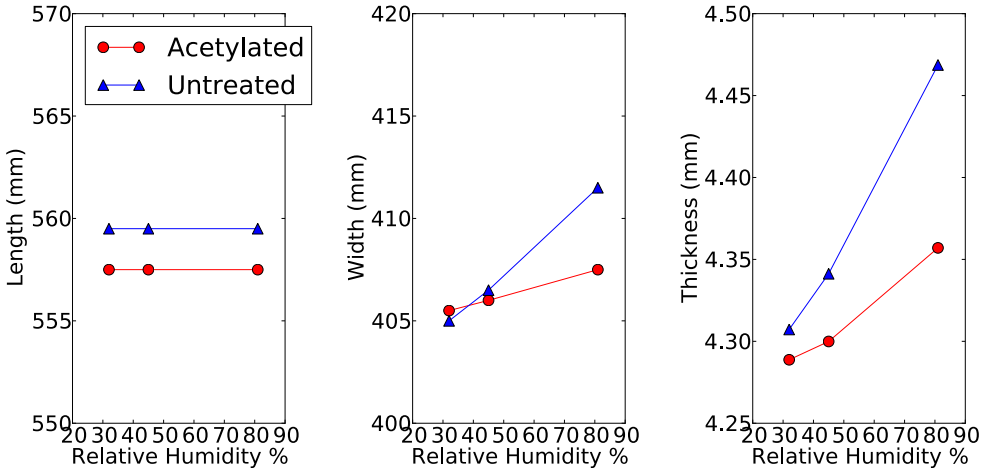

Figure 6.5: Dimensional change of the test plates at various RH levels.

It is observed that the acetylated board varied significantly less in thickness and width versus the untreated board. In the radial (width) direction the untreated board can be seen to expand 6.5 mm while the acetylated board varied by approximately 2 mm. The length direction for both plates did not vary significantly.

Variations in mass, moisture content, and density as a function of RH are presented in figure 6.6. The mass is the parameter which is directly measured, with the MC and density calculated from the mass and dimensions of the plate. The oven dry mass used in the calculation of MC was observed to be 399 g for the untreated plate and 509 g for the acetylated plate.

Again, the acetylated board can be seen to have significantly smaller variations in all parameters as a direct result of less swelling/shrinkage due to fewer available hydroxyl bonding sites. MC varies from about 6% to 13% for the untreated plate, but only from about 2% to 4% for the acetylated board over the same RH range. The acetylated board is observed to be significantly more dense in all RH conditions due to the higher molar mass of the acetyl group that is bonding to the hydroxyl groups present in the wood in comparison to lighter water molecule that occupies the same sites in the untreated panel.

One final indication of the improved stability of the acetylated board is seen in figure 6.7. This figure shows the permanent damage caused by oven drying both sample plates after the boards have been allowed to reacclimatize to normal indoor humidity conditions for one week. The acetylated board shows much less distortion in comparison to the untreated board.

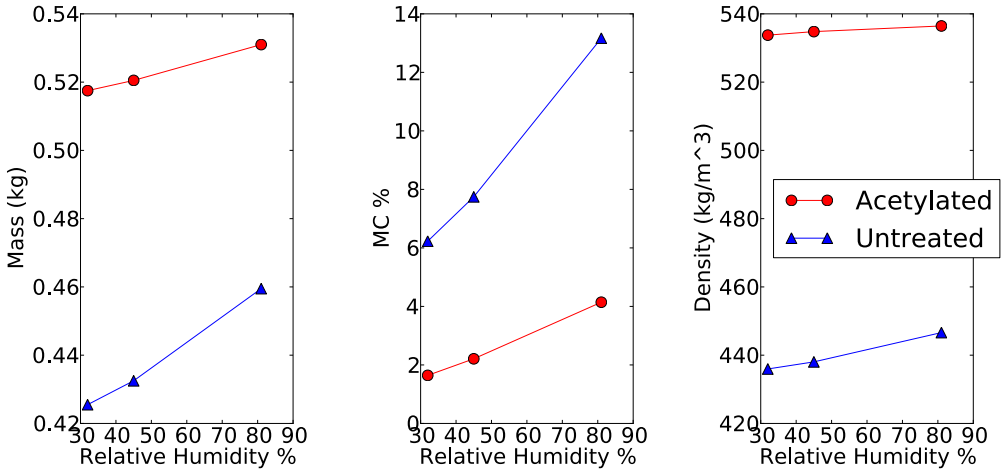

Figure 6.6: Mass, moisture content, and density of the test plates at various RH levels.

6.3.2 Modal Analysis

To simplify the analysis the modal results are reported in terms of the first three vibration modes for both plates. Modal frequency as a function of RH for the three clamped vibration modes C00, C01, and C10 are provided in figure 6.8.

A general decreasing trend can be seen from low to high humidity for all three modes as expected, with the exception of the acetylated board for mode C10 at the medium humidity level. In all cases the change in frequency of the modes was less for the acetylated boards in comparison to the untreated board. As a wooden plate absorbs water it tends to decrease in terms of the elastic moduli [3], and correspondingly the less stiff plate would expect to see a drop in modal frequencies. The opposite is true in terms of modal damping, with an increase expected at higher RH levels. This result can be seen in figure 6.9 where modal damping percentages are plotted against RH.

The observations of modal damping show that the untreated plate varies more in terms of damping percentage, with a particularly large effect noticed for the first vibration mode and the expected general trend of increasing damping with increasing RH. The behaviour of the acetylated board is less consistent, but also varies less than the untreated board. Measurements of the free boundary condition plate were also conducted for use in the calculation of Young's modulus in the longitudinal direction using Larsson's method [72]. Modal frequency values for the plates at varying RH are presented in figure 6.10.

The general behaviour is similar to the previous results, with a general decrease in the F20 mode's frequencies as the boards absorb moisture and become less stiff and more dense. The untreated board has a larger change in frequency than the

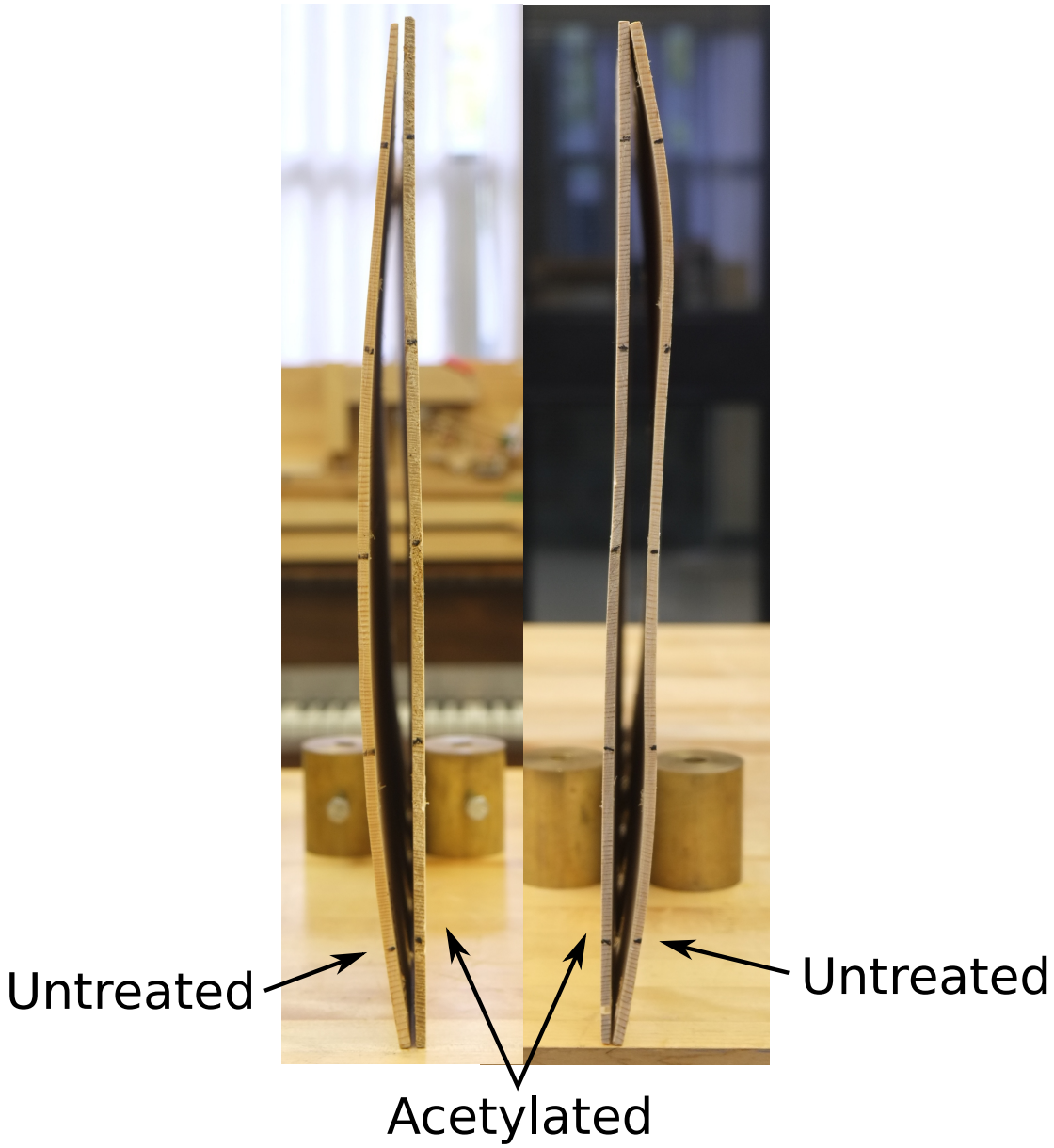

Figure 6.7: Permanent warping of acetylated and untreated plates after oven drying and reacclimatization at normal indoor humidity levels for one week.

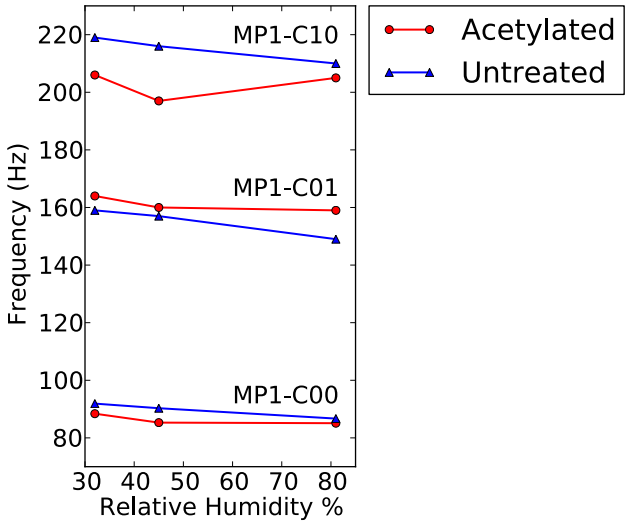

Figure 6.8: Modal frequency values measured at MP1 for modes C00, C01, and C10 plotted against relative humidity.

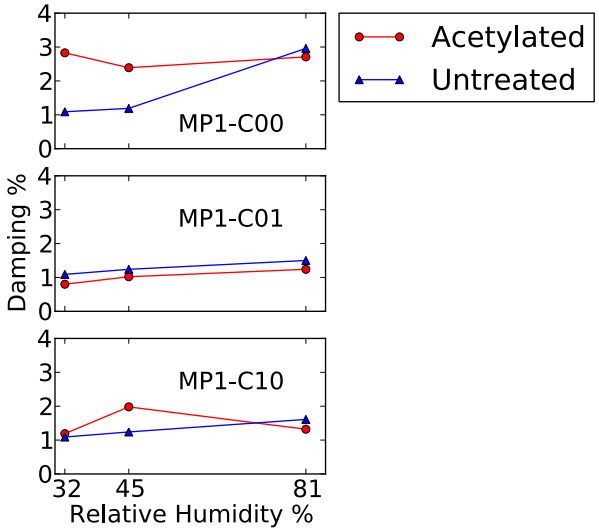

Figure 6.9: Modal damping values measured at MP1 for modes C00, C01, and C10 plotted against relative humidity.

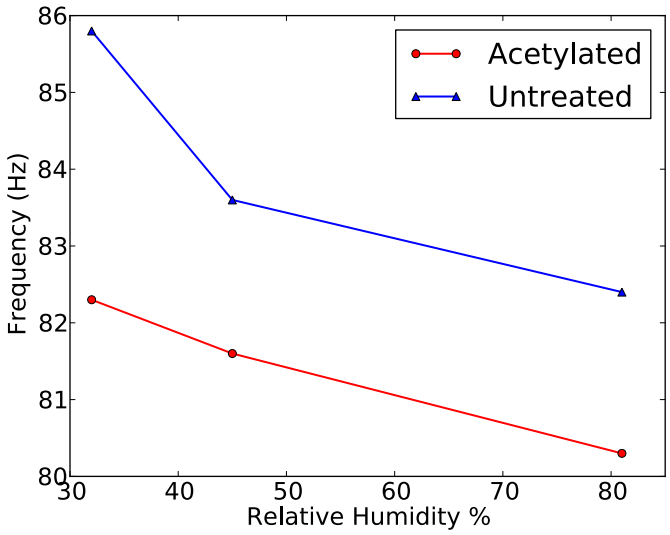

Figure 6.10: Modal frequency values measured at MP1 for mode F20 plotted against relative humidity.

acetylated board and this difference plays directly into the calculation of Young's modulus, E_L from equation 6.1. Values calculated for the two plates are shown in figure 6.11.

As expected the Young's modulus of the acetylated board is about 15% higher than the untreated board, but also varies less as a function of RH. The values calculated for the untreated board seem slightly high for typical values of Norway Spruce (12-14 GPa) [4, 11], but as the wood is soundboard grade increased density and E_L are expected. Yoshikawa [5] presents a value of 16 GPa for Norway Spruce which is directly in line with the observed values. Ultimately the relative behaviour of the plates as a function of humidity is the most important aspect of this study, so these values were considered acceptable.

6.3.3 Impedance

Another common measurement used for comparison purposes in musical acoustics is impedance (or its inverse mobility). Impedance curves are presented for measurements at MP2 in figures 6.12 and 6.13 after acclimatizing the plates at the three different RH values.

For both the untreated and acetylated plates the largest differences occur above 300 Hz, but a more quantitative method of comparing the similarity of the curves is useful. By treating each impedance curve as an n-dimensional vector, where n is

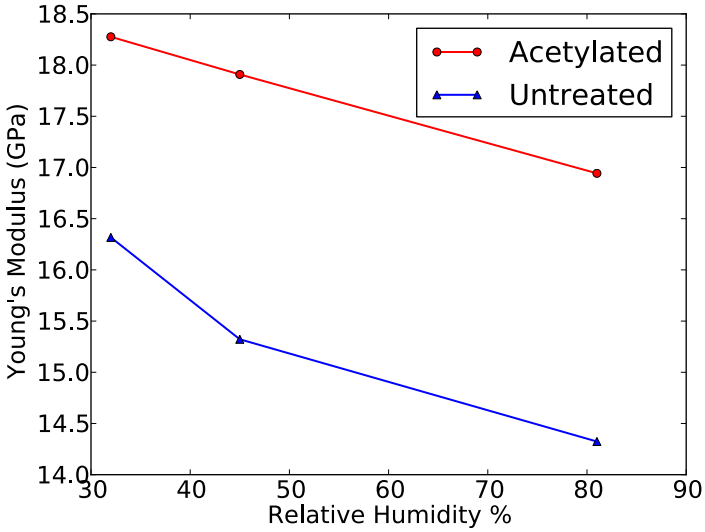

Figure 6.11: Young's modulus in the longitudinal direction calculated from modal frequencies of mode F20 plotted against relative humidity.

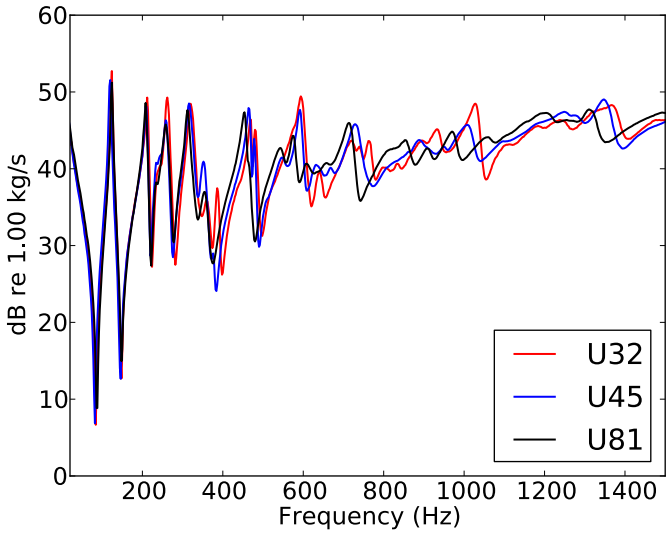

Figure 6.12: Impedance measured at MP2 of the untreated plate for 32% RH (U32), 45% RH (U45), and 81% RH (U81).

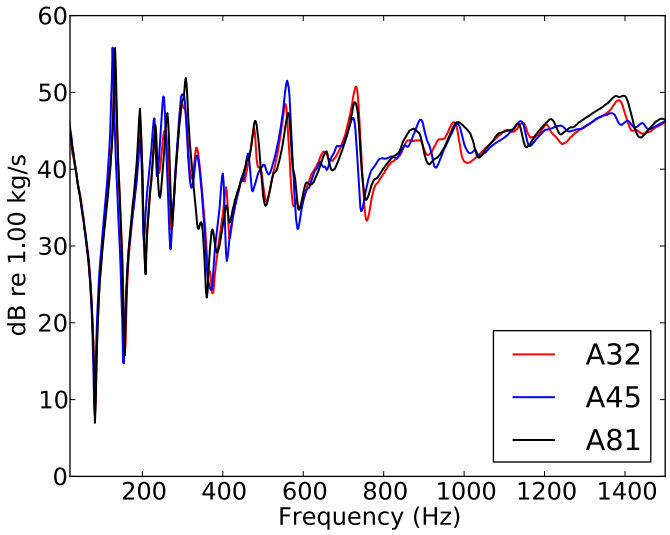

Figure 6.13: Impedance measured at MP2 of the acetylated plate for 32% RH (A32), 45% RH (A45), and 81% RH (A81).

Table 6.1: Cosine Similarity of Impedance Curves by Plate Treatment

RH Comparison	Untreated	Acetylated
32% - 32%	1.0	1.0
32% - 45%	0.9981	0.9980
32% - 81%	0.9968	0.9988

the number of data entries in the curve, the cosine similarity can be calculated as:

$$\text{similarity} = \cos\theta = \frac{A \cdot B}{||A||\,||B||} \tag{6.6}$$

where A and B are the vectors being compared and the similarity value varies between -1 and 1, with 1 meaning exactly the same, 0 indicating independence, and -1 meaning the vectors are exactly the opposite [73]. Cosine similarity values comparing the behaviour of the two test panels against themselves at different RH levels are presented in table 6.1.

In the grand scheme the variations in the impedance curves as a function of RH can thought to be quite minor, but it is interesting to note that again, the untreated board has a larger difference than the acetylated board in terms of cosine similarity from 32% to 81% RH. In other words, the acetylated board is observed to be more stable.

Typically the vibrational performance of soundboards of musical instruments is discussed in terms of a modal region in the lower frequency bands and an impedance

region in the higher frequency bands [74, 75]. This type of behaviour is exactly what was seen in the performance of both plates, with the acetylated plate being more stable in terms of both low order modal values and high frequency impedance values. A final comparison of impedance values is seen in figure 6.14 which compares the untreated and acetylated board directly at 32% RH.

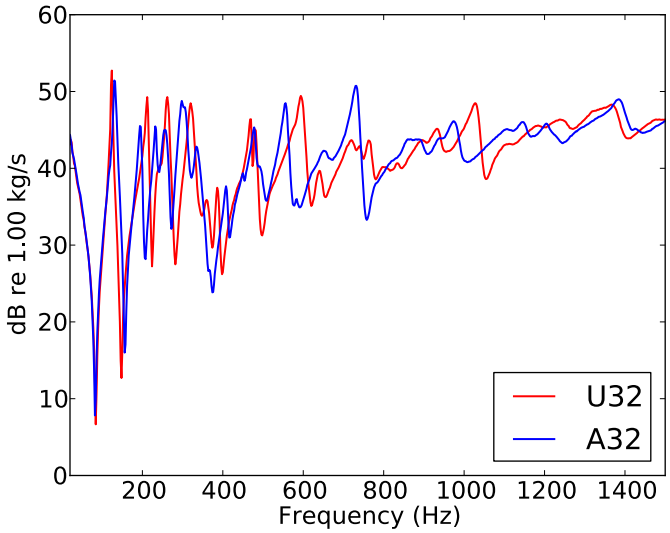

Figure 6.14: Impedance measured at MP2 of the acetylated (A32) and untreated (U32) plates at 32% RH

Although not identical, the general behaviour of both curves at 32% RH is quite similar (cosine similarity of 0.9936 comparing the untreated and acetylated boards) and supports the idea that using acetylated wood improves stability, but does not significantly alter the vibrational properties of a wooden plate typical of musical instrument soundboards. Figures 6.15 and 6.16 show the same type of general behaviour for the 45% RH comparison (cosine similarity of 0.9949) and the 81% RH comparison (cosine similarity of 0.9949) respectively.

6.3.4 Wood Classification

Finally, the wood classification studies of Wegst [1] and Yoshikawa [5] provide another avenue by which to compare the performance of the test panels not only to themselves, but against typical woods used in musical instrument soundboards.

Two of Wegst's plots are recreated herein, one that plots density and Young's modulus seen in figure 6.17, and another that plots loss coefficient versus sound radiation coefficient in figure 6.18.

In figure 6.17 both the untreated and acetylated plates have material properties that land within the typical range observed by Wegst. The acetylated plate is

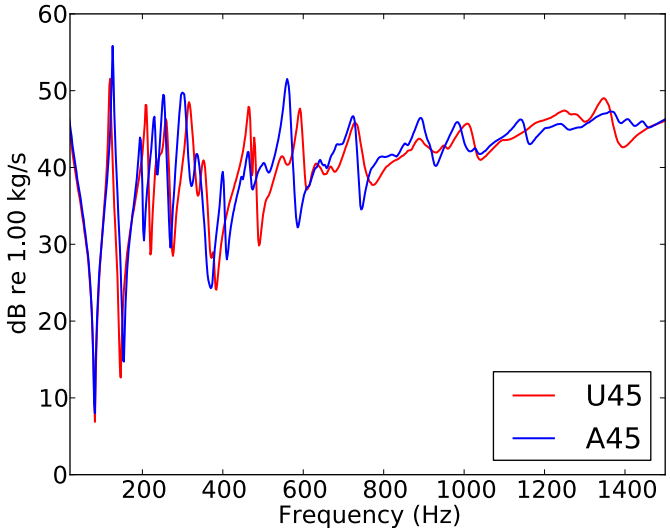

Figure 6.15: Impedance measured at MP2 of the acetylated (A45) and untreated (U45) plates at 45% RH

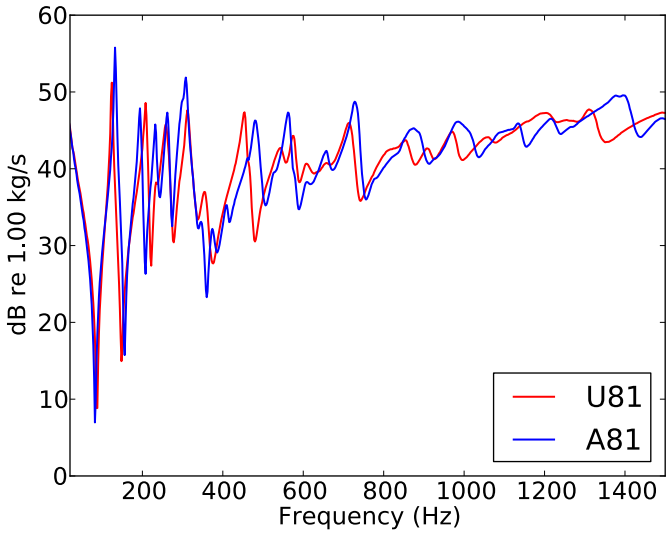

Figure 6.16: Impedance measured at MP2 of the acetylated (A81) and untreated (U81) plates at 81% RH

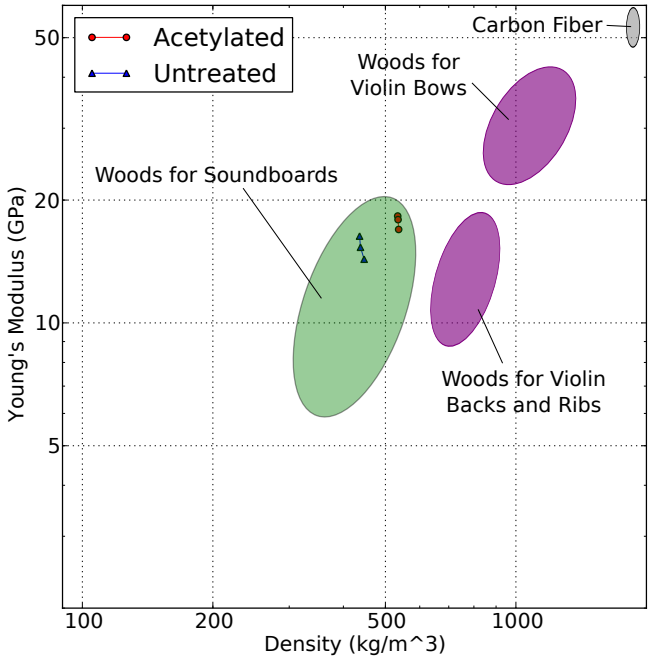

Figure 6.17: Material properties density and Young's modulus for both acetylated and untreated boards with varying humidity plotted on the Wegst [1] classification scheme for soundboard woods (replotted from the original). The green ellipse represents the range of material properties typical of woods used as musical instrument soundboards.

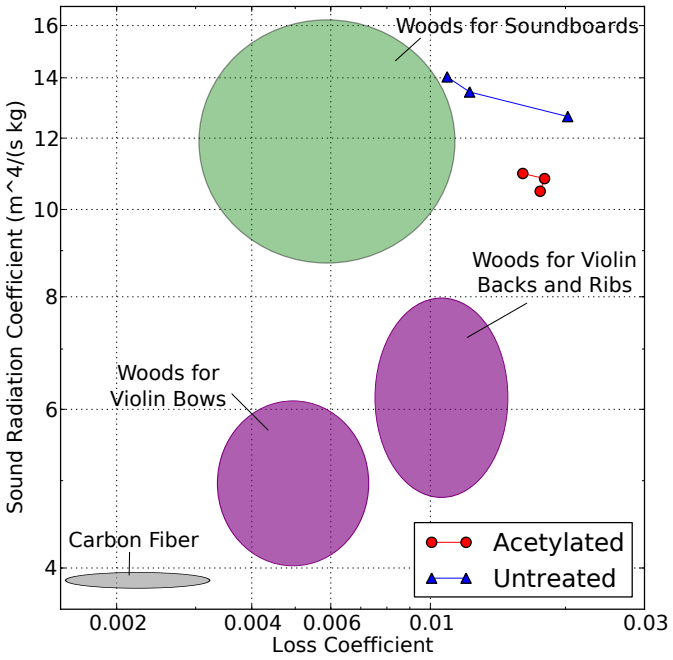

Figure 6.18: Material properties loss coefficient and sound radiation coefficient for both acetylated and untreated boards with varying humidity plotted on the Wegst [1] classification scheme for soundboard woods (replotted from the original). The green ellipse represents the range of material properties typical of woods used as musical instrument soundboards.

again observed to vary less than the untreated plate as expected from the previous results discussed above. Figure 6.18 also presents a similar result with the acetylated plate observed to be more stable than the untreated plate, but with both materials having higher loss coefficient values than those reported by Wegst. One of the challenges when working with a material like wood is that measurements are affected by the environmental conditions and natural variability in the test samples themselves, something that is often underreported in the literature. Unfortunately the methods by which the loss coefficients were determined are not reported by Wegst and it is quite possible that the differences in measurement technique and sample preparation could create these kinds of differences between the observed results for the two test plates and those presented by Wegst for typical soundboard woods. Inquiries into the experimental methods were made, but no reply was received. Loss coefficient is a frequency dependent property and the reported numbers in figure 6.18 were calculated as an average of the damping values of the first three modes. If Wegst used data selected from only one mode, or made an assumption of frequency independence like Yoshikawa [5] below 1 kHz, then the difference between their reported values and those observed herein can be explained. It should be noted that damping is a difficult property to measure, particularly in this context, and the ideal method of comparison would be to have all researchers use the same test methodology in their measurements. The overall magnitude of the loss coefficient parameter is ultimately not as important in the comparison of the stability of the acetylated panel versus the untreated panel, as the acetylated plate can be seen to vary less than the untreated plate in Wegst's classification scheme.

In Yoshikawa's classification scheme two parameters are defined: antivibration parameter (AVP) and transmission parameter (TP) and observed values for these parameters are seen in figure 6.19 as a function of RH.

The large variability of the untreated plate is again visible here with the acetylated plate seen to be much more stable than the untreated plate. It should be noted again that in a similar manner to the Wegst data the effect of measurement technique and environmental conditions may be influencing the results. If it is assumed that the observed damping values are slightly high for the untreated and acetylated plates tested as part of this study the effect of normalizing them would be to shift them upwards along the transmission parameter axis, closer to Yoshikawa's reported values. Yoshikawa does report the measurement technique used to calculate damping, but this varies from the technique used herein and in Yoshikawa's method is only measured at one frequency and is assumed frequency independent below 1000 Hz, a simplifying assumption.

Typical values of soundboard woods reported by Yoshikawa are also plotted to provide a context for the applicability of the two test panels as musical instrument soundboards. Once again both the untreated and acetylated boards are observed to be within the range typically reported for woods used in musical instrument soundboards. The soundboard woods cluster near the regression line, with fairly large variations among the different wood species. Yoshikawa's data are taken from

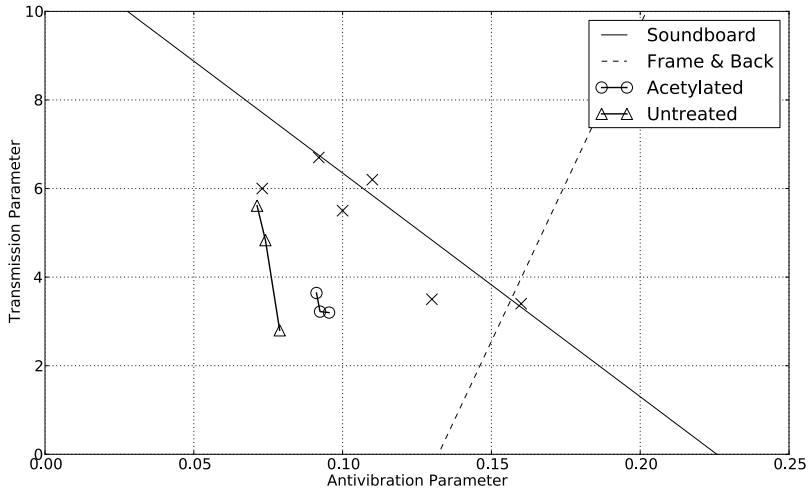

Figure 6.19: Material properties antivibration parameter and transmission parameter for both acetylated and untreated boards with varying humidity plotted on the Yoshikawa [5] classification scheme for soundboard woods. The solid line represents a regression fit for standard soundboard woods and the dashed line represents a regression fit for woods used in the frame and backs (for violins, guitars, etc.) of stringed musical instruments as defined by Yoshikawa.

the scientific literature and the MC's of the test samples are not reported. The large variation of the untreated plate as a function of RH is more evidence that MC is an important factor that needs to be reported with any wood testing as it can be seen to have a significant effect on the observed results.

6.4 Conclusions

Further experimental studies of a larger scale would be needed to confirm these results, but as a preliminary assessment it can be seen that the use of acetylated wood products as more stable alternatives in musical instrument construction is quite promising. Compared to untreated wood it has been shown that the acetylated board is more stable in terms of damping, modal frequencies, Young's modulus, density, and also derived parameters used in classification studies such as those presented by Wegst [1] and Yoshikawa [5]. Listening tests similar to those of chapters 2 and 3 would likely also be useful to provide a comparison in terms of perceived stability.

In summary, acetylated Norway spruce wood is shown to perform mechanically in a similar way to untreated wood. An increase in both stiffness and density is noted for acetylated wood related to the chemical process utilized in stabilization, yet even after modification the wood properties still remain within the range of

acceptable material choices used for soundboard woods in musical instruments. For Yoshikawa's [5] classification the parameters are combinations of density and stiffness, or damping and stiffness, so if both increase by similar amounts little overall effect will be observed. With this added stability musical instrument builders could fine tune their instruments with more confidence in the stability of their tone in a broader range of RH conditions without having to use a material like carbon fiber that can have properties far removed from those of typical soundboard woods [1] depending on composition and layup. That said, Ono and Isomura [76] have explored carbon fiber's application in relation to guitars and there are currently a number of commercially available instruments on the market. The reception of these instruments has been mixed with regards to both tone and aesthetics.

The recent commercialization of the acetylation process provides even more motivation for the use of stabilized wood products in musical instruments as this material can be more readily acquired. Currently there are no resources specifically producing acetylated musical instrument grade woods, but this is a promising possible direction for commercial development. Beyond just soundboard woods, any of the wooden components used in musical instruments would theoretically benefit from stabilization. An example can be seen in the piano keys themselves, which are made from long pieces of wood and are finely adjusted by a piano technician to ensure a consistent feel for the performer and the proper actuation of the action mechanism itself. From the fine components of a grand piano action to the entire woodwind family, stabilized products would reduce variation in tone and mechanical performance, and would likely be welcomed by instrument builders as long as the properties of these stabilized materials can be shown to not vary significantly from the materials traditionally used for these purposes.

Chapter 7

Conclusions and Future Work

The motivation for the present research was to explore the role of ambient humidity, and correspondingly, moisture content (MC), on the tone of musical instruments made of wood; and to develop new techniques for understanding the links between tone and design. Two instruments proved to be the focus for this work, the piano and the guitar, and a number of experimental and analytical techniques were used to assess the behaviour of these instruments as a function of MC. The first step was to quantitatively show that MC changes are perceptible as changes in tone. A finite difference model was then developed to allow fine control over the MC parameter that was not possible using real instruments and real wood. The model was verified against the preliminary listening tests used as the basic motivation for this thesis, and a just-noticeable difference level was established using an adaptive three alternative forced choice method (3AFC). The concept of wavelet based psychoacoustical signal parameters was also explored both theoretically and practically, with an application of the technique presented through a study of historical pianos. Finally, an experimental examination of stabilized wood was conducted to assess its applicability in musical instrument construction to help control an instrument's tone. Conclusions drawn from each of these research components will be presented below.

7.1 Conclusions

7.1.1 3AFC Guitar Testing

The primary purpose of the 3AFC guitar testing was to quantitatively provide evidence for the anecdotal claim that musical instrument tone varies with changes in humidity. A guitar was acclimatized at three different relative humidity (RH) levels, corresponding to 7%, 9%, and 11% MC, and recordings were made of the six open strings. A 3AFC testing procedure was then used to conduct a series of listening tests to see if tonal differences were perceptible between the low, medium,

and high MC levels. Other factors such as pitch and loudness were normalized to ensure the only free variable was related to tonal aspects of the sound affected by MC differences. The results of this experiment were promising as changes in MC were found to be highly perceptible within the range of normal indoor seasonal variations in RH. A pitch effect was also observed with higher pitches being more readily distinguished, or in other words, being more significantly effected by changes in MC. This study provided the basic motivation for the subsequent research in this thesis as it strongly supports the hypothesis that variations in MC are perceptible as variations in tone.

7.1.2 Simulation, Validation, and JND Levels

The ability to finely control the MC property was then needed to further investigate the role of MC in tone. Controlling the MC of the wood in a real instrument provides a significant challenge, and as such a mathematical model was developed to allow for this desired level of control using simulated sounds. A finite difference method was adapted from Bilbao's [13] approach and material property data from Pérez et. al. [4] was used as inputs to an orthotropic Kirchhoff thin plate model. The behaviour of the model was validated by performing a second set of listening tests in the same 3AFC style and experimental conditions described above, with the only difference being that instead of real recordings from an actual guitar the sounds samples were created using the computer model. The model was considered validated after comparing the average subject response to both the real and simulated sounds which aligned quite closely.

The validated model was then used in an adaptive 3AFC approach to find a just-noticeable difference (JND) level of approximately 0.7%MC (i.e. sounds simulated at 7.0% and 7.7%MC are just-noticeably different). In terms of relative humidity this corresponds to approximately a 10% difference, or that instruments acclimatized at 30% RH and 40% RH would be just noticeably different. This result highlights the sensitivity of human tone perception and provides motivation for the introduction of stable alternatives into the construction of musical instruments. If humans are this highly tuned to tonal differences then finding materials which are less sensitive to variations in RH may be considered to be an improvement. The challenge with establishing a goal like this, however, is to choose to either use materials that vary dramatically from wood in both mechanical properties and appearance, or to try to retain a traditional sound and appearance by finding materials that are stable and also retain the traditional qualities of wood.

7.1.3 Wavelets

The application of wavelet methods has been explored in a variety of fields [53, 54] and has provided many interesting results. Although used in certain music analysis and compression tasks, the use of wavelets in psychoacoustical signal parameters

(PSPs) has not previously been explored. PSPs are conventionally calculated from the time signal and its Fast Fourier Transform (FFT) frequency domain representation, something that poses a challenge for representing the short, impactive components typically found in the excitation portion of a musical instrument sound. This challenge is due to the FFT's inability to accurately represent non-periodic components in the frequency domain. By replacing the FFT representation of the signal with a wavelet transform version a much more accurate representation of the impactive components can be made in the 'frequency' domain, which then in turn can be used in the calculation of wavelet domain based PSPs.

A series of test signals with idealized impactive components were analyzed using both traditional and wavelet domain PSPs to determine if the theoretical improvements achieved through the use of the wavelet transform were real. The results clearly indicated that the wavelet domain PSPs were more sensitive to changes in the impactive sound components than their Fourier equivalents, as expected.

The biggest drawback to using the wavelet approach is that the transform produces a 2D time-scale output which is more difficult to interpret. Instead of using pure sinusoids to decompose the signal, like the FFT, the wavelet transform can use a wide variety of different wavelets to do this decomposition. As a result the interpretation of the wavelet transform does not occur at discrete pure frequencies, but instead at an equivalent Fourier frequency that is the primary frequency component of the wavelet at a particular scale. All of this makes the interpretation of results in the wavelet domain that much more complicated; but it is this added cost that results in increased time and frequency resolution not possible with PSPs based on Fourier transforms. In general it can be concluded that wavelet methods can provide a better representation in sound analysis where aperiodic sound components are present. The usefulness of the wavelet approach was also demonstrated in the context of MC where an increased sensitivity in terms of wavelet scale centroid was observed for guitar sounds recorded at different MC levels in comparison to conventional PSPs calculated in the Fourier domain.

7.1.4 The Evolution of Piano Design

The design of the piano has evolved over the centuries from the small fortepiano, with leather wrapped hammers, to the large modern design of the grand piano, with felt hammers and wound strings. An improved bass response and the presence of more energy in the upper partials was observed in the tonemaps of modern grand pianos, particularly in the bass notes, in comparison to those of the smaller fortepiano. These differences are explained by an increase in soundboard area, the introduction of longer string scale lengths, and the use of wound strings for bass notes in the modern design.

One observation put forth by Breitman [70] describes the sound of early fortepianos as being more clear and less 'muddled'. The results of psychoacoustical signal parameter analysis do lend some support to this observation. In particular, the

increased temporal centroid in the bass range of the modern grand piano versus the fortepiano would indicate that these notes have more sustain. In terms of spectral centroid a trend toward lower values for more modern instruments that is due to their increased bass response was observed, something that is likely due to their larger soundboards and the development of wound strings. With an improved bass response these modern instruments could be considered to have a more harmonically complex sound that could be interpreted as being more 'muddled' when directly compared. The challenges of linguistically describing instrument tone are evident.

A serendipitous conclusion was also drawn from the examination of the spectral centroid values of a modern style Hardman grand piano. A relatively smooth change in spectral centroid value was expected from note to note, but at certain points sudden jumps in spectral centroid values were observed. A connection was made between the intersection of the bridge and the ribs of the soundboard near to note attachment points and these sudden fluctuations in spectral centroid. To do this the change in impedance of notes near to one of these intersections was examined and significant differences were observed for adjacent notes, where one note was attached to the bridge near to a bridge-rib intersection and the other was located in between these bridge-rib intersections. Further impedance testing would be needed to fully support this explanation, but was not feasible with a fully strung instrument due to accessibility issues.

7.1.5 Stabilized Wood for Soundboards

To provide long term tonal stability requires stability in terms of both the geometry and structure of a musical instrument, and also stability in terms of the material properties of the vibrating system. Structural changes are related to things such as the crowning of a piano soundboard or the curvature imparted to a guitar top. As untreated wood expands and contracts with variations in MC the dimensions and geometry of the instrument will also change and in turn create changes in tone. MC has also been shown to have an effect on the material properties such as density and Young's modulus. Generally speaking increases in MC result in increased density and mass, and decreased values of all the elastic moduli, with internal friction/damping also effected.

Examining this effect experimentally was the goal of the final chapter of this thesis and the acetylation technique was chosen to produce the stabilized wood. Acetylation is a technique that bonds acetyl groups to the hydroxyl groups present in wood that are the normal sites for moisture absorption. By occupying these sites with acetyl groups the acetylated wood becomes less susceptible to variations in material properties and dimension due to changes in MC. The performance of this stabilized wood was then examined with regards to its vibrational properties and compared to an untreated sample of the same species. The properties of both samples were also plotted against existing wood classification studies that identified target ranges for woods typically used in the soundboards of musical instruments.

Although acetylated wood is already known to be stabilized in terms of its dimensional and mass properties [27], the tests completed herein of its application as a guitar soundboard also showed increased stability in terms of vibrational properties. Acetylated wood was observed to not be perfectly stable, but it was shown that it does greatly increase stability while still retaining acceptably similar material properties in comparison to untreated wood. Both the untreated and acetylated test panels were found to have properties typical of soundboards as categorized by Wegst [1] and Yoshikawa [5]. It should be noted that the classification schemes reported by Wegst and Yoshikawa did not consider or control MC and the types of variations in material properties discussed throughout this thesis. From the observed experimental results MC was seen to have a significant effect on the performance of wood in these classification schemes. Acetylation was also shown to create an increase in density and stiffness in comparison to the untreated test panel while modal analysis and impedance measurements were seen to be fairly consistent in terms of overall behaviour. The tradeoff between added stiffness and mass due to the acetylation process seemed to cancel out in terms of vibrational properties allowing the acetylated panel to score similarly to the untreated panel in the classification schemes of Wegst [1] and Yoshikawa [5].

One of the existing methods to deal with MC issues in musical instrument is to replace wooden components with materials like carbon fibre. The problem with this approach is that even though these anhygroscopic materials are more stable, they are also significantly different than the traditional soundboard woods in terms of material properties [1]. By applying a method like acetylation to create stabilized materials with similar mechanical properties to the existing woods used in soundboards builders can retain a traditional sound and appearance while benefiting from added tonal stability. With added tonal stability musical instrument makers can more confidently fine tune their instruments for a desired sound over a broader range of humidity conditions, something that cannot be done with traditional untreated wood.

7.2 Future Work

Several components of this research work provide a foundation for more extensive future work. Further development of the thin plate soundboard model outlined in chapter 3 would be beneficial to researchers looking to realistically model musical instrument sounds. Including MC as a factor in modelling assumptions would ultimately make the most realistic models and would also allow the perceptual effects noted in this thesis to be tested in more specific situations.

The development of wavelet domain PSP toolboxes would also provide an excellent avenue for future work. The largest challenge with any techniques using the wavelet transform is to provide an understandable context within which to interpret results. A focus on making the transforms as musically relevant as possible would also aid in their adoption. The benefits of using wavelet approaches have

been documented in many fields [53, 54] and their application in musical acoustics where signals are composed of periodic and aperiodic components should be just as beneficial. In the high notes of the piano, which are characterized by a more percussive sound, it was observed that the wavelet PSPs saw larger variations in comparison to traditional PSPs. Perceptual testing of the wavelet domain PSPs would be needed to determine if their improved mathematical representation of sound signals is aligned with the perceived differences in these sounds.

Finally, the testing of an acetylated wood panel carried out in chapter 6 provided excellent preliminary results. The existing understanding of the acetylation process and its effect on wood was confirmed and the improved stability of an acetylated panel in terms of its vibrational response was observed. A larger, more detailed study of acetylated wood would provide a more statistically significant result, and would likely be considered to be more convincing to the musical instrument industry, an industry which is firmly rooted in traditional construction methods. Other applications of stabilized wood in musical instruments could also be explored, with a particularly relevant example found in the action and keyboard components of pianos which require very well controlled precision and stability for proper function. The acetylation technique appears to have a great deal of potential for use in controlling the tone and performance of musical instruments constructed from wood by providing a stable alternative that retains similar material properties to, and the appearance of, untreated wood.

References

[1] U. G. K. Wegst, "Wood for sound," *American Journal of Botany*, vol. 93, no. 10, 2006. iii, xv, 2, 10, 37, 105, 115, 117, 118, 120, 121, 126

[2] Steinway model d grand piano. [Online]. Available: http://www.ptg.org/userfiles/image/History/steinway.jpg ix, 3

[3] B. R. Hoadley, *Understanding Wood: a craftsman's guide to wood technology.* Taunton Press, 2000. ix, 3, 4, 5, 6, 9, 11, 22, 23, 24, 25, 35, 58, 109

[4] M. Pérez Martinez, P. Poletti, and L. Espert Gil, "Vibration testing for the evaluation of the effects of moisture content on the in-plane elastic constants of wood used in musical instruments," in *Vibration and Structural Acoustics Analysis.* Springer, 2011, pp. 21–57. x, 3, 10, 47, 56, 112, 123, 143

[5] S. Yoshikawa, "Acoustical classification of woods for string instruments," *The Journal of the Acoustical Society of America*, vol. 122, p. 568, 2007. xv, 2, 10, 105, 112, 115, 119, 120, 121, 126

[6] S. Levarie and E. Levy, *Tone: A Study in Musical Acoustics*, 2nd ed. Connecticut: Greenwood Press, 1981. 6

[7] G. Peeters, "A large set of audio features for sound description (similarity and classification) in the cuidado project," IRCAM, Ircam, Analysis/Synthesis Team, 1 pl. Igor Stravinsky, 75004 Paris, France, Tech. Rep. pp. 1-25, April 2004. 6, 15, 24, 30, 32, 61, 62, 65, 67, 82, 92

[8] T. Rahne, C. Rasinski, and K. Neumann, "Measuring timbre discrimination with cross-faded synthetic tones," *Journal of Neuroscience Methods*, vol. 189, pp. 176–179, 2010. 7, 14, 15, 25

[9] H. F. D. Ing and E. Z. D. Ing, "Just-noticeable sound changes," in *Psychoacoustics.* Springer, 2007, pp. 175–202. 7, 13

[10] D. Fandrich, "From the forest to the concert hall," Presentation Handout, PTG Seminar, May 2007. 7

[11] D. Green, J. Winandy, and D. Kretschmann, "Wood handbook: Wood as an engineering material," Forest Products Laboratory, Madison, WI., General Technical Report FPL-GTR-113 Chapter 4, 1999. 9, 22, 24, 112

[12] J. L. Romanillos, *Antonio de Torres - Guitar Maker - His Life and Work*. Westport, CT, USA: The Bold Strummer Ltd., 1990. 10, 22

[13] S. Bilbao, *Numerical Sound Synthesis: Finite Difference Schemes and Simulation in Musical Acoustics*, 1st ed. John Wiley & Sons, Ltd, 2009. 11, 12, 13, 39, 40, 41, 43, 123, 136

[14] ——, *Wave and scattering methods for numerical simulation*. Wiley, 2004. 11

[15] A. Chaigne and C. Lambourg, "Time-domain simulation of damped impacted plates. i. theory and experiments," *The Journal of the Acoustical Society of America*, vol. 109, p. 1422, 2001. 12, 48

[16] G. Derveaux, A. Chaigne, P. Joly, and E. Becache, "Time-domain simulation of a guitar," *The Journal of the Acoustical Society of America*, vol. 112, p. 2409, 2002. 12

[17] F. Fontana and S. Serafin, "Modeling savart's trapezoidal violin using a digital waveguide mesh," in *Proc. Stockholm Musical Acoustics Conference (SMAC-03)*, vol. 1, 2003, pp. 51–53. 12

[18] J. O. Smith III, "Efficient synthesis of stringed musical instruments," 1993. 12

[19] C. Lambourg, A. Chaigne, and D. Matignon, "Time-domain simulation of damped impacted plates. ii. numerical model and results," *The Journal of the Acoustical Society of America*, vol. 109, p. 1433, 2001. 12

[20] R. Glowinski, T.-W. Pan, and J. Periaux, "A fictitious domain method for dirichlet problem and applications," *Computer Methods in Applied Mechanics and Engineering*, vol. 111, no. 3, pp. 283–303, 1994. 13

[21] N. Henrich, G. Sundin, D. Ambroise, C. d'Alessandro, M. Castellengo, and B. Doval, "Just noticeable differences of open quotient and asymmetry coefficient in singing voice," *Journal of Voice*, vol. 17, no. 4, pp. 481–494, 2003. 14, 54

[22] C. Torrence and G. Compo, "A practical guide to wavelet analysis," *Bulletin of the American Meterological Society*, vol. 79, no. 1, pp. 61–78, January 1998. 15, 62, 63, 65

[23] A. Askenfelt, "Observations on the transient components of the piano tone," *STL-QPSR*, vol. 34, no. 4, pp. 15–22, 1993. 16, 20, 62

[24] X. He and M. Scordilis, *Psychoacoustic Music Analysis Based on the Discrete Wavelet Packet Transform*. Hindawi Publishing Corporation, 2008, no. 346767. 16, 62

[25] H. Abe and J. Fujii, "Method for manufacturing modified wood," Yamaha Corporation, U.S. Patent 6,667,429 B2, 2003. 16, 17, 103

[26] H. Yano and K. Minato, "Controlling the timbre of wooden musical instruments by chemical modification," *Wood science and technology*, vol. 27, no. 4, pp. 287–293, 1993. 16, 103

[27] R. M. Rowell, "Acetylation," *For. Prod. J*, vol. 56, pp. 4–12, 2006. 17, 103, 104, 126

[28] (2013, September) Accsys technologies. [Online]. Available: http://www.accsysplc.com 18, 103

[29] M. Ramsden, F. Blake, and N. Fey, "The effect of acetylation on the mechanical properties, hydrophobicity, and dimensional stability of pinus sylvestris," *Wood Science and Technology*, vol. 31, no. 2, pp. 97–104, 1997. 18, 104

[30] J.-Z. Li, T. Furuno, S. Katoh, and T. Uehara, "Chemical modification of wood by anhydrides without solvents or catalysts," *Journal of wood science*, vol. 46, no. 3, pp. 215–221, 2000. 18

[31] E. Obataya, K. Minato, and B. Tomita, "Influence of moisture content on the vibrational properties of hematoxylin-impregnated wood," *Journal of wood science*, vol. 47, no. 4, pp. 317–321, 2001. 19

[32] E. Obataya, M. Norimoto, and J. Gril, "The effects of adsorbed water on dynamic mechanical properties of wood," *Polymer*, vol. 39, no. 14, pp. 3059–3064, 1998. 22

[33] M. Matsunaga, K. Minato, and F. Nakatsubo, "Vibrational property changes of spruce wood by impregnation with water-soluble extractives of pernambuco (guilandina echinata spreng.)," *J Wood Sci*, vol. 45, pp. 470–474, 1999. 22

[34] E. Obataya, K. Minato, and B. Tomita, "Influence of moisture content on the vibrational properties of hematoxylin-impregnated wood," *J Wood Sci*, vol. 47, pp. 317–321, 2001. 22

[35] A. Caclin, S. McAdams, B. Smith, and S. Winsberg, "Acoustic correlates of timbre space dimensions: A confirmatory study using synthetic tones," *J. Acoust. Soc. Am.*, vol. 118, no. 1, pp. 471–482, July 2005. 24, 30, 61, 67, 88

[36] H. K. Davis, E. N. Geelhoed, and A. W. MacRae, "Sensory analysis of trout tainted by diesel fuel in ambient water," *Wat. Sci. Tech*, vol. 25, no. 2, pp. 11–18, 1992. 25

[37] Q.-J. Fu, J. Galvin, X. Wang, and G. Nogaki, "Moderate auditory training can improve speech performance of adult cochlear implant patients," *Acoustics Research Letters Online*, vol. 6, no. 3, pp. 106–111, 2005. 25

[38] H. Pobloth and W. B. Kleijn, "On phase perception in speech," in *Acoustics, Speech, and Signal Processing, 1999. Proceedings.*, IEEE, Ed., vol. 1, 1999, pp. 29–32. 25

[39] M. Hansen and B. Kollmeier, "On the relative importance of individual critical bands for the perception of speech quality," *Contributions to Psychological Acoustics*, pp. 611–618, 1996. 25

[40] B. Kollmeier, T. Brand, and B. Meyer, "Perception of speech and sound," in *Springer handbook of speech processing*, J. Benesty, M. M. Sondhi, and Y. Huang, Eds. Springer, 2008, p. 65. 26

[41] W. Hartmann, *Signals, Sound, and Sensation*, ser. Modern Acoustics and Signal Processing. American Inst. of Physics, 1997, no. pp. 545-549. [Online]. Available: http://books.google.ca/books?id=3N72rIoTHiEC 26

[42] (2013, January) Sennheiser hd 280 pro headphones. [Online]. Available: http://www.sennheiser.ca/live/senn/produit/en/275/13/ 26, 55

[43] (2009, January) M-audio mobile pre usb. [Online]. Available: http://www.m-audio.com/products/en_us/MobilePreUSB.html 26, 55

[44] (2013, January) Industrial acoustics sound isolation chamber. [Online]. Available: http://www.industrialacoustics.com/usa/index.asp 26, 55

[45] (2009, January) Bk pulse software. [Online]. Available: http://www.bksv.com/Products/PULSEAnalyzerPlatform/ 33

[46] (2009, January) Mescope vibration analysis software. [Online]. Available: http://www.vibetech.com/go.cfm/en-us/content/mescope/x? 33

[47] P. Piezotronics, "Model 086c02 impact hammer installation and operating manual," Electronic Datasheet, 12 7. 35

[48] R. Bogtrykerri, "Bruel and kjaer 8336 laser doppler vibrometer datasheet," Electronic Datasheet, 4 2007. 35

[49] D. Blackstock, *Fundamentals of Physical Acoustics*. John Wiley & Sons, Ltd, 2000. 48

[50] (August, 2013) Climate data. [Online]. Available: http://climate.weather.gc.ca 55

[51] E. K. Moscicki, E. F. Elkins, H. M. Baurn, and P. M. McNarnara, "Hearing loss in the elderly: an epidemiologic study of the framingham heart study cohort," *Ear and hearing*, vol. 6, no. 4, pp. 184–190, 1985. 56

[52] A. a. Wieczorkowska, J. Wróblewski, and P. Synak, "Application of temporal descriptors to musical instrument sound recognition," *Journal of Intelligent Information Systems*, vol. 21, no. 1, pp. 71–93, 2003. 60

[53] M. Farge, "Wavelet transforms and their applications to turbulence," *Annu. Rev. Fluid Mech.*, vol. 24, pp. 395–457, 1992. 60, 80, 123, 127

[54] I. Daubechies, "The wavelet transform, time-frequnecy localization and signal analysis," *IEEE Transactions on Information Theory*, vol. 36, no. 5, pp. 961–1005, 1990. 61, 62, 80, 123, 127

[55] T. J. Ulrych, "Application of homomorphic deconvolution to seismology," *Geophysics*, vol. 36, no. 4, pp. 650–660, 1971. 61

[56] A. J. Berkhout, "Least-square inverse filtering and wavelet deconvolution," *Geophysics*, vol. 42, no. 7, pp. 1369–1383, 1977. 61

[57] E. Schubert and J. Wolfe, "Does timbral brightness scale with frequency and spectral centroid?" *Acta Acustica united with Acustica*, vol. 92, pp. 820–825, 2006. 61, 67

[58] P. Lee, "Wavelet filter banks in perceptual audio coding," Masters Thesis, University of Waterloo, 1-144 2003. 62

[59] Y. Hu, "Incorporating a psychoacoustical model in frequency domain speech enhancement," *IEEE Signal Processing Letters*, vol. 11, no. 2, pp. 270–273, 2004. 62

[60] C. Delfs, "Classification of piano sounds using time-frequency signal analysis," in *Acoustics, Speech, and Signal Processing.* IEEE, 1997, pp. 2093–2096. 62

[61] D. Sinha and A. Tewfik, "Low bit rate transparent audio compression using adapted wavelets," *IEEE Transactions on Signal Processing*, vol. 41, no. 12, pp. 3463–3479, 1993. 62

[62] P. Srinivisan and L. Jamieson, "High-quality audio compression using an adaptive wavelet packet decomposition and psychoacoustic modeling," *IEEE Transactions on Signal Processing*, vol. 46, no. 4, pp. 1085–1093, 1998. 62

[63] E. Wang, "Application of wavelets to analysis of piano tones," Ph.D. dissertation, National University of Singapore, 2009. 62

[64] V. Välimäki, H. Penttinen, J. Knif, M. Laurson, and C. Erkut, "Sound synthesis of the harpsichord using a computationally efficient physical model," *EURASIP Journal an Applied Signal Processing*, vol. 7, pp. 934–948, 2004. 62

[65] J. Woodhouse, "On the synthesis of guitar plucks," *Acta Acustica united with Acustica*, vol. 90, pp. 928–944, 2004. 62

[66] M. K. Mandal, S. Panchanathan, and T. Aboulnasr, "Choice of wavelets for image compression," *Lecture Notes in Computer Science*, vol. 1133, pp. 239–249, 1996. 63, 74, 80

[67] C. R. J. Jr., E. Hendricks, I. Berezhnoy, E. Brevdo, and S. Hughes, "Image processing for artist identification," *IEEE Signal Processing Magazine*, pp. 37–48, July 2008. 63

[68] I. Daubechies, "Where do wavelets come from? - a personal point of view," *Proceedings of the IEEE*, vol. 84, no. 4, pp. 510–513, 1996. 80

[69] M. Borland, "Investigation of piano soundboard voicing techniques and their impact on tone," Master's thesis, University of Waterloo, 2009. 82, 88, 91

[70] D. Breitman, "Discussion of historic piano construction." Personal Conversation, July 2011. 82, 83, 100, 124

[71] H. A. Conklin, "Design and tone in the mechanoacoustic piano. part ii. piano structure," *J. Acoust. Soc. Am.*, vol. 100, no. 2, pp. 695–708, 1996. 97

[72] D. Larsson, "Using modal analysis for estimation of anisotropic material constants," *Journal of engineering mechanics*, vol. 123, no. 3, pp. 222–229, 1997. 105, 109

[73] Wikipedia. (2013, September) Cosine similarity. [Online]. Available: http://en.wikipedia.org/wiki/Cosine_similarity 114

[74] N. Giordano, "Mechanical impedance of a piano soundboard," *J. Acoust. Soc. Am.*, vol. 103, no. 4, pp. 2128–2133, 1998. 115

[75] ——, "Simple model of a piano soundboard," *J. Acoust. Soc. Am.*, vol. 102, no. 2, pp. 1159–1168, 1997. 115

[76] T. Ono and D. Isomura, "Acoustic characteristics of carbon fiber-reinforced synthetic wood for musical instrument soundboards," *Acoustical science and technology*, vol. 25, no. 6, pp. 475–477, 2004. 121

Appendix

Standard Note Names and Frequencies

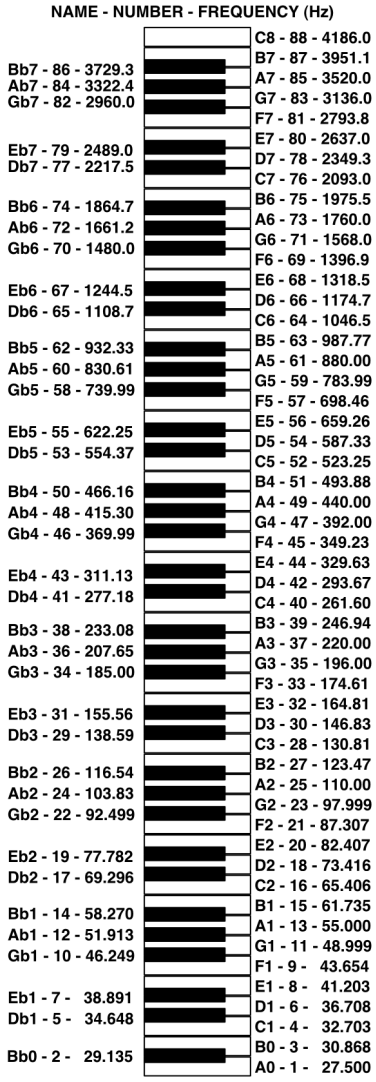

Simulation Code

The orthotropic thin plate simulation discussed in chapter 3 is calculated from the following four Python scripts:

- *Orthotropic-Thin-Plate-Model.py* - the main program
- *Output-process.py* - script used to process plate displacement into sound
- *MCproperties.py* - function called by the main program to determine material properties
- *FDSNeumann2D.py* - function called by the main program to establish 2D difference matrices

Orthotropic-Thin-Plate-Model.py

The main program which calculates string and plate displacement as a function of initial and boundary conditions following the method described by Bilbao [13].

```
from pylab import *
from scipy import *
from scipy.io import wavfile
from scipy.signal import *
from scipy.stats import *
from scipy.sparse import *
import scipy.io as sio
import math
import wave
import sys
import os

STAB = 1.1

# Guitar Notes (Hz) - E2: 82.4, A2: 110.0, D3: 146.8, G3:196.0, B3: 246.9, E4: 329.6
gnotes = array([82.4, 110.0, 146.8, 196.0, 246.9, 329.6])

for fn in gnotes:

    for MC in arange(7.0,11.1,1.0):
        for icN in range(4,5):

            from pylab import *
            from scipy import *
            from scipy.io import wavfile
            from scipy.signal import *
            from scipy.stats import *
            from scipy.sparse import *
            import scipy.io as sio
            import math
            import wave
            import sys
            import os
            import numpy.ma
            from scipy.signal import cspline1d, cspline1d_eval

            ### Simulation Parameters ###

            Fs = 44100.0                    # Sampling Rate in Hz
            Tdur = 2.0                      # Total duration of simulation (s)
            Nframes = int(floor(Tdur*Fs))   # Duration of simulation (samples)
            tsim = arange(0,Tdur,1/Fs)
            tsim = tsim[0:Nframes]          # Time Vector
            k = 1.0/Fs                      # Time step of simulation

            ### Stiff String - Implicit Matrix form ###
            ### Clamped Boundary Conditions
            ### EQN 7.30b Bilbao ###

            STRicTYPE = icN # 1 for RC, 2 for Pluck, 3 for Pluck+RC

            STRB = 0.0001                   # inharmonicity parameter see eq 7.21
            STRf0 = fn                      # Fundamental Frequency
            STRctr = 1.0/8.0                # Center of Excitation
            STRwid = 0.1                    # Width of Excitation
            STRu0ID = 1.0                   # Max Initial Displacement
            STRv0ID = 0.0                   # Max Initial Velocity
            STRrp = 0.3                     # Position of readout (0-1)
            STRloss = [100.0, 10.0, 5000.0, 3.0]   # loss [freq.(Hz), T60(s), freq.(Hz), T60(s)]
            STRtheta = 1.0                  # implicit scheme free parameter (>0.5)


            STRgamma = 2*STRf0                  # gammma parameter
            STRkappa = sqrt(STRB)*(STRgamma/pi)  # kappa parameter from inharmonicity constraint
                  eq 7.21


            # Stability and scheme parameters

            STRh = sqrt((STRgamma**2*k**2+sqrt(STRgamma**4*k**4+16*STRkappa**2*k**2*(2*STRtheta
                 -1)))/(2*(2*STRtheta-1))) # eqn 7.26

            STRN = floor(1.0/STRh)        # Number of grid points
            STRh = 1.0/STRN               # Actual grid space
            STRmu = STRkappa*k/STRh**2 # eqn 7.12 - similar to courant number
            STRlmbda = STRgamma*k/STRh  # Actual lambda

            STRN = STRN + 0 # BC Clamped - Clamped
            STRN = STRN + 1 # BC Clamped - Free
            STRN = STRN + 2 # BC Free - Free


            # Readout interpolation parameters
```

```
STRrp_int = int(1+floor(STRN*STRrp))        # Rounded grid index for readout
STRrp_frac = 1+STRrp/STRh-STRrp_int          # Fractional part for interpolation

# Scheme Loss Parameters - eqn 7.29

STRzeta1 = (-STRgamma**2+sqrt(STRgamma**4+4*STRkappa**2*(2*pi*STRloss[0])**2))/(2*
    STRkappa**2)
STRzeta2 = (-STRgamma**2+sqrt(STRgamma**4+4*STRkappa**2*(2*pi*STRloss[2])**2))/(2*
    STRkappa**2)
STRsig0 = 6.0*log(10.0)/(STRzeta2-STRzeta1)*(STRzeta2/STRloss[1]-STRzeta1/STRloss
    [3])
STRsig1 = 6.0*log(10.0)/(STRzeta2-STRzeta1)*(-1.0/STRloss[1]+1.0/STRloss[3])

### Create Initial Conditions

if STRicTYPE == 1:
    # Raised Cosine - Struck
    STRxax = arange(0,STRN-1)*STRh
    STRind = (-(STRxax-STRctr-STRwid/2)*(STRxax-STRctr+STRwid/2)>0)+zeros(STRN-1)
    STRrc = 0.5*STRind*(1+cos(2*pi*(STRxax-STRctr)/STRwid))
    STRIC = STRrc
    ICname = "RC"

elif STRicTYPE == 2:
    # Plucked IC
    STRxax = arange(0,STRN-1)*STRh
    pluck = 1/STRctr*STRxax
    pluck[floor((STRN-1)*STRctr):] = -1/(1-STRctr-STRh)*STRxax[floor((STRN-1)*STRctr
        ):]+1/(1-STRctr)
    pluck[-1] = 0
    STRIC = pluck
    ICname = "Pluck"

elif STRicTYPE == 3:
    # Shifted Sinc

    N1 = floor(STRctr*(STRN-1))
    N2 = STRN-1-N1
    x1 = mgrid[-pi/2.1:0:N1*1j]
    x2 = mgrid[0:pi/2.1:N2*1j]

    y1 = sinc(x1)
    y2 = sinc(x2)

    SincPluck = concatenate([y1,y2])
    SincPluck = SincPluck-SincPluck[0]
    SincPluck = SincPluck/max(SincPluck)
    STRIC = SincPluck
    ICname = "SincPluck"

else:
    STRxax = arange(0,STRN-1)*STRh
    pluck = 1/STRctr*STRxax
    pluck[floor((STRN-1)*STRctr):] = -1/(1-STRctr-STRh)*STRxax[floor((STRN-1)*STRctr
        ):]+1/(1-STRctr)
    pluck[-1] = 0
    y = copy(pluck)
    dx = STRxax[1]-STRxax[0]
    cj = cspline1d(y,lamb=1)
    splinePluck = cspline1d_eval(cj, STRxax, dx=dx,x0=STRxax[0])
    splinePluck[0] = 0
    splinePluck[-1] = 0
    STRIC = splinePluck
    ICname = "SplinePluck"

# Initial Grid Functions and Outputs

STRu0 = STRu0ID*STRIC
STRu1 = (STRu0ID+k*STRv0ID)*STRIC
STRu2 = zeros(STRN-1)
STRout = zeros(Nframes)

### make into (N,1) sized arrays - i.e. 1D
STRu0 = reshape(STRu0,[size(STRu0),1])
STRu1 = reshape(STRu1,[size(STRu1),1])
STRu2 = reshape(STRu2,[size(STRu2),1])

### Create Coefficient matrices ###

# A Matrix

### Dxx ###

# Make diagonals
tpa = zeros(STRN-1)
tpa[0] = -2
tpa[1] = 1

Dxx = 1.0/STRh**2*linalg.toeplitz(tpa,tpa)
Dxx = csc_matrix(Dxx)

### Dxxxx ###
```

```
# Make diagonals
tpa = zeros(STRN-1)
tpa[0] = 6
tpa[1] = -4
tpa[2] = 1

Dxxxx = 1.0/STRh**4*linalg.toeplitz(tpa,tpa)
Dxxxx = csc_matrix(Dxxxx)

### A ###

STRA = (1+STRsig0*k)*eye(STRN-1,STRN-1)-STRsig1*k*Dxx
STRA = csc_matrix(STRA)

### B ###

STRB = -2*eye(STRN-1,STRN-1)-STRgamma**2*k**2*Dxx+STRkappa**2*k**2*Dxxxx
STRB = csc_matrix(STRB)

### C ###

STRC = (1-STRsig0*k)*eye(STRN-1,STRN-1)+STRsig1*k*Dxx
STRC = csc_matrix(STRC)

#### Convert from sparse to dense for sparse solver to work
STRB = STRB.todense()
STRC = STRC.todense()


### Kirchoff Thin Plate - Implicit Matrix form ###
### Neumann Clamped Boundary Conditions
# Assuming orthotropic, with x = longitudinal (with grain) and y = radial (cross
    grain)

### Dimensional and Material Parameters ###

from FDSNeumann2D import *
from MCproperties import *

Lx = 0.507          # Plate X dimension in longitudinal direction (m)
Ly = 0.355          # Plate Y dimension in radial direction (m)
H = 0.003        # Plate thickness dimension (m)

### Moisture Content as a percentage ###

El, Er, Glr, rhoW, vrl, vlr = matprops(MC)

rho = rhoW     # Density of plate (kg/m**3)

Ex = El    # Young's Modulus in longitudinal direction (Pa)
Ey = Er     # Young's Modulus in radial direction (Pa)
Gxy = Glr    # Shear Modulus (Pa)

vxy = vlr    # Poisson's ratio xy
vyx = vrl    # Poisson's ratio yx

Dx = (Ex*H**3)/(12*(1-vxy*vyx)) # Stiffness Constant - X direction
Dy = (Ey*H**3)/(12*(1-vxy*vyx)) # Stiffness Constant - Y direction
Dxy = vyx*Dx+vxy*Dy+Gxy*H**3/3  # Stiffness Constant - Shear direction

L = sqrt(Lx*Ly) # Characteristic Length

kappax = sqrt(Dx/(rho*H*L**4))       # Plate Stiffness Parameter - longitudinal
kappay = sqrt(Dy/(rho*H*L**4))       # Plate Stiffness Parameter - radial
kappaxy = sqrt(Dxy/(rho*H*L**4))     # Plate Stiffness Parameter - shear

print 'kappax = ' + str(kappax)
print 'kappay = ' + str(kappay)
print 'kappaxy = ' + str(kappaxy)

### Other Parameters ###

loss = [100.0, 3.0, 1000.0, 1.0]    # loss [freq.(Hz), T60(s), freq.(Hz), T60(s)] -
    from Sitka-tap.wav
apx = 0.2                           # Center of Attachment X
apy = 0.3                           # Center of Attachment Y
awid = 0.1                            # Width of Attachment
u0ID = 1.0                          # Max Initial Displacement
v0ID = 0.0                          # Max Initial Velocity
epsilon = Lx/Ly                     # Domain Aspect Ratio
sig0 = 0.05
sig1 = 0.4

# Stability and scheme parameters

r = sqrt(kappay/kappax)

hx = STAB*(4*k**2*(kappax**2+kappay**2/r**4+kappaxy**2/r**2))**0.25
hy = r*hx
Nx = floor(sqrt(epsilon)/hx)
Ny = floor(1.0/(sqrt(epsilon)*hy))
```

```
hx = 1.0/Nx # Actual Grid Spacing X
hy = 1.0/Ny # Actual Grid Spacing Y
ss = (Nx-1)*(Ny-1)

# Difference Matrix and Scheme Parameters
dxx = Dxx(Nx-1,Ny-1,hx,hy)
dyy = Dyy(Nx-1,Ny-1,hx,hy)
dxxxx = Dxxxx(Nx-1,Ny-1,hx,hy)
dyyyy = Dyyyy(Nx-1,Ny-1,hx,hy)
dxxyy = Dxxyy(Nx-1,Ny-1,hx,hy)

A = (1+sig0*k)*np.eye(ss,ss)-sig1*k*(dxx+dyy)
B = 2*np.eye(ss,ss)-k**2*kappax**2*dxxxx-k**2*kappay**2*dyyyy-k**2*kappaxy**2*dxxyy
C = (-1+sig0*k)*np.eye(ss,ss)-sig1*k*(dxx+dyy)

### Make A sparse ###
A = csc_matrix(A)

# Create Spreading Function for String Attachment - 2D Raised Cosine
X, Y = meshgrid(arange(0,Nx-1)*hx,arange(0,Ny-1)*hy)
dist = sqrt((X-apx)**2+(Y-apy)**2)
ind = ((-dist+awid/2.0)>0)+0
J = 0.25*ind*(1+cos(2*pi*dist/awid))
J = reshape(J,[ss,1])
J = J/sum(J)

### Initial Grid Functions and Outputs

u0 = u0ID*zeros([ss,1])
u1 = (u0ID+k*v0ID)*zeros([ss,1])
u2 = zeros([ss,1])

### make into (ss,1) sized arrays - i.e. 1D
u0 = reshape(u0,[size(u0),1])
u1 = reshape(u1,[size(u1),1])
u2 = reshape(u2,[size(u2),1])

# Define Mass Ratio between String and Plate

STRrho = 8000.0 # Density of Steel kg/m^3
gnotes = array([82.4, 110.0, 146.8, 196.0, 246.9, 329.6])
if fn == 82.4:
    STRdia = 0.0014
elif fn == 110.0:
    STRdia = 0.0011
elif fn == 146.8:
    STRdia = 0.00085
elif fn == 196.0:
    STRdia = 0.0006
elif fn == 246.9:
    STRdia = 0.0004
elif fn == 329.6:
    STRdia = 0.0003
else:
    STRdia = 0.001

STRArea = pi*(STRdia/2.0)**2 # String Cross Sectional Area (1mm diameter)
STRL = 0.635 # String length (m)

MR = (STRrho*STRArea*STRL)/(rho*H*Lx*Ly)

stringOUT = zeros([size(STRu0),Nframes])
plateOUT = zeros([size(u0),Nframes])

### Start main loop ###
print 'Start_of_main_loop'

for n in range(2,Nframes):

    # String to plate force modfied by spreading function
    F1 = -k**2*J*MR*STRgamma**2*(STRu1[-2,0]-STRu1[-1,0])/STRh # see Bilbao pg 348 -
         forward spatial difference - force is proportional to slope

    # Plate Solution
    u2 = scipy.sparse.linalg.spsolve(A,(dot(B,u1)+dot(C,u0)-F1))
    u0 = copy(u1)
    u1 = copy(u2.T)

    plateOUT[:,n] = copy(u2)

    # String Solution
    STRu2 = scipy.sparse.linalg.spsolve(STRA,(-dot(STRB,STRu1)-dot(STRC,STRu0)))

    # Enforce string BC at Bridge
    STRu2[-1,0] = mean(ma.masked_array(J,J==0)*u2) # end of string displacement is
         average plate displacement at bridge using spreading function

    # Update previous string time steps
    STRu0 = copy(STRu1)
    STRu1 = copy(STRu2.T)

    stringOUT[:,n] = copy(STRu2)
```

```
### Save Data outpue for Post Processing ###
DATA_OUTPUT_FILENAME =   'OP/' + str(STRf0) + '-' + str(MC) + 'MC-' + ICname + '.mat'

sio.savemat(DATA_OUTPUT_FILENAME, {'plateOUT':plateOUT, 'stringOUT':stringOUT, 'Lx':Lx
    , 'Ly':Ly, 'hx':hx, 'hy':hy, 'Nx':Nx, 'Ny':Ny, 'Fs':Fs, 'Nframes':Nframes, 'ICname':
    ICname}, oned_as='row')
```

Output-process.py

This script is called after the main program to calculate the Rayleigh integral from the plate acceleration which is used to simulate sound pressure at a point in the sound field.

```
from pylab import *
from scipy import *
from scipy.io import wavfile
from scipy.signal import *
from scipy.stats import *
from scipy.sparse import *
import scipy.io as sio
import math
import wave
import sys
import os

gnotes = array([82.4, 110.0, 146.8, 196.0, 246.9, 329.6])

for fn in gnotes:

    for nIC in range(4,5):

        ### Set up initial properties ###
        ICType = nIC # 1 for RC, 2 for Pluck, 3 for RCpPluck
        STRf0 = fn # String frequency
        HDiameter = 0.2  # Head Diameter (m)
        Lp = array([0.8,0.2,0.5]) # Listening Point (x,y,z)
        c0 = 340 # Speed of sound (m/s) of air
        p0 = 1.21 # Density (kg/m^3) of air


        if ICType == 1:
            ICname = "RC"
        elif ICType ==2:
            ICname = "Pluck"
        elif ICType ==3:
            ICname = "SincPluck"
        else:
            ICname = "SplinePluck"


        # Run Loop for different Moisture Content Levels
        for MC in arange(9.0,11.1,1.0):

            print 'MC: ' + str(MC) + ' IC: ' + ICname

            ### Load Parameters from Data File ###
            DATA_INPUT_FILENAME =  'OP/' + str(STRf0) + '-' + str(MC) + 'MC-' + ICname + '.mat'
            m = sio.loadmat(DATA_INPUT_FILENAME)

            plateOUT = m['plateOUT']
            Lx = m['Lx']
            Ly = m['Ly']
            hx = m['hx'][0]
            hy = m['hy'][0]
            Nx = m['Nx'][0][0]
            Ny = m['Ny'][0][0]
            Fs = m['Fs'][0]
            Nframes = m['Nframes'][0]

            ### Calculation of the Rayleigh Integral ###

            # Spatial Grid corresponding to nodes - remove boundary from calculation
            x,y = mgrid[hx:Lx-hx:(Nx-1)*1j,hy:Ly-hy:(Ny-1)*1j]

            # Time Vector
            t = arange(0,Nframes/Fs,1.0/Fs)

            # Distance from listening point to plate
            R = sqrt((Lp[0]-x)**2+(Lp[1]-y)**2+Lp[2]**2)
            delay = R/c0

            delayIndex = delay/(1.0/Fs)
            delayIndex = delayIndex.astype(numpy.int64)
            delayMin = delayIndex.min()
            delayIndex = delayIndex-delayMin
            delayMax = delayIndex.max()

            # Reshape Arrays to match plateOUT format
            R = reshape(R,[size(R),1])
            delayIndex = reshape(delayIndex,[size(delayIndex),1])

            # Plate displacement matrix
            u = plateOUT
```

```
# Time Step
dt = 1.0/Fs

# Take the derivatives to find acceleration
#     v = 1.0/dt*diff(u,axis=1)
a = (1.0/dt)**2*diff(u,n=2,axis=1)

### Calculate Rayleigh Integral - Method 2 - shifted array
aSize = shape(a)[1]
aShift  = zeros([shape(a)[0],shape(a)[1]+delayMax])

for n in range(size(delayIndex)):
    aShift[n,delayIndex[n]:aSize+delayIndex[n]] = p0*a[n,:]/(4*pi*R[n])

P = sum(aShift,axis=0)
P = P[:aSize]

fname = 'OP/' + str(STRf0) + '-' + str(MC) + 'MC-' + ICname + '.wav'

### Normalize to 0.8 max amplitude
wav = int16(0.8*32768*P/max(abs(P)))
Fs = int(Fs)
wavfile.write(fname, Fs, wav)

del m
del u
del a
del aShift
del plateOUT
```

MCproperties.py

This function file is called by the main program to calculate material properties as a function of MC for use in the orthotropic plate finite-difference scheme. Returned material property values are calculated from a polynomial fit to data reported by Pérez et al. [4].

```
from scipy.signal import *
from scipy import *
from pylab import *

def matprops(inputMC):

    ### Data from Perez and Poletti for Norway Spruce ###
    ### MC only allowed from 0-25 percent ###
    ## Picea Abies properties ##

    MC = array([0.11,1.43,6.01,9.38,15.73,17.22,18.82,20.37,21.80,24.71])

    # Pa
    El = 1e6*array([13102.0, 13871.0, 13080.0, 12439.0, 12065.0, 10685.0, 10736.0, 10347.0,
        9919.0, 9491.0])
    Er = 1e6*array([887.8, 923.0, 938.6, 890.1, 725.6, 692.3, 653.9, 618.3, 579.4, 497.6])
    Glr = 1e6*array([845.0, 914.0, 1004.8, 974.9, 942.7, 956.1, 903.7, 846.1, 800.4, 668.1])
    ElEr = El/Er

    # Density in kg/m^3
    rho = array([443.8, 447.5, 458.4, 467.0, 478.5, 481.6, 484.7, 487.8, 488.3, 492.8])

    ### Curve Fit Values ###

    a = polyfit(MC,El,2)
    Elfit = polyval(a,inputMC)

    a = polyfit(MC,Er,2)
    Erfit = polyval(a,inputMC)

    a = polyfit(MC,Glr,2)
    Glrfit = polyval(a,inputMC)

    a = polyfit(MC,rho,2)
    rhofit = polyval(a,inputMC)

    # Poisson's Ratio
    vrl = 0.36 # For Norway Spruce from Kuenecke, Hering, Niemz
    vlr = vrl*Erfit/Elfit

    return Elfit, Erfit, Glrfit, rhofit, vrl, vlr
```

FDSNeumann2D.py

This function file is called by the main program to calculate the 2D difference matrices used in the orthotropic plate finite-difference scheme.

```
from pylab import *
from scipy import *
from scipy.signal import *
from scipy.stats import *
from scipy.sparse import *
import scipy.io as sio
import math

### Following grid stacking convention as laid out in CH10 of NSS - Bilbao ###
# All matrices adjusted for Neumann BC's
# Neumann BC's drop outside nodes - need to adjust size of nx,ny below as appropriate
# i.e. for a plate with Nx divisions, you have Nx+1 nodes, subtract both ends gives Nx-1
# nx,ny below are post adjustment (i.e. they are already adjusted)

### Definitions of Difference Matrices 2-D ###

# hx - X Spatial Step
# hy - Y Spatial Step

# nx - number X Grid Points
# ny - number Y Grid Points

# returns a sparse matrix


### Dyy ###
def Dyy(nx,ny,hx,hy):

    # Make diagonals
    tpa = zeros(ny)
    tpa[0] = -2
    tpa[1] = 1

    # Make infinite matrix
    D1yy = linalg.toeplitz(tpa,tpa)

    # Adjust for Neumann BC's
    D1yy[0,1] = 2
    D1yy[-1,-2] = 2

    # Make full 2D matrix
    D2yy = kron(eye(nx,nx),D1yy)

    # Scale by spatial step
    D2yy = 1.0/hy**2*D2yy

    # Make sparse to speed up computation
    D2yy = csc_matrix(D2yy)

    return D2yy


### Dyyyy ###
def Dyyyy(nx,ny,hx,hy):

    # Make diagonals
    tpa = zeros(ny)
    tpa[0] = 6
    tpa[1] = -4
    tpa[2] = 1

    # Make infinite matrix
    D1yyyy = linalg.toeplitz(tpa,tpa)

    ## Adjust for Neumann BC's

    #Row 1
    D1yyyy[0,0] = 5
    D1yyyy[0,1] = -6
    #Row 2
    D1yyyy[1,1] = 7
    #Row ny-1
    D1yyyy[-2,-2] = 7
    #Row ny
    D1yyyy[-1,-1] = 5
    D1yyyy[-1,-2] = -6

    # Make full 2D matrix
    D2yyyy = kron(eye(nx,nx),D1yyyy)

    # Scale by spatial step
    D2yyyy = 1.0/hy**4*D2yyyy
```

```
    # Make sparse to speed up computation
    D2yyyy = csc_matrix(D2yyyy)

    return D2yyyy


### Dxx ###
def Dxx(nx,ny,hx,hy):

    # Make infinite matrix
    D2xx = -2*eye(nx*ny,nx*ny)+eye(nx*ny,nx*ny,-ny)+eye(nx*ny,nx*ny,ny)
    D2xx = D2xx.todense()

    ## Adjust for Neumann BC's
    D2xx[0:ny,ny:2*ny] = 2*D2xx[0:ny,ny:2*ny]
    D2xx[-ny:,-2*ny:-ny] = 2*D2xx[-ny:,-2*ny:-ny]

    # Scale by spatial step
    D2xx = 1.0/hx**2*D2xx

    # Make sparse to speed up computation
    D2xx = csc_matrix(D2xx)

    return D2xx


### Dxxxx ###
def Dxxxx(nx,ny,hx,hy):

    # Make infinite matrix
    D2xxxx = (6*eye(nx*ny,nx*ny)-4*eye(nx*ny,nx*ny,-ny)-4*eye(nx*ny,nx*ny,ny)+eye(nx*ny,nx*ny
        ,-2*ny)+eye(nx*ny,nx*ny,2*ny))
    D2xxxx = D2xxxx.todense()

    ## Adjust for Neumann BC's

    # Block Row 1
    D2xxxx[0:ny,0:ny] = 5.0/6.0*D2xxxx[0:ny,0:ny]
    D2xxxx[0:ny,ny:2*ny] = 6.0/4.0*D2xxxx[0:ny,ny:2*ny]
    # Block Row 2
    D2xxxx[ny:2*ny,ny:2*ny] = 7.0/6.0*D2xxxx[ny:2*ny,ny:2*ny]

    # Block Row Nx-1
    D2xxxx[-2*ny:-ny,-2*ny:-ny] = 7.0/6.0*D2xxxx[-2*ny:-ny,-2*ny:-ny]

    # Block Row Nx
    D2xxxx[-ny:,-2*ny:-ny] = 6.0/4.0*D2xxxx[-ny:,-2*ny:-ny]
    D2xxxx[-ny:,-ny:] = 5.0/6.0*D2xxxx[-ny:,-ny:]

    # Scale by spatial step
    D2xxxx = 1.0/hx**4*D2xxxx

    # Make sparse to speed up computation
    D2xxxx = csc_matrix(D2xxxx)

    # Convert back to dense
    D2xxxx = D2xxxx.todense()

    return D2xxxx


### Dxxyy ###
def Dxxyy(nx,ny,hx,hy):

    # Make sub-matrices

    m1 = (-2*eye(ny,ny)+eye(ny,ny,-1)+eye(ny,ny,1)).todense()
    m1[0,1] = 2.0
    m1[-1,-2] = 2.0

    km1 = (eye(nx,nx,1)+eye(nx,nx,-1)).todense()
    km1[0,:] = 0
    km1[-1,:] = 0

    m2 = (4*eye(ny,ny)-2*eye(ny,ny,-1)-2*eye(ny,ny,1)).todense()
    m2[0,1] = -4.0
    m2[-1,-2] = -4.0

    km2 = eye(nx,nx).todense()
    km2[0,:] = 0
    km2[-1,:] = 0

    m3 = (-4*eye(ny,ny)+2*eye(ny,ny,-1)+2*eye(ny,ny,1)).todense()
    m3[0,0] = -3.0
    m3[-1,-1] = -3.0

    km3 = zeros([nx,nx])
    km3[0,1] = 1
```

```
km3[-1,-2] = 1

m4 = (4*eye(ny,ny)-2*eye(ny,ny,-1)-2*eye(ny,ny,1)).todense()
m4[0,1] = -3.0
m4[-1,-2] = -3.0

km4 = zeros([nx,nx])
km4[0,0] = 1
km4[-1,-1] = 1

D2xxyy = kron(km1,m1)+kron(km2,m2)+kron(km3,m3)+kron(km4,m4)

# Scale by spatial step
D2xxyy = 1.0/(hx**2*hy**2)*D2xxyy

# Make sparse to speed up computation
D2xxyy = csc_matrix(D2xxyy)

# Convert back to dense
D2xxyy = D2xxyy.todense()

return D2xxyy
```